The Pennsylvania State University

The Graduate School

DEPOSITION OF MAGNETITE IN HIGH TEMPERATURE BOILER ENVIRONMENTS

A Dissertation in

Energy and Mineral Engineering

by

Balaji Raman

Submitted in Partial Fulfillment

of the Requirements

for the Degree of

Doctor of Philosophy

August 2017

The dissertation of Balaji Raman was reviewed and approved* by the following:

Serguei N. Lvov
Professor of Energy and Mineral Engineering &
Materials Science and Engineering
Director of Electrochemical Technologies Program
Dissertation Advisor
Chair of Committee

Sarma V. Pisupati
Professor of Energy and Mineral Engineering

Zuleima T. Karpyn
Professor of Petroleum and Natural Gas Engineering
Quentin E. and Louise L. Wood Faculty Fellow in Petroleum and Natural Gas
Engineering
FCMG Chair in Fluid Behavior and Rock Interactions

James H. Adair
Professor of Materials Science and Engineering,
Biomedical Engineering and Pharmacology

Sanjay Srinivasan.
Professor of Petroleum and Natural Gas Engineering
Interim Associate Department Head for Graduate Education
John & Willie Leone Family Department of Energy and Mineral Engineering

*Signatures are on file in the Graduate School

ABSTRACT

Suspended magnetite particles in boiler water may deposit in lower orifice headers in forced circulation boilers, impeding flow and causing inefficiencies, ultimately leading to overheating boiler tube failures. The surface charge and zeta potential developed by the suspended particles could be a driving factor in this process. To study the mechanism behind the deposition of suspended magnetite on stainless steel, laboratory-scale experiments were carried out under a range of standard boiler water chemistry, simulating fouling experienced in boiler units. A high-temperature–high-pressure electrophoretic deposition cell with provisions to test deposition on metal substrates has been developed. The trends in the deposition processes for the various chemistry were validated using visual observations, surface microscopy, and in situ electrochemical impedance spectroscopy (EIS). A three-electrode assembly design was developed to carry out the in situ electrochemical measurements in various boiler water environments. The experimental setup was successfully used to test boiler water chemistry at 300°C (572°F) and 10 MPa (1450 psi). The chemistry tested included all-volatile treatment (AVT; oxidizing and reducing using hydrazine), caustic treatment (CT), phosphate treatment (PT), and a filming amine (GE HRSG-02). In addition, the effect of particle size on the deposition process was studied.

The experimental results have been explained using established principles of suspended oxide behavior in aqueous environments. The results indicated that the presence of suspended magnetite particles at a $pH_{25°C} = 9.3$, controlled by ammonium hydroxide, caused the particles to aggressively deposit on the stainless steel surface. On the other end of the AVT spectrum, when tested at $pH_{25°C} = 9.8$, no visually observable deposits were found on the surface of the steel. Operating close to the point of zero charge of magnetite at 300 °C resulted in deposition and moving away from the point of zero charge mitigated deposition. In case of the caustic treatment and phosphate treatment, it was seen that the compression of the double layer due to the additional electrolytes in the system could influence the deposition process even when the pH of the system was away from the point of zero charge of magnetite at 300°C. No significant influence of hydrazine was observed on the deposition of magnetite. Impedance spectroscopy was successfully used in these tests to identify *in situ* the cases where deposition occurred.

The filming amine chemistry did not mitigate deposition completely, but the presence of the HRSG-02 affected the nature of deposits observed on the substrate. Macroscopically the substrate appeared to be covered with deposits and some darker regions. The results of the

iv

filming amine study point to possible interactions between the amine-substrate and amine-magnetite. Increasing the particle size distribution clearly showed a decrease in the deposition even though the boiler water chemistry was conducive for deposition. Although, controlling the particle size is not an option for utility boilers, these tests provide further insight into understanding deposition at high temperatures in boiler type environments.

In addition to experimental results, the Derjaguin-Landau-Verwey-Overbeek (DLVO) theory has been used to model the behavior of the suspended particles under the AVT boiler water chemistry regime. The DLVO interaction energy curves and the calculated agglomeration probabilities support the experimental observations regarding the deposition of magnetite under the AVT regime. Such calculations can be extended to other treatment chemistries as well providing means to predict the behavior of suspended particles in boiler water.

In summary, this study has clearly established a link between the solution chemistry at 300 °C (572 °F) to the deposition of magnetite on 304 SS. The results show that the zeta potential, which is influenced by the pH of the solution, could be the major factor dictating the susceptibility of deposition at these conditions. EIS was used successfully to establish that magnetite deposition results in high values ($> 10^6 \Omega$) of the magnitude of the impedance. Although qualitative, this could provide valuable information when monitoring boilers and power plants for deposition. These results also proved the success of the experimental setup developed in this project for simulating the boiler environments of interest and for studying the deposition phenomena commonly faced in boilers. This study is a one of a kind study focusing purely on the particle attachment aspect of deposition across a wide range of boiler water treatment chemistries with the results supported by surface analyses, impedance spectroscopy and theoretical calculations.

TABLE OF CONTENTS

LIST OF FIGURES

LIST OF TABLES

Preface to the Dissertation

This research work explores the effects of different boiler water chemistry on the deposition of magnetite on 304 stainless steel in boiler environments. The test conditions, choice of substrate, temperature and pressure parameters were all decided based on the interactions with Electric Power Research Institute (EPRI), DTE Energy, Consumer's Energy and Alstom Power. The research work was tailored to solve the issues of magnetite deposition currently faced by DTE Energy, Consumer's Energy and Alstom Power. This work was funded by EPRI.

A significant portion of this dissertation has been published as an EPRI Technical Report and is cited as *Deposit Mechanisms & Control of Lower Orifice Header Fouling in Forced Circulation Units*, EPRI, Palo Alto, CA: 2016. 3002009262.

Parts of this dissertation have also been published as,

1. B. Raman, D.M. Hall, S.J. Shulder, M.F. Caravaggio, S.N. Lvov, Colloids Surfaces A Physicochem. Eng. Asp. (2016).

2. B. Raman, D.M. Hall, S.N. Lvov, S. J. Shulder and M. Caravaggio, '*Electrochemical Impedance Spectroscopy as a Tool to Link Cycle Chemistry Properties to Fouling in Power Generating Systems*', in 11th International Conference on Cycle Chemistry in Fossil & Combined Cycle Plants with Heat Recovery Steam Generator (Saint Louis: EPRI, 2015).

3. B. Raman, D.M. Hall, S.J. Shulder, M. Caravaggio, S.N. Lvov, ECS Trans. 66(21) (2015) 43–56. 10.1149/06621.0043ecst.

ACKNOWLEDGEMENTS

Chapter 1

Introduction

Discussion of Research Need

A current problem in high-pressure forced circulation boilers (~2200 psi [15.2 MPa]) is the fouling of the lower header flow control orifices (see Figure 1-1). The material fouling these orifices was found to be friable deposits of magnetite observed on the circumference of the orifice. When these large quantities of magnetite deposited on the circumference of the orifice opening, they restricted flow and increased the differential pressure across the orifice. Large accumulations can result in tube failures from overheating due to insufficient flow. To mitigate any failures, these deposits must be removed despite the resulting costly unit shutdowns.
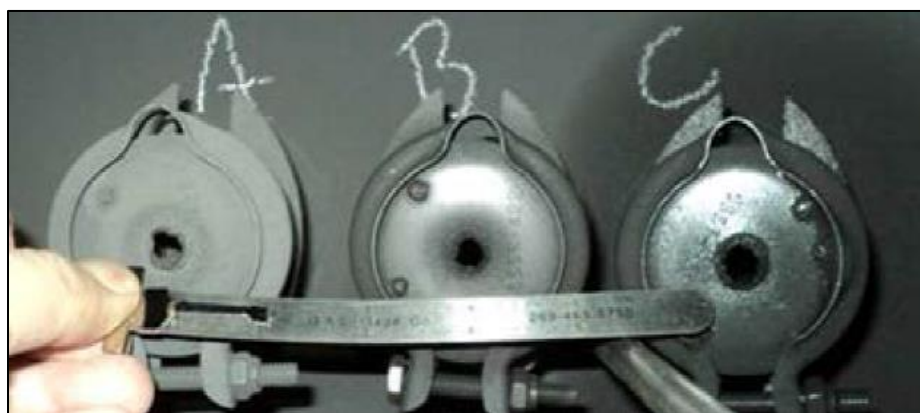
Figure 1-1 Picture of lower header flow control orifice fouling. *Used with permission from C. Dunham, Consumers Energy*

It is generally believed that the origin of the magnetite particles is products of corrosion processes within the feedwater cycle. However, the factors that govern this fouling problem have yet to be well defined. Some think that boiler water chemistry (reducing or solid alkalizing agents) influence this fouling process; others suggest that the formation of these deposits may be influenced by the zeta potential of the suspended particles. Given these uncertainties, there is a need for research that provides evidence to link boiler water treatments to the susceptibility of fouling in lower header forced circulation boilers.

Fouling and deposition of iron oxides is a major issue in fossil fuel fired power plants and often have been found to lead to boiler tube failures [1]. Under de-aerated conditions, the iron in steel oxidizes to magnetite. The simplified reaction is given as follows

$$3 \text{ Fe(s)} + 4 \text{ H}_2\text{O(l)} \rightarrow \text{Fe}_3\text{O}_4\text{(s)} + 4 \text{ H}_2\text{(g)} \tag{1}$$

Magnetite forms a dark, passive and protective layer on the boiler tube surface, limiting further corrosion. Corrosion product transport in feed water piping can lead to magnetite particles being transported downstream where, under certain conditions, the oxide particles can adhere to the tube walls or other surfaces. Fouling due to magnetite deposition has been observed frequently on boiler tube walls and sometimes on orifice plates [2]. Deposits on orifice plates restrict the flow and insufficient flow could eventually lead to failure due to overheating. Minimizing corrosion and boiler tube failures by means of establishing guidelines for the various boiler water and feedwater treatment regimes has been a priority for several years [1,3-8]. Typically, boiler water is de-aerated and the pH is maintained in the alkaline range to minimize corrosion [2]. All-volatile treatment (AVT) is a common treatment regime where the feedwater pH is controlled using ammonium hydroxide. Sometimes a solid alkali treatment is employed, where tri-sodium phosphate or sodium hydroxide to the boiler in addition to the ammonium hydroxide coming from the feedwater.

Magnetite deposition on various metal and alloy surfaces has been researched previously under different conditions [9-11]. Newson et al. (1983) studied the deposition of suspended magnetite over a range of temperatures up to 75 $^{\circ}$C [12]. Turner and Godin (1994) studied the deposition of magnetite on Alloy 600 under boiling and non-boiling conditions at temperatures up to 290 °C and determined that the deposition was limited either by the transport of the magnetite particles to the surface or by the possibility of attachment of the particle to the surface [11]. The deposits in these studies were analyzed using a destructive technique or by using radioactively tagged magnetite particles. The researchers speculate that, under certain conditions the attachment of the particles is dependent on the particle-surface interaction, which is governed primarily by the London-van der Waals forces and electrostatic interactions [13]. Burill (1977) also discusses the possibility of surface charge and zeta potential of magnetite influencing deposition onto isothermal tubes.

Controlling deposition of magnetite is of key interest to the power industry. The surface properties of magnetite and it's behavior are influenced by physicochemical environment, of which temperature is an integral part. It is imperative to study the deposition process at relevant temperatures. This study presents a novel experimental approach to study the influence of boiler water chemistry on fouling and deposition by focusing purely on the effect of inter-particle interactions and particle substrate interactions in boiler type environments. In this study, a high pressure high temperature deposition cell capable of investigating the influence of boiler water chemistry on deposition on metal substrates was developed. To closely match boiler type environments, magnetite deposition on 304 stainless steel was studied at 300 °C and 10 MPa (1450 psi). 304 stainless steel was chosen as the material of interest based on the input from the boiler units experiencing orifice plate fouling. In fossil plants, boiler water is typically tuned to a set of chemistry conditions to prevent corrosion and damage to infrastructure. There are multiple such chemistry and guidelines for which are provided by Electric Power Research Institute [14]. The system developed and presented here provides a way to test the influence of different boiler water chemistry on suspended magnetite particles and how it affects deposition from a particle attachment point of view. In real systems, the deposition could occur over a number of days or even months. In order to accelerate the deposition process, an excess of iron (II, III) oxide (magnetite) was added to the system. Particle deposition has been shown to be dependent on transport of particles to surface and the probability of attachment [9]. The excess magnetite particles ensured that the deposition process was not limited by the availability of suspended magnetite particles, eliminating the dependence on particle transport to the surface. As such, the addition of the excess magnetite focused the study to whether the aqueous environment increases the probability of attachment and the susceptibility of fouling. The experimental system was also designed to carry out in-situ electrochemical impedance spectroscopy measurements (EIS). The capabilities of EIS for monitoring and characterizing surface-solution interactions have been well-studied. By studying the impedance response across a range of frequencies, EIS can identify the different phenomena occurring at the interface based on their timescales. In theory, the occurrence of a deposit will create a new interface between the solution and substrate. This could add an additional capacitor type behavior at the high frequencies or, in the case of porous deposits, affect the low frequency behavior by influencing the diffusion processes [15-18]. The EIS data collected from these tests were used to monitor changes on the solution-substrate interface due to deposition. *In situ* electrochemical measurements provide scope for electrochemical monitoring of the solution-substrate interface in extreme environments and this

has potential applications in the industry. In summary, this paper aims to present a test system capable of monitoring the solution substrate interface, real time and *in situ*, for particle deposition at temperatures and in solution chemistry that are pertinent to power plant steam generators.

Objectives

This project was developed to evaluate the susceptibility of different water chemistry to the deposition of suspended magnetite particles on stainless steel (SS). It is intended that the results of this study will provide some data to develop an understanding of whether the fouling process of interest follows the trends expected of one influenced by the zeta potential of magnetite. To accomplish this task, the following objectives were formed:

- Develop a high-temperature electrophoretic deposition cell to investigate the effect of boiler water chemistry on magnetite deposition to a 304 stainless steel substrate at 300°C (572°F) and 10 MPa (1450 psi).

- Develop a novel electrode assembly to electrochemically monitor changes in the impedance of the steel surface–solution interface via electrochemical impedance spectroscopy (EIS).

- Identify whether the deposition of suspended magnetite particles can be observed in a simulated boiler environment.

- Use the data collected to infer whether deposition trends observed can be correlated to properties of the suspended magnetite solution and possible orifice fouling mechanisms.

- Determine whether certain boiler water chemistry reduced the potential for orifice fouling.

The substrate (304 SS), the temperature and pressure were chosen based on typical operating ranges in regions of boiler units where magnetite deposition was observed frequently. This information was obtained by contacting the Electric Power Research Institute and three other utilities.

Summary of Test Conditions

Table 1-1 Summary of the various boiler water treatments tested in this study.

Test Condition / Boiler Water Chemistry	Chemicals & Concentrations	304 SS Sample	pH_{25C}	Referred as
AVT	NH_4OH (4.4 10^{-5} mol kg^{-1})	AVT-1	9.3	AVT Low
	NH_4OH (32 10^{-5} mol kg^{-1})	AVT-2	9.8	AVT High
	NH_4OH (4.4 10^{-5} mol kg^{-1}) without magnetite	AVT-1C	9.3	Control
	NH_4OH (32 10^{-5} mol kg^{-1}) without magnetite	AVT-2C	9.8	Control
Phosphate Treatment	NH_4OH (4.4 10^{-5} mol kg^{-1}) + 3 ppm Na_3PO_4	PT-1	9.49	High Phosphate
	NH_4OH (4.4 10^{-5} mol kg^{-1}) + 0.3 ppm Na_3PO_4	PT-2	9.3	Low Phosphate
Caustic Treatment	NH_4OH (4.4 10^{-5} mol kg^{-1}) + 1.2 ppm NaOH	CT-1	9.59	High Caustic
	NH_4OH (4.4 10^{-5} mol kg^{-1} + 0.5 ppm NaOH)	CT-2	9.43	Low Caustic
Hydrazine	NH_4OH (4.4 10^{-5} mol kg^{-1}) + 30 ppb N_2H_4	AVTH-1	9.3	
	NH_4OH (4.4 10^{-5} mol kg^{-1}) + 90 ppb N_2H_4	AVTH-2	9.3	
Filming Amine	2.5 ppm HRSG-02	FFA-1	9.3	
	5 ppm HRSG-02	FFA-2	~10	
Particle Size	Particle size < 5 μm (NH_4OH 4.4 10^{-5} mol kg^{-1})	AVTPS	9.3	

The choices of test conditions were based on available literature and interactions with utilities experiencing magnetite deposition in their forced circulation units. The utilities and manufacturer contacted were Consumers Energy, DTE Energy, and Alstom Power, respectively. The $pH_{25°C}$ of the feedwater and boiler water was maintained in the range of 8.9–9.3. Consumers Energy employed phosphate-based treatments for its boiler water. The feedwater was brought up to a $pH_{25°C}$ of 9.15 using ammonium hydroxide, and trisodium phosphate was added to the boiler. The unit experiencing problems with deposition had a target boiler $pH_{25°C}$ range of 9.2–9.6. Alstom Power provided a specifications document with its recommended operational $pH_{25°C}$ ranges. Based on the Alstom guidelines, the feedwater $pH_{25°C}$ was maintained between 9.0 and 9.6, and the boiler water $pH_{25°C}$ was elevated using trisodium phosphate to stay in the range of 9.0–10.0. The suggested range of phosphate concentration was from 2 ppm to 6 ppm. The International Association for the Properties of Water and Steam (IAPWS) also has technical guidance documents that suggests $pH_{25°C}$ ranges and amounts of phosphate for different types of boilers and treatments [19, 20]. The recommended $pH_{25°C}$ of the boiler water is between 9.0 and 9.4, and the suggested phosphate range is from 0.3 ppm to 2 ppm. EPRI's Comprehensive Cycle Chemistry Guidelines for Fossil Plants provides detailed recommendations for feedwater and boiler water chemistry based on the feedwater metallurgy and type of boiler [14]. For units with mixed metallurgy and reducing feedwater treatment, all-volatile treatment reducing, or AVT(R), should be used with pH maintained via ammonia addition (or a neutralizing amine with lower volatility than ammonia) and a reducing agent (usually hydrazine or carbohydrazide). For all-ferrous systems, an oxidizing treatment is used in which pH is maintained with ammonia, no reducing agent is applied, and sufficient oxygen residual ensures an oxidizing condition, AVT(O), in the feedwater. On once-through units and some drum units, oxygen is added along with ammonia. Subcritical drum units may be operated under AVT chemistry with no chemical addition to the boiler drum. A solid alkali drum treatment may also be employed to maintain the boiler water pH through the addition of trisodium phosphate (Na_3PO_4) (phosphate treatment [PT], caustic addition (NaOH) (caustic treatment [CT]), or phosphate with a small amount of caustic. Solid alkali treatments provide a sodium-based alkalinity for pH control and the ability to neutralize acidic contaminant ingress and should be used for units with brackish or salt water cooling water. Boiler water pH should be corrected for ammonia so that solid alkali is always present. The EPRI-suggested feedwater and boiler water treatment specifications are provided in

Table 1-2 Normal Chemistry Operating Specifications

Location	Parameter	AVT(R)	AVT(O)	OT
Condensate Pump Discharge (CPD)	Dissolved oxygen (O_2), ppb	≤10	≤20	≤20
Deaerator Inlet	Oxidation reduction potential (ORP), mV	-150 to -250	>+0	>100
Economizer Inlet (Feedwater)	pH			
	Drum	9.0–9.3	9.2–9.6	9.0–9.6
	Once-through			8.5–9.0
	Dissolved oxygen (O_2), ppb			
	Drum	≤5	5–10	30–50
	Once-through			50–200
Boiler Water	pH	9.0–9.6	9.0–9.6	NA

Boiler water pH specifications are pressure dependent. For units on PT and pressure >2000 psi (13.8 MPa), the range is 9.0–9.6 while at pressures <2000 psi (13.8 MPa), the range is 9.2–9.8. Phosphate addition should be used to maintain the ammonia-corrected pH and not to achieve a specific phosphate residual. For units on CT, the ammonia-corrected pH should be 9.1–9.4; CT is not recommended for use above 2500 psi (17.2 MPa).

In this study, the range of test conditions included the AVT range, wherein $pH_{25°C}$ of 9.3, 9.6, and 9.8 were tested. All pH values were controlled using $NH_4OH(aq)$. For the caustic treatment, two concentrations were chosen: 0.5 ppm (referred to as low caustic) and 1.2 ppm (referred to as high caustic). For the phosphate treatment, two concentrations were chosen: 0.3 ppm (referred to as low phosphate) and 3 ppm (referred to as high phosphate). For the caustic and phosphate treatments, the deionized water was brought up to a $pH_{25°C}$ of 9.3 using $NH_4OH(aq)$. A reducing agent was not added for any of these tests.

In addition to the traditional boiler water chemistry mentioned above, some other chemistry and conditions were tested. Hydrazine, a traditional reducing agent (oxygen scavenger), was used in testing the AVT(R) chemistry. The 30 ppb and 90 ppb hydrazine residuals were selected as the two conditions for testing the influence of hydrazine. The hydrazine residuals were suggested by the EPRI project manager as representative residual values for high-

pressure boiler units. The synthetic boiler water was prepared by conditioning deaerated, deionized water to a $pH_{25°C}$ of 9.3 using $NH_4OH(aq)$.

Almost all fossil power plants use some form of an amine treatment in their feedwater water chemistry. These amines could be aqueous ammonia, anhydrous ammonia gas, neutralizing amine blends, and, more recently, film-forming products/amines. Polyamine treatment is a relatively new class of boiler water treatment developed by GE Power & Water, which employs a multifunctional, volatile organic amine corrosion inhibitor [21]. The polyamine program typically employs a long-chain fatty diamine corrosion inhibitor combined with a blend of neutralizing amines. The polyamine used in the testing was the GE Steamate HRSG-02. The polyamine was added as received product. The composition of HRSG-02 is given in Table 1-3. The HRSG-02 product has approximately 1 part film-forming compound per four parts of HRSG-02 product. The product is a blend of traditional neutralizing amines and organic amine filming compounds.

Table 1-3 Composition of Steamate HRSG-02

Chemical	Percentage	Role
Alkyl diaminopropane	10–20%	Filming compound
Cyclohexylamine	10–20%	Neutralizing amine
Ethanolamine	10–20%	Neutralizing amine
Oleylamine 1	2.5–10%	Filming compound
Diethanolamine	0.1–1%	Neutralizing amine

The 2.5 ppm HRSG-02 and 5 ppm HRSG-02 levels were chosen based on the manufacturer's experience with multiple boiler units employing the polyamine treatment. The two concentrations chosen here result in boiler water pH between 9.3 and 10; this allows for a comparison with the AVT(R) conditions tested earlier.

To identify possible factors (apart from the chemistry) influencing the deposition, the effect of a different particle size on magnetite deposition was studied. When testing the different boiler water chemistry, magnetite particles in the size range of 50–100 nm were used. To provide a contrast and comparison to the previous work, commercially obtained magnetite particles with size <5 μm were used in this study. Using a suspension having such a wide range of particle sizes takes the study a step closer to real boiler environments, where there is little control over the particle size distribution. It must be noted that the particle sizes compared here are at the

beginning of the test, when particles are added in the system. **Error! Reference source not f ound.** summarizes the various boiler water chemistry tested in this study.

References

[1] B. Dooley, A vision for reducing boiler tube failures, Power Eng. 96 (1992). http://www.osti.gov/scitech/biblio/5428734 (accessed July 25, 2014).

[2] B. Buecker, Power Plant Water Chemistry: A Practical Guide, PennWell Publishing Company, 1997.

[3] B. Buecker, The Evolution of Power Plant Water/Steam Chemistry, Power Eng. 10 (2012). http://scholar.google.com/scholar?hl=en&btnG=Search&q=intitle:The+Evolution+of+Power+Pla nt+Water/Steam+Chemistry#0 (accessed August 10, 2014).

[4] B. Buecker, Utility water chemistry update, Power Eng. 105 (2001) 12. http://ezaccess.libraries.psu.edu/login?url=http://search.proquest.com/docview/221063450?accou ntid=13158.

[5] B. Buecker, Monitoring the chemistry program change of the condensate/feedwater in a utility drum boiler, Mater. Perform. 44 (2005) 42–45. http://cat.inist.fr/?aModele=afficheN&cpsidt=16481858 (accessed August 10, 2014).

[6] B. Dooley, A vision for reducing boiler tube failures. Part 2, Power Eng. 95 (1992). http://www.osti.gov/scitech/biblio/5116302 (accessed July 25, 2014).

[7] R.B. Dooley, R. Tilley, Guidelines for controlling flow-accelerated corrosion in fossil and combined cycle plants, EPRI Rep. 1008082 (2005).

[8] O. Jonas, Effective cycle chemistry control, in: Proc. ESAA Power Stn. Chem. Conf. Rockhampton, Queensland, Aust. May 15, 2000.

[9] C.W. Turner, D.H. Lister, D.W. Smith, The Deposition and removal of sub-micron particles of magnetite at the surface of alloy 800, in: Steam Gener. Heat Exch. Conf., Toronto, 1994. http://www.iaea.org/inis/collection/NCLCollectionStore/_Public/27/015/27015059.pdf (accessed September 30, 2014).

[10] D.J. Wesolowski, M.L. Machesky, D.A. Palmer, L.M. Anovitz, Magnetite surface charge studies to 290°C from in situ pH titrations, Chem. Geol. 167 (2000) 193–229. doi:10.1016/S0009-2541(99)00209-0.

[11] C. Turner, M. Godin, Mechanisms of magnetite deposition in pressurized boiling and non-boiling water, Ontario, 1994. http://inis.iaea.org/search/search.aspx?orig_q=RN:27005796 (accessed July 21, 2014).

[12] I. Newson, T. Bott, C. Hussain, Studies of magnetite deposition from a flowing suspension, Chem. Eng. …. 20 (1983) 335–353. http://www.tandfonline.com/doi/abs/10.1080/00986448308940597 (accessed July 25, 2014).

[13] N. Kallay, Adhesion of Fine Particles at Solid/Solution Interfaces, MRS Bull. 15 (1990) 41–47. doi:10.1557/S0883769400060723.

[14] EPRI, Comprehensive Cycle Chemistry Guidelines for Fossil Plants, Palo Alto, CA, 2011. doi:1021767.

[15] M.E. Orazem, B. Tribollet, Electrochemical Impedance Spectroscopy, John Wiley & Sons, Inc., 2008. doi:10.1002/9780470381588.

[16] B. Tribollet, G. Galicia, N. Pebere, V. Vivier, Corrosion Study of an AZ91 Magnesium alloy by EIS and LEIS, in: ECS Trans., ECS, 2006: pp. 157–168. doi:10.1149/1.2215499.

[17] H.R. Zebardast, S. Rogak, E. Asselin, Electrochemical detection of corrosion product fouling in high temperature and high pressure solution, Electrochim. Acta. 100 (2013) 101–109. doi:10.1016/j.electacta.2013.03.108.

[18] V. Balashov, M. Fedkin, S. Lvov, B. Dooley, Experimental System For Electrochemical Corrosion Studies In High Temperature Aqueous Solutions, (2007) 12. https://www.onepetro.org/conference-paper/NACE-07403.

[19]. D. Friend and R. Dooley, Technical Guidance Document: Volatile Treatments for the steam-water circuits of fossil and combined-cycle/HRSG power plants. Niagara Falls, Canada, 2010. http://www.iapws.org/techguide/Volatile.pdf.

[20]. K. Daucik and R. Dooley, Technical Guidance Document: Phosphate and NaOH treatments for steam-water circuits of drum boilers of fossil and combined-cycle/HRSG power plants. Plzen, Czech Republic, 2011. http://www.iapws.org/techguide/PhosphateCaustic.pdf.

[21]. GE Power and Water, Polyamine Boiler Treatment Technology-A Discussion in Question & Answer Format, 2011.

Chapter 2

Background & Theory

Deposition Mechanism

Under isothermal conditions, deposition of suspended particles onto a surface can be considered as a two-step process. First is the transport step which is the transport of the particle from the bulk of the aqueous medium to the proximity of the substrate. The second step is the attachment step, which determines whether the particle will adhere to the substrate. The transport step is dependent on the initial flux of depositing particles, which can be linked to the concentration of the suspended particles in the bulk solution and the hydrodynamics in the system. The attachment step is dependent on the interaction between the particle and the substrate. Typically, these interactions are governed by London-van-der-Waals forces and electrostatic forces, both of which can be attractive or repulsive. The electrostatic interactions depend on the nature of the charges developed on the particle and substrate, which are in turn influenced by the physicochemical environment [1,2].

In this study, the focus is on the influence of the boiler water chemistry on the deposition of magnetite on 304 SS. Boiler water chemistry is a key aspect of the physicochemical environment and will influence the attachment step of the deposition process. The transport step will depend on flow and hydrodynamics in the boiler tube, aspects which are not of focus in this study. This scope of this study is limited to the particle-substrate interactions and how the physicochemical environment affects the interactions.

Surface Charge Development and DLVO Theory

Metal oxides in an aqueous solution develop a surface electric charge due to dissociation of surface groups and preferential adsorption of ions or substitutions in the lattice [3]. Metal oxides in an aqueous environment have hydroxyl groups on their surfaces, which can accept or donate protons based on their interaction with H^+(aq) or OH^-(aq) ions in solution. Multiple sites

on the oxide surface will contribute to the surface charge. The interactions with the aqueous environment can be depicted in a very simple, qualitative manner using the following reactions [4,5,6]:

Under acidic conditions,

$$\equiv M\text{-}OH + H^+ \rightarrow \equiv M\text{-}OH_2^+ \tag{2}$$

and under alkaline conditions,

$$\equiv M\text{-}OH + OH^- \rightarrow \equiv M\text{-}O^- + H_2O \tag{3}$$

There is a pH dependence for the surface charge developed and this is a well-known phenomenon [6]. The condition when the net charge on the particles is zero is called the point of zero charge (PZC) for the suspension. pH at the PZC is denoted at pH_{PZC} [6]. The electrokinetic properties of oxides in aqueous environments can be studied by measuring the zeta potential, which in turn is directly dependent on the surface charge. Around pH_{PZC}, the absolute value of zeta potential is very small and it is zero at pH_{PZC} as a result of the net zero surface charge [6].

The Derjaguin-Landau-Verwey-Overbeek (DLVO) theory of colloidal stability depends on the sum of the repulsive electrostatic forces and the attractive van der Waals forces between the two suspended particles and surfaces [3]. Particle aggregation is determined by the balance between the repulsive electrostatic forces and the attractive van der Waals forces [7,8]. Since the aqueous environment influences the surface charge on the suspended oxide particle, a similar charge is developed on all the suspended particles of a given type in the medium. This may cause a repulsive interaction between the particles. It has been demonstrated that the zeta potential of magnetite particles is positive in acidic pH and is negative in basic solutions [9,5,10-12]. With increasing temperature, the PZC of magnetite drops from around $pH_{25°C} = 7$ to around $pH_{300°C} = 5.5$ [10,13]. This shift in the PZC is also accompanied by a shift in the pH of pure water with increasing temperature [14]. At the PZC, the attractive forces dominate due to a lack of surface charge, hence favoring aggregation and deposition.

The Physicochemical Environment at 300 °C: At Temperature pH & Surface Charge

It has been established that the surface charge generated is influence by the pH. Since the surface characteristics of magnetite are governed by the immediate physicochemical

environment, it is important to consider the solution properties at the operating conditions. In this case, the operating conditions were 300 °C and 100 bar, chosen to closely simulate a boiler like environment. Although boiler water chemistry guidelines are set for target pH at ambient conditions, for understanding the surface charge development on magnetite, one must know the pH at conditions of interest, which in this case are 300 °C and 100 bar. All the high temperature calculations were carried out using OLI Analyzer, a thermodynamic modeling software. The reliability of the software was verified by comparing the results from the OLI Analyzer with calculations made using thermodynamic data from a different source.

The outline of steps for verifying the results from OLI Analyzer with thermodynamic calculations using other sources is shown below for the AVT $pH_{25°C} = 9.3$ case. With the aim being to simulate a boiler type environment, the base used in this case is dissolved ammonia, $NH_3(aq)$, which can also be represented as $NH_4OH(aq)$, ammonium hydroxide. The hydrolysis of ammonia can be written as,

$$NH_3(aq) + H_2O(l) \leftrightarrow NH_4^+(aq) + OH^-(aq) \tag{3}$$

The system also has water ionization occurring as another reaction,

$$H_2O\ (l) \leftrightarrow H^+(aq) + OH^-(aq) \tag{4}$$

In the case of AVT $pH_{25°C} = 9.3$, the total concentration of $NH_3(aq)$ used in preparing the test solution was $4.4\ 10^{-5}$ mol/kg. The species in the system at equilibrium are $NH_3(aq)$, $H^+(aq)$, $OH^-(aq)$, $NH_4^+(aq)$, $H_2O(l)$. The equilibrium speciation at 300 °C and 100 bar was calculated by simultaneously solving the expressions for the thermodynamic hydrolysis constant of ammonia, K_{NH3}, the ionization constant of water, K_{H2O} at 300 °C and 100 bar, the electroneutrality constraint and elemental mass constraints. The standard Gibbs energies of formation from OLI Analyzer [15] were used to calculate K_{NH3} and K_{H2O}. The activity coefficient for all species were calculated using the Debye-Hückel equation and iterative approach [16]. The results of the speciation calculation in the form of concentrations on the molal scale, b, is given in Table 2-1.

Table 2-1 Equilibrium composition, in mol/kg H_2O, at 300 °C, 100 bar

Species	b_i, /[mol/kg]
H^+(aq)	$1.24\ 10^{-6}$
NH_3(aq)	$4.16\ 10^{-5}$
NH_4^+(aq)	$2.42\ 10^{-6}$
OH^-(aq)	$3.67\ 10^{-6}$

The pH of $4.4\ 10^{-5}$ mol/kg ammonia in water at 300 °C, 100 bar, was calculated to be 5.907. The pH was also calculated using K_{NH3} value from SUPCRT92 [17] with K_{H2O} value from IAPWS formulation [14] and different combinations of OLI Analyzer, SUPCRT92 and IAPWS dissociation constant values. The different sources gave a $pH_{300\ °C}$ of 5.91 ± 0.01. This confirms that pH of the dilute ammonia aqueous solution at 300 °C and 100 bar is consistent between thermodynamics data sources with a precision of about ± 0.01 and that OLI Analyzer can be reliably used to calculate the at-temperature pH in other cases.

Figure 2-1 shows how the pH of ammonium hydroxide varies with increasing temperature for the AVT tests. The low dissociation constant of ammonium hydroxide at 300 °C results in the solution having a pH very close to neutral pH (pH of pure water) at 300 °C. The pH values shown in Figure 2-1 were calculated using OLI Analyzer, a thermodynamic modeling software. A pH 9.3 solution of ammonium hydroxide at room temperature has a pH of 5.8 at 300 °C. At 300 °C, the pH_{PZC} of suspended magnetite particles is around 5.7 [10,18]. As the solution pH approaches the pH_{PZC}, the deposition rate has been observed to increase due to the negligible repulsive interactions [8]. The stainless steel, being predominantly iron, in boilers will be covered with a passive magnetite layer and some oxides of chromium [19]. Test data provided by the utilities revealed the orifice plate deposits (fouling product) to be predominantly magnetite. Hence, under these conditions the surface properties and behavior of the substrate can be considered similar to the suspended magnetite. The theory indicates that at 300 °C, boiler water conditioned at a $pH_{25°C} = 9.3$ using ammonium hydroxide (AVT) may favor deposition of suspended iron oxide particles on stainless steel surfaces. Extending this to the other end of the AVT spectrum, when boiler water is conditioned to $pH_{25°C} = 9.8$ using ammonium hydroxide, the pH at 300 °C is away from the point of zero charge of magnetite at 300 °C. The magnetite surface develops negative charges at pH values higher than the point of zero charge. At the higher

end of the AVT range, the magnetite surface is expected to be charged at 300 °C, meaning there would be repulsive interactions in the system. In this case, we would expect less or no deposition to occur.
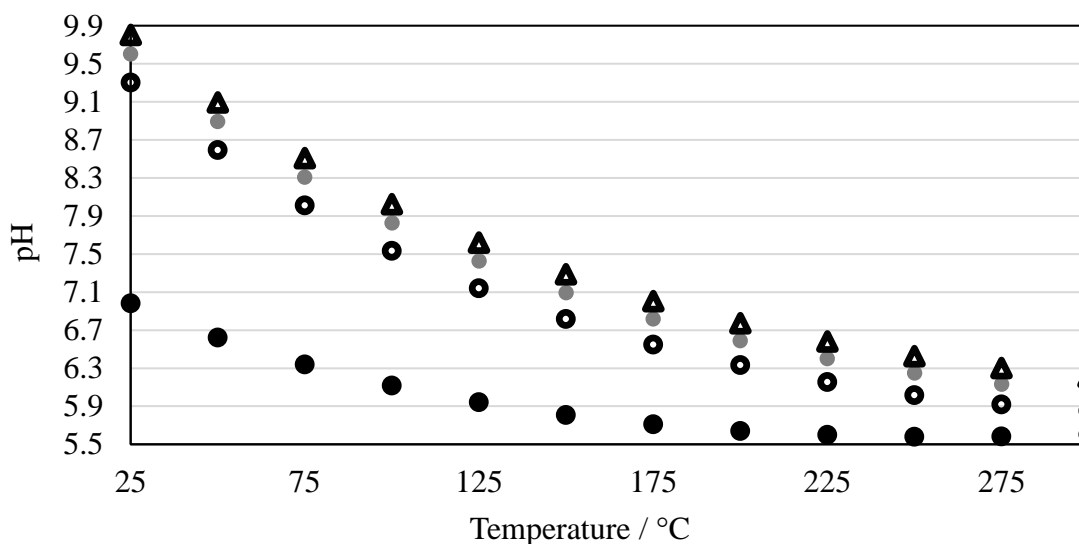
Figure 2-1 Variation of pH with temperature for NH₄OH(aq) and pure water: (●) pure water, (○) NH₄OH(aq) with $pH_{25°C}$ = 9.3, (●) NH₄OH(aq) with $pH_{25°C}$ = 9.6, (Δ) NH₄OH(aq) with $pH_{25°C}$ = 9.8.

In the case of the phosphate treatment, OLI Analyzer's mixed-solvent electrolyte model was used with Gibbs energy minimization method to predict the properties of the boiler water at 300 °C and 100 bar. Mixed-solvent electrolyte model uses standard state thermochemical properties of the solution species with terms to account for the excess Gibbs energy [15]. The pH at 300 °C and 100 bar obtained for the high phosphate case using OLI was comparable to the pH calculated using the HCh Unitherm software, which uses to HKF model [20] and input data from SUPCRT92 [21] to calculate the thermodynamic properties of the aqueous species. This once again verified the reliability of OLI Analyzer in making the high temperature calculations. Figure 2-2 show the pH as a function of temperature for the phosphate treatment tests, $pH_{25 °C}$ = 9.3 NH₄OH(aq) + 0.3 ppm Na₃PO₄(aq) and $pH_{25 °C}$ = 9.3 NH₄OH(aq) + 3 ppm Na₃PO₄(aq).
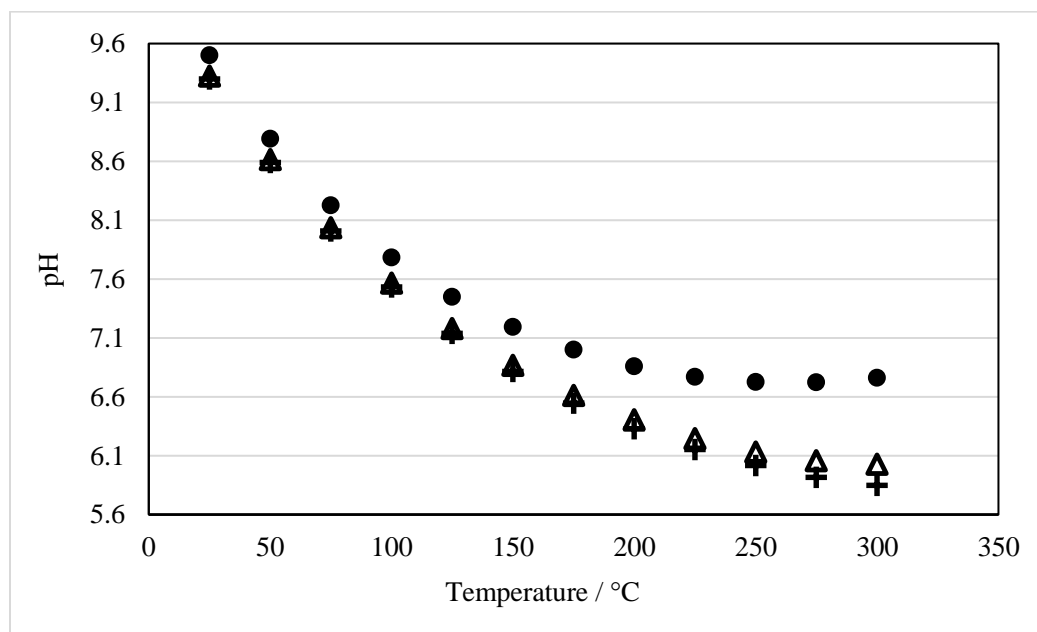
Figure 2-2. Solution pH as a function of temperature for the 2 cases in Phosphate Treatment. (+) $NH_4OH(aq)$ with $pH_{25°C} = 9.3$, (Δ) $pH_{25°C} = 9.3$ $NH_4OH(aq) + 0.3$ ppm $Na_3PO_4(aq)$, ($\bullet$) $pH_{25°C} =$ 9.3 $NH_4OH(aq) + 3$ ppm $Na_3PO_4(aq)$.

When phosphate treatment, both high and low concentration, is employed, the $pH_{300°C}$ is higher than the AVT Low $pH_{300°C}$ and further away from the pH_{PZC} of magnetite at 300 °C, which is between around 5.7. Being away from the pH_{PZC}, one would expect surface charges on the magnetite particles. The presence of similar charges will lead to repulsive interactions and hence will not favor deposition and aggregation.

A similar explanation can be offered for the caustic case. The $pH_{300°C}$ when caustic treatment is employed is higher than the pH_{PZC} of magnetite at 300 °C. NaOH being a stronger base than Na_3PO_4, the $pH_{300°C}$ for the lower concentration caustic is further away from the conventional AVT $pH_{300°C}$. Due to the presence of surface charges, repulsive interactions are expected to occur and prevent any deposition or aggregation.
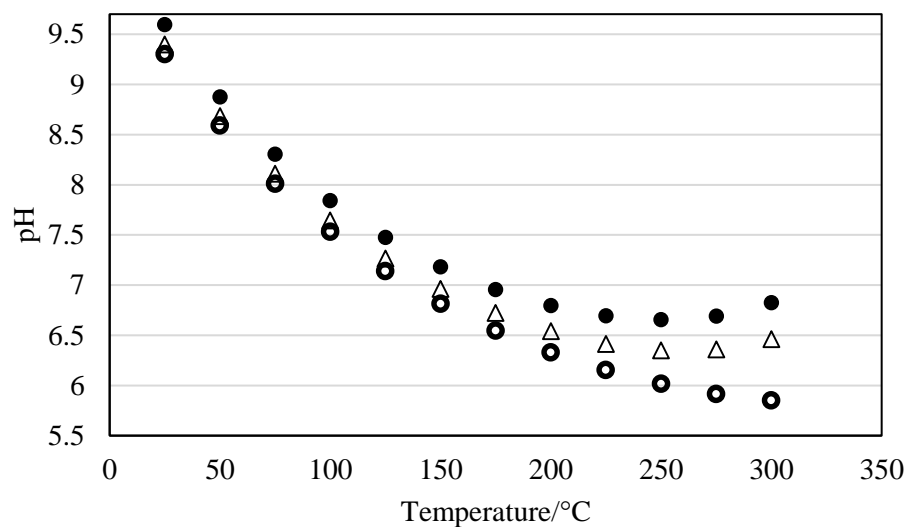
Figure 2-3. Solution pH as a function of temperature for the 2 cases in Caustic Treatment. (○) $NH_4OH(aq)$ with $pH_{25°C} = 9.3$, (Δ) $pH_{25 °C} = 9.3$ $NH_4OH(aq) + 0.5$ ppm $NaOH(aq)$, (●) $pH_{25 °C} = 9.3$ $NH_4OH(aq) + 1.2$ ppm $NaOH(aq)$.

However, in the case of the phosphate and caustic treatments, the ionic strength must also be taken into consideration. Ionic strength can influence inter particle interactions by means of double layer compression or expansion [6]. This adds to the importance of the considering the boiler physicochemical environment for understanding the behavior of suspended magnetite.

If the particle interactions are governed by DLVO theory and surface charges, the immediate physicochemical environment, temperature, pH, ionic strength and ionic equilibria are key parameters. Boiler water chemistry can be broken down in pH and ionic strength and according to this hypothesis, it is potentially possible to control and mitigate deposition by adjusting the physicochemical environment i.e. boiler water chemistry. This however has not been tested. This study serves to demonstrate the hypothesis presented above and introduce a test system capable of studying and understanding the deposition process in harsh environments across a range of aqueous systems.

References

[1] M. Basset,, N. Arbeau,, J. Mclnerney,, D.H. Lister, 3rd Int. Steam Generator and Heat Exchanger Conference, 1998, pp. 677–93.

[2] S.M. Vidojkovic,, M.P. Rakin, Surface properties of magnetite in high temperature aqueous electrolyte solutions: A review., Adv. Colloid Interface Sci. (2016).

[3] R. Oliveira, Understanding adhesion: A means for preventing fouling, Exp. Therm. Fluid Sci. 14 (1997) 316–322. doi:10.1016/S0894-1777(96)00134-3.

[4] C. Turner, M. Godin, Mechanisms of magnetite deposition in pressurized boiling and non-boiling water, Ontario, 1994. http://inis.iaea.org/search/search.aspx?orig_q=RN:27005796 (accessed July 21, 2014).

[5] Z.-X. Sun, F.-W. Su, W. Forsling, P.-O. Samskog, Surface Characteristics of Magnetite in Aqueous Suspension, J. Colloid Interface Sci. 197 (1998) 151–159. doi:10.1006/jcis.1997.5239.

[6] R. Hunter, Foundations of Colloid Science, Oxford University Press, 2001.

[7] O. Malysheva, T. Tang, P. Schiavone, Adhesion between a charged particle in an electrolyte solution and a charged substrate: Electrostatic and van der Waals interactions., J. Colloid Interface Sci. 327 (2008) 251–60. doi:10.1016/j.jcis.2008.07.019.

[8] D.C. Prieve, E. Ruckenstein, Role of surface chemistry in particle deposition, J. Colloid Interface Sci. 60 (1977) 337–348. doi:10.1016/0021-9797(77)90293-4.

[9] M. Erdemoğlu, M. Sarıkaya, Effects of heavy metals and oxalate on the zeta potential of magnetite, J. Colloid Interface Sci. 300 (2006) 795–804. doi:10.1016/j.jcis.2006.04.004.

[10] S. Vidojkovic, V. Rodriguez-Santiago, M. V. Fedkin, D.J. Wesolowski, S.N. Lvov, Electrophoretic mobility of magnetite particles in high temperature water, Chem. Eng. Sci. 66 (2011) 4029–4035. doi:10.1016/j.ces.2011.05.021.

[11] M.A. Blesa, N.M. Figliolia, A.J.. Maroto, A.E. Regazzoni, The influence of temperature on the interface magnetite—aqueous electrolyte solution, J. Colloid Interface Sci. 101 (1984) 410–418. doi:10.1016/0021-9797(84)90052-3.

[12] A.E. Regazzoni, M.A. Blesa, A.J.. Maroto, Interfacial properties of zirconium dioxide and magnetite in water, J. Colloid Interface Sci. 91 (1983) 560–570. doi:10.1016/0021-9797(83)90370-3.

[13] D.J. Wesolowski, M.L. Machesky, D.A. Palmer, L.M. Anovitz, Magnetite surface charge studies to 290°C from in situ pH titrations, Chem. Geol. 167 (2000) 193–229. doi:10.1016/S0009-2541(99)00209-0.

[14] A. V. Bandura, S.N. Lvov, The Ionization Constant of Water over Wide Ranges of Temperature and Density, J. Phys. Chem. Ref. Data. 35 (2006) 15. doi:10.1063/1.1928231.

[15] OLI Systems, OLI Analyzer, (2014).

[16] J.N. Butler, Ionic equilibrium: a mathematical approach, Addison-Wesley Reading, MA, 1964.

[17] G.M. Anderson, How to use SUPCRT92, in: Thermodyn. Nat. Syst., Cambridge University Press, 2009: pp. 601–604.

[18] R. Fernandez-Prini, A.H. Harvey, D.A. Palmer, Aqueous systems at elevated temperatures and pressures: Physical chemistry in water, steam and hydrothermal solutions, Academic Press, 2004.

[19] B. Buecker, Power Plant Water Chemistry: A Practical Guide, PennWell Publishing Company, 1997.

[20] H.C. Helgeson,, D.H. Kirkham,, G.C. Flowers, Am. J. Sci. 281(10) (1981) 1249–516.

[21] J.W. Johnson,, E.H. Oelkers,, H.C. Helgeson, Comput. Geosci. 18(7) (1992) 899–947. 10.1016/0098-3004(92)90029-Q.

Chapter 3

Experimental Setup and Methods

A schematic of the experimental setup used is shown in Figure 3-1. The electrophoretic deposition cell comprised of a high temperature-high pressure electrochemical cell to simulate the boiler environment with inlet/outlet tubing system designed to pump the synthetic boiler water. A 650 mL Parr 4560 Mini Bench Top reactor with a built-in controller for temperature and stir rate, served as the electrophoretic deposition cell. A boiler type test environment of 300 °C and 10 MPa was simulated inside of this autoclave vessel. The test solution was prepared in an Argon environment inside of a glove bag. De-ionized (DI) water, with resistivity of 18.2 MΩ cm (Milli-Q water) measured at 25 °C, was first de-aerated by bubbling with Argon. The concentration of dissolved oxygen (DO) was monitored with the Oakton DO 6+ dissolved oxygen meter with a resolution of 10 ppb. Following the industry standards for de-aeration, sparging of the DI water was continued until the DO level was below 10 ppb. Dissolved oxygen kits from CHEMetrics were also used to verify the oxygen concentration. A ChromTech Series III HPLC pump was used to pump the test solution into the autoclave at room temperature. 316 SS tubing was used to provide the inlet and outlet for the solution. A dip tube was used as an outlet from the autoclave to withdraw any samples. This dip tube was connected to a pressure relief value via a cooling loop. The system pressure was maintained at 10 MPa using the pressure relief valve. The system design allows for safe control of the pressure. At the end of the test, the pressure relief valve can be opened, drawing the test solution out for sampling and to bring the deposition cell back to ambient pressure.
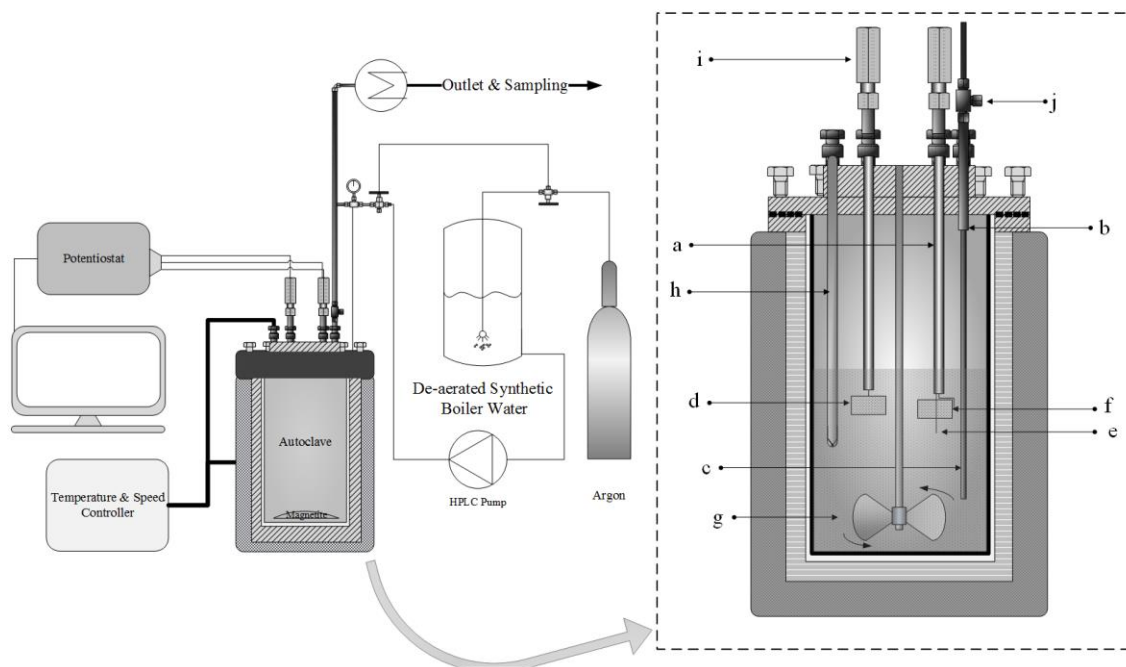
Figure 3-1 Schematic of the experimental system illustrating the electrode assembly inside the autoclave: (a) alumina ceramic tube to isolate the leads, (b) ¼ inch 316 SS inlet tube, (c) 1/8 inch 316 SS dip tube-outlet, (d) 304 SS working electrode/substrate, (e) platinum quasi-reference electrode, (f) large area 304 SS counter electrode, (g) stirrer to maintain suspension inside the autoclave, (h) Inconel thermocouple sheath housing the thermocouple, (i) Conax® high pressure sealing gland, (j) inlet into the autoclave.

To carry out *in situ* electrochemical measurements a three electrode assembly was designed. The inset in Figure 3-1 illustrates in detail the electrode assembly. The working electrode was the material of interest (substrate), which was a 304 SS coupon. A similar coupon served as the counter electrode and a platinum wire was used as a quasi-reference electrode. The stainless steel electrodes were machine cut from a large 304 SS sheet to dimensions of 1.27 cm by 2.54 cm. The commercially obtained 304 SS sheet was pre-polished to a mirror finish with a protective cover to preserve the finish. This cover was not removed until before the experiments. 304 SS wire was welded on to the edges of the coupons to serve as the leads. Soldering was avoided as the commonly used solders melt at temperatures less than 300 °C. Before the experiments, the protective cover was removed and the coupon surface was roughened with P60 grade sandpaper. The coupons were then sonicated for around 20 minutes in iso-propyl alcohol followed by another round of sonication in de-ionized water.

Hollow ceramic tubes (alumina) were used to electrically isolate the leads inside the autoclave. The ceramic tube was filled with Cotronics Resbond™ 919 adhesive to hold the leads

in place inside the tube. The leads were run through 316 SS tubing via a Conax® high pressure
sealing gland. Outside the autoclave, the leads were insulated by sheathing them with shrinkable
PTFE tubing. The tubing around the sealing glands were continuously cooled to prevent any
PTFE decomposition.

Commercial magnetite (50-100 nm, 97% Trace metals basis, Sigma Aldrich) was used in
this study. In actual boiler units, the deposition of magnetite occurs over an extended duration. To
accelerate the deposition process, a set amount of magnetite, 0.2 grams, was added to the
autoclave before sealing the vessel. The commercially obtained magnetite was characterized
using FESEM. Figure 3-2 is an FESEM image of the commercially obtained magnetite at a
magnification of 10000x. All the particles are uniform in shape and appearance. A higher
magnification (50000x), Figure 3-3 clearly shows octahedral shaped particles, a feature attributed
to magnetite. An EDS map of the samples did not show the presence of any element other than
iron or oxygen.

Although the oxide deposits observed in utility scale boilers are typically mixed oxides
along with other precipitates, this study primarily focuses on the deposition of magnetite. The
FESEM images and EDS spectra confirm that the nanoparticles used in the study are magnetite
and lack any significant impurities.
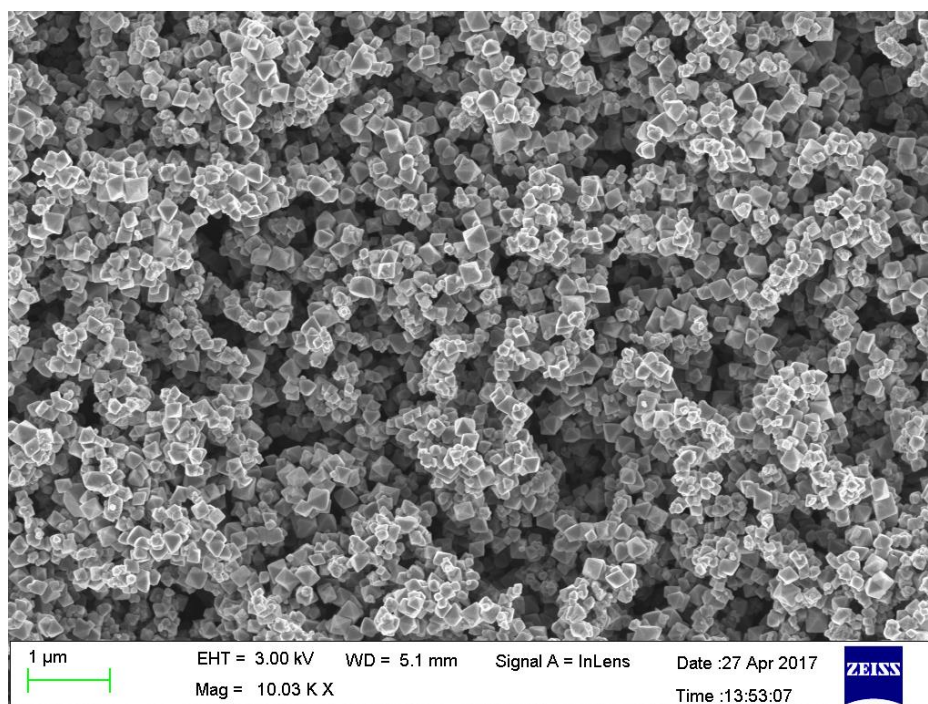
Figure 3-2 FESEM image of commercially obtained magnetite nanoparticles. The uniform shape of the particles indicates lack of significant amounts of impurities.
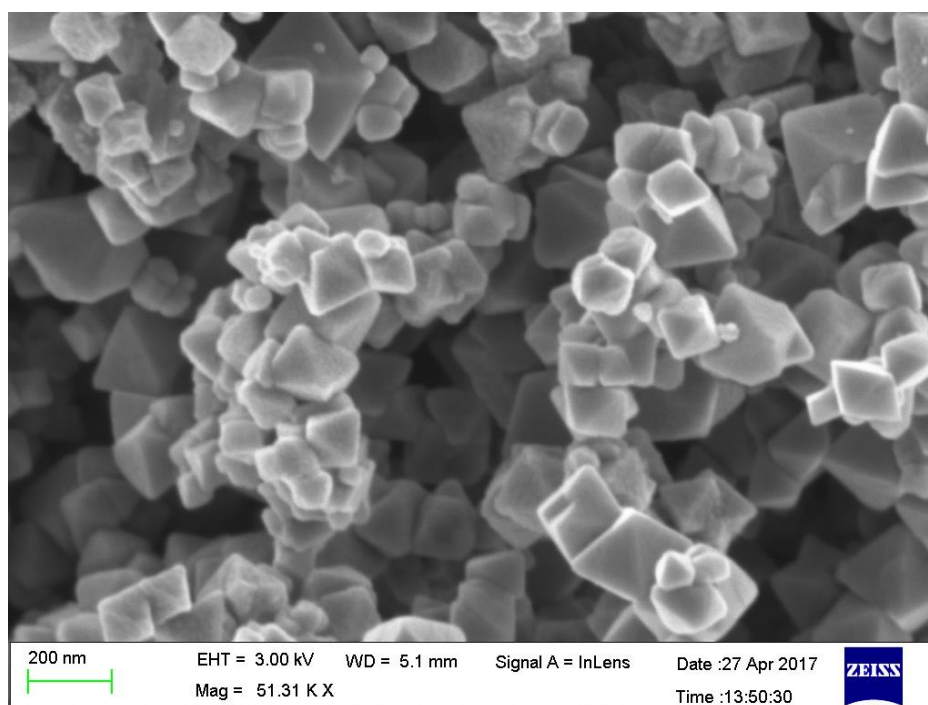
Figure 3-3 FESEM image of magnetite nanoparticles at higher magnification (51000x). The particles exhibit the octahedral shape attributed to magnetite.

The autoclave vessel came fitted with a stirrer, which helped keep the magnetite particles in suspension in the synthetic boiler water over the duration of the test. The stirrer setting was kept between 300- 350 rpm across all the tests. The commercial magnetite was assumed to behave in the same manner as the magnetite particles found in boilers. However, in an actual boiler, the morphology and the purity of the oxide deposits could be different and can be tested in the system if a sample is provided. The autoclave was sealed and pressurized up to around 1 MPa using argon and the test solution was then pumped into the autoclave until a pressure of 9 MPa was established. The temperature was then ramped up in steps of 50 °C until the system temperature reached 300 °C. So, the argon acted like a piston during the temperature ramp up, pushing some excess solution out and maintaining a gas phase above the aqueous one. The pressure relief valve was adjusted so that the system pressure during the temperature ramp up was always 10 MPa. Three tests were carried out at $pH_{25°C} = 9.3$ with the suspended magnetite particles and a fourth control experiment was carried out at the same pH but without the addition magnetite. The duration of each test was 65 hours.

The potentiostat used for EIS measurements was a Gamry Instruments Reference 3000 Potentiostat/Galvanostat/ZRA. An ac perturbation potential of 10 mV around the measured open circuit potential (OCP) was used in making the impedance measurements. Measurements were made between 0.1 Hz to 100 kHz with 5 points of measurement per decade. All the post-test analyses were performed ex-situ at ambient conditions. A Malvern Zetasizer was used to measure the particle size after exposure at 300 C. Surface analyses of the stainless steel samples were carried out at Materials Research Institute of the Pennsylvania State University. Scanning Electron Microscope (SEM) images were obtained using FEI ESEM Quanta 200. Energy Dispersive Spectroscopy analyses were carried out using Aztec EDS by Oxford Instruments. Between the exposure tests and the surface analyses, the samples were stored in closed storage containers in a desiccator, which was flushed with Argon. These precautions were taken in order to minimize exposure of the sample surface to air.

Chapter 4

Results

Preface to Chapter 4

The following chapter presents the results of the research study. The results are categorized in sub-sections based on the specific test condition i.e. boiler water chemistry studied. For each test, the results and observations were corroborated by three techniques: (i) visual observations, (ii) surface analysis and (iii) EIS results. Each sub-section presents the results of the: (i) visual observations, (ii) surface analysis and (iii) EIS for the boiler water chemistry studied.

Table 4-1 Summary of deposition results for different the different test conditions.

Test Condition	Sample	$pH_{300°C}$	$I_{300°C}$ [μmol/kg]	Deposition
AVT $pH_{25°C}$ 9.3	AVT-1	5.8	3.66	High
AVT $pH_{25°C}$ 9.8	AVT-2	6.2	10.02	Negligible
AVT + high Na_3PO_4	PT-1	6.8	54.84	Moderate
AVT + low Na_3PO_4	PT-2	6.0	14.61	Negligible
AVT + high NaOH	CT-1	6.7	32.80	Moderate
AVT + low NaOH	CT-2	6.4	8.53	Negligible
AVT + 30 ppb N_2H_4	AVTH-1	5.89	3.72	High
AVT + 90 ppb N_2H_4	AVTH-2	5.91	3.83	High
HRSG-02 2.5 ppm	FFA-1	5.81*		Moderate
HRSG-02 5.0 ppm	FFA-1	5.91*		Moderate
AVT $pH_{25°C}$ 9.3 Increased Particle Size	AVTPS	5.8	3.66	Low

Approximate model developed accounting only for neutralizing amines in the amine blend. Film forming amines were excluded for pH calculation.

All-Volatile Treatment

AVT: Visual Observations

Figure 4-1 shows the stainless-steel coupons tested at $pH_{25°C} = 9.3$ with suspended magnetite (deposition susceptibility test on the left) and without suspended magnetite (control; on the right). A clear difference can be seen between the visual appearances of the specimens collected from tests with and without magnetite. When magnetite was added to the system, the stainless-steel coupons were coated with black non-dense coatings that were friable. However, in the case of the control samples, no visible deposits were found on the surface.
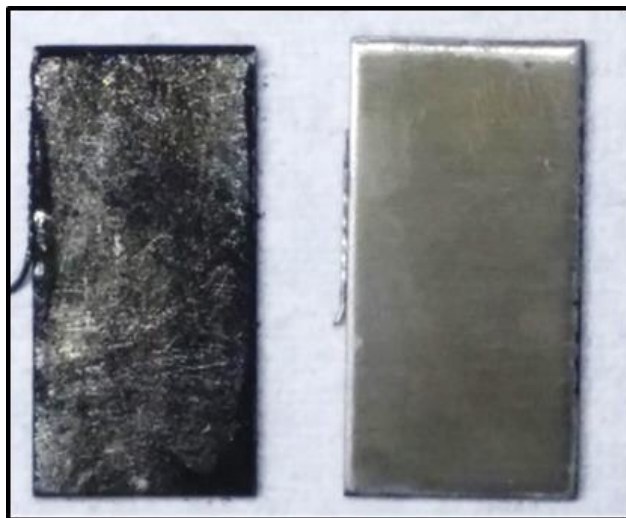
Figure 4-1. Samples subjected to testing at $pH_{25°C} = 9.3$: AVT-1 with magnetite (left), AVT-1C without magnetite (right). Exposure time = 65 hours. Temperature 300 °C. AVT-1 showed good surface coverage with black colored particles whereas AVT-C showed lack of any surface coverage.

Figure 4-2 contains images of the stainless-steel samples exposed to tests conditions with AVT $pH_{25°C}$ 9.8 with (AVT-2) and without magnetite (AVT-2C). In contrast to sample AVT-1, sample AVT-2 does not show any readily observable deposits. Similarly, the control experiment with sample AVT-2C did not show any visible signs of deposits on the surface. The slight tint on the surface in the image below was due to a minor reflection in lighting.
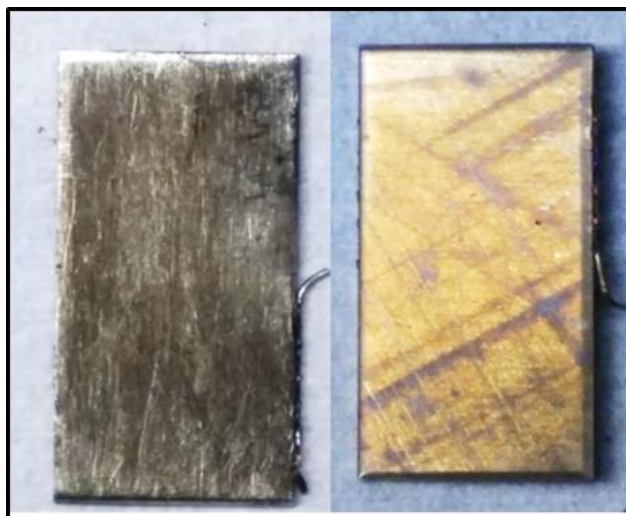
Figure 4-2. Samples subjected to testing at $pH_{25°C} = 9.8$. Sample AVT-2 with magnetite (left), Sample AVT-2C without magnetite (right). Exposure time = 65 hours. Temperature 300 °C. Neither sample showed any significant surface coverage.

In all the AVT cases, control experiments, with sample AVT-1C and AVT-2C, were carried out without magnetite in the system and in each of the control tests run no surface coloration was observed in any of the samples. The control test results supported the conclusion that the deposits observed were only due to the suspended magnetite attaching to the surface and not the formation of magnetite during the exposure time.

AVT: Microscopy & Surface Analysis

Conclusions made from visual observation comparisons between the upper and lower pH AVT conditions were corroborated using surface analysis. Secondary electron (SEM) and back-scattered electron (BSE) images of the samples were used to identify the presence of deposits on collected steel samples. Figure 4-3 is the SEM image of sample AVT-1 with magnetite deposits on the surface.

HV	Mag	WD	Spot	HFW	Sig	Pressure	⊢————50.0µm————⊣
20.0 kV	1916x	10.5 mm	4.0	0.14 mm	SE	---	
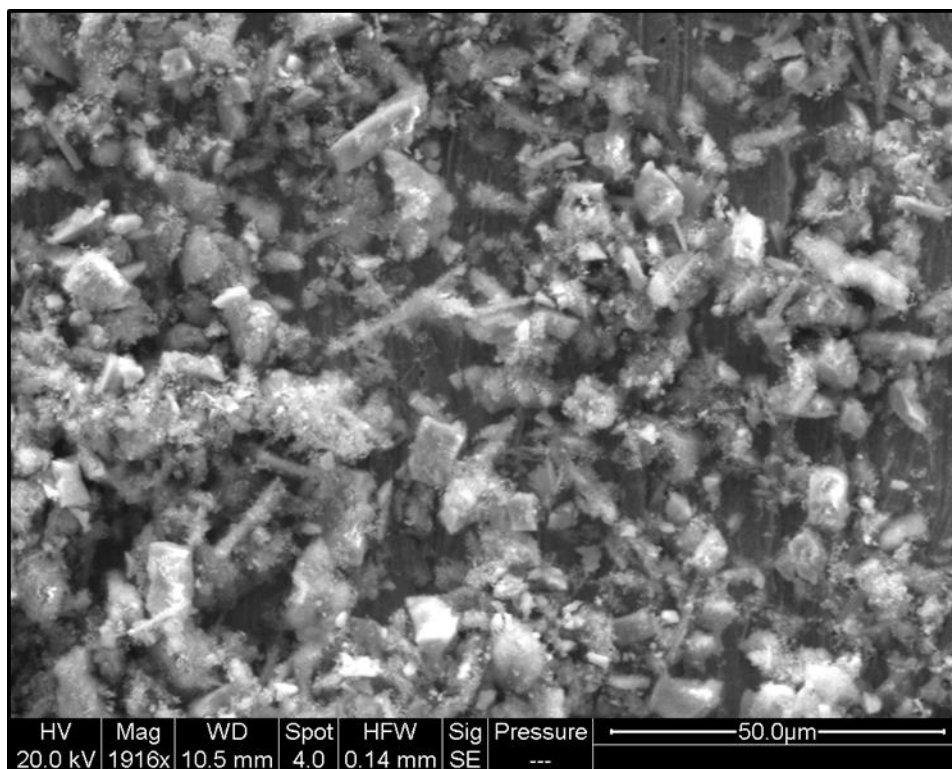
Figure 4-3. Secondary Electron Image (1900x) of sample AVT-1 showing deposits partially covering the surface. Test solution is $pH_{25\ °C}$ = 9.3 $NH_4OH(aq)$ with magnetite. Exposure time = 65 hours. Temperature 300 °C. Magnetite particles can be seen on the surface along with the cement particles (ZrO and MgO). The cement was used as a part of the electrode assembly.

For comparison, Figure 4-4 shows the SEM image of the surface of sample AVT-1C, from the control experiment (without magnetite). The surface was relatively clearer except for a few glowing specks. The glow was indicative of charge accumulation which occurred when nonconductive substances were imaged. In this instance, the glowing specks were attributed to trace amounts of the ceramic particles used inside the alumina tube. Specks like these were also observed on the surface of the sample with the magnetite deposit but less easily spotted due to the heavy deposits of the iron oxide.
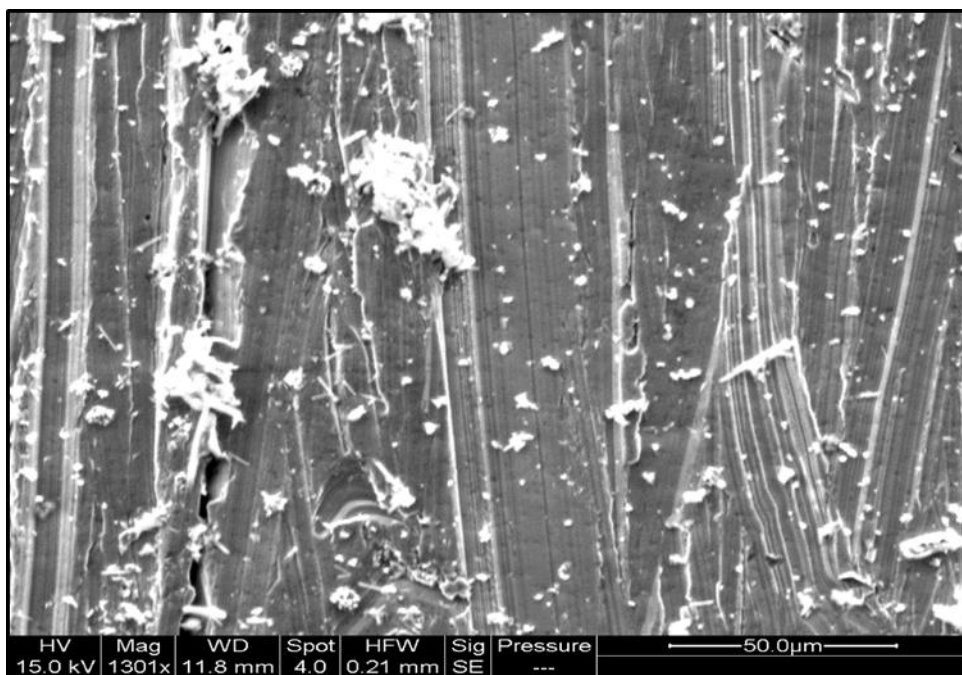
Figure 4-4. Secondary Electron Image (1300x) of sample AVT-1C from the control experiment. Test solution is $pH_{25\,°C} = 9.3$ NH$_4$OH(aq) without magnetite. Exposure time = 65 hours. Temperature 300 °C. ZrO and MgO (from the cement) particles can be seen on the surface, but there is a lack of magnetite particles on the surface.

To better assess the thickness of the deposits, a cross sectional SEM and BSE images of sample AVT-1 were obtained. The sample AVT-1 was embedded in epoxy and was imaged along one of the edges of the steel coupon. A deposit on the substrate can be clearly seen in Figure 4-5 and Figure 4-6. These images indicated the presence of a deposit on the surface of the sample. There appears to a thin, tightly bound inner layer above which is a second layer of deposit. The SEM images do not indicate any morphological differences between the two layers. However, there also appears to be a third outermost layer, which consists of large particles deposited on top of the middle layer. This could be an indication that there is agglomeration of magnetite in the bulk solution as well as deposition of magnetite on the substrate.
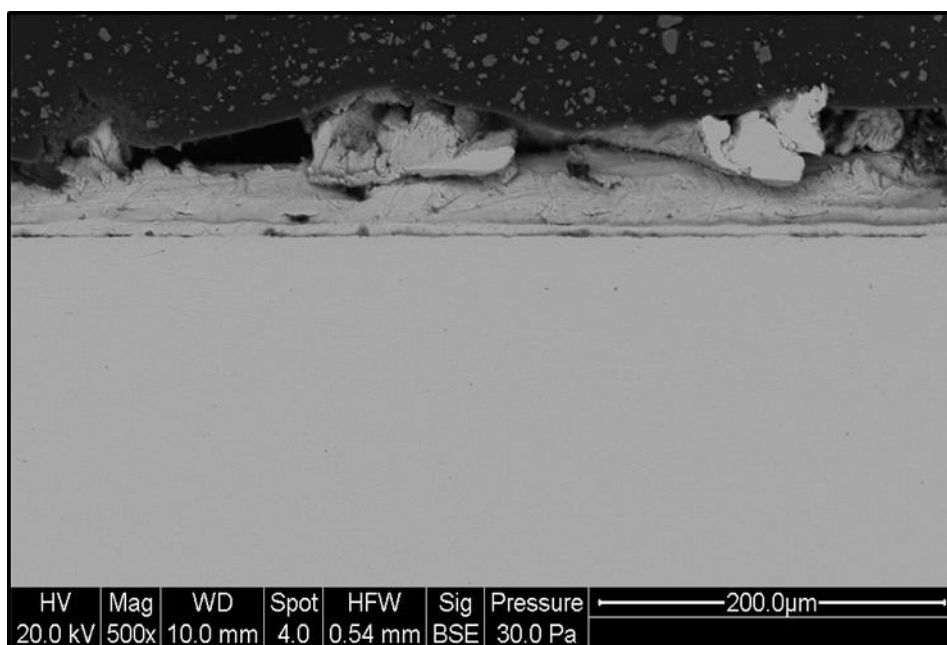
Figure 4-5. Back Scattered Electron Image (500x) showing layers of deposition on sample AVT-1. Test solution is $pH_{25\,°C} = 9.3$ $NH_4OH(aq)$ with magnetite. Exposure time = 65 hours. Temperature 300 °C.
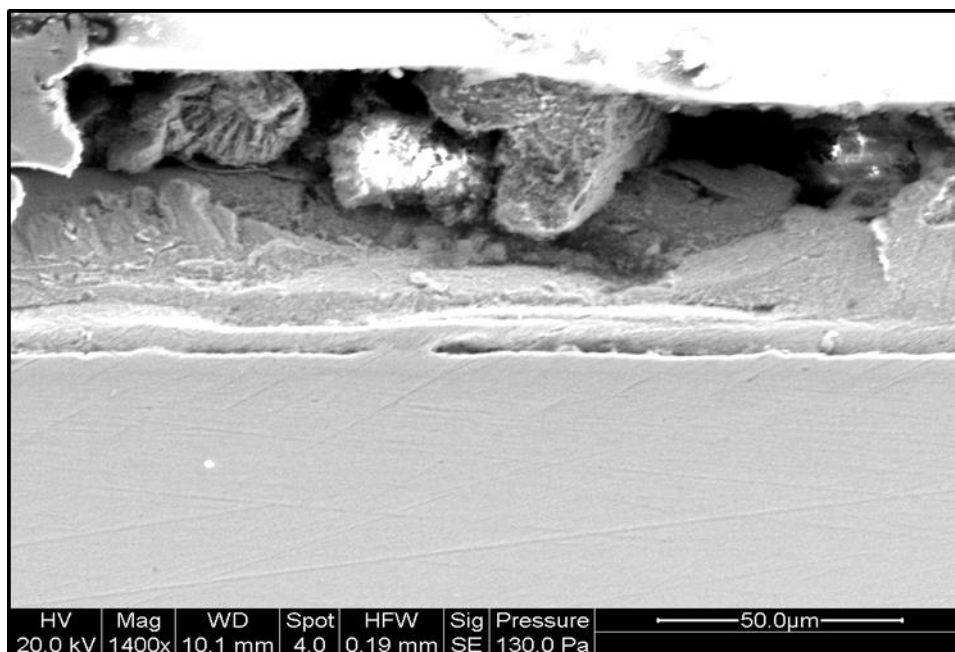
Figure 4-6. Secondary Electron Image (1400x) indicating crystalline deposits on sample AVT-1. Test solution is $pH_{25\,°C} = 9.3$ $NH_4OH(aq)$ with magnetite. Exposure time = 65 hours. Temperature 300 °C.

Energy Dispersive Spectroscopy (EDS) was used to qualitatively determine the elemental composition of the surface. EDS analyses of the deposits from the cross-sectional images of the samples (Figure 4-6) indicated that the deposit was primarily composed of iron and oxygen elements, suggestive of an iron oxide deposit. The presence of iron and oxygen was consistently observed throughout the deposit. Figure 4-7 is the elemental spectrum of the EDS analysis of a region on the deposit. The high quantities of Fe and O indicates that the deposit is primarily an iron oxide. The multiple small peaks, typically attributed to calcium and phosphorus observed could be stray signals picked up from any impurities in the ceramic adhesive or the epoxy used in preparing the cross-sectional sample.
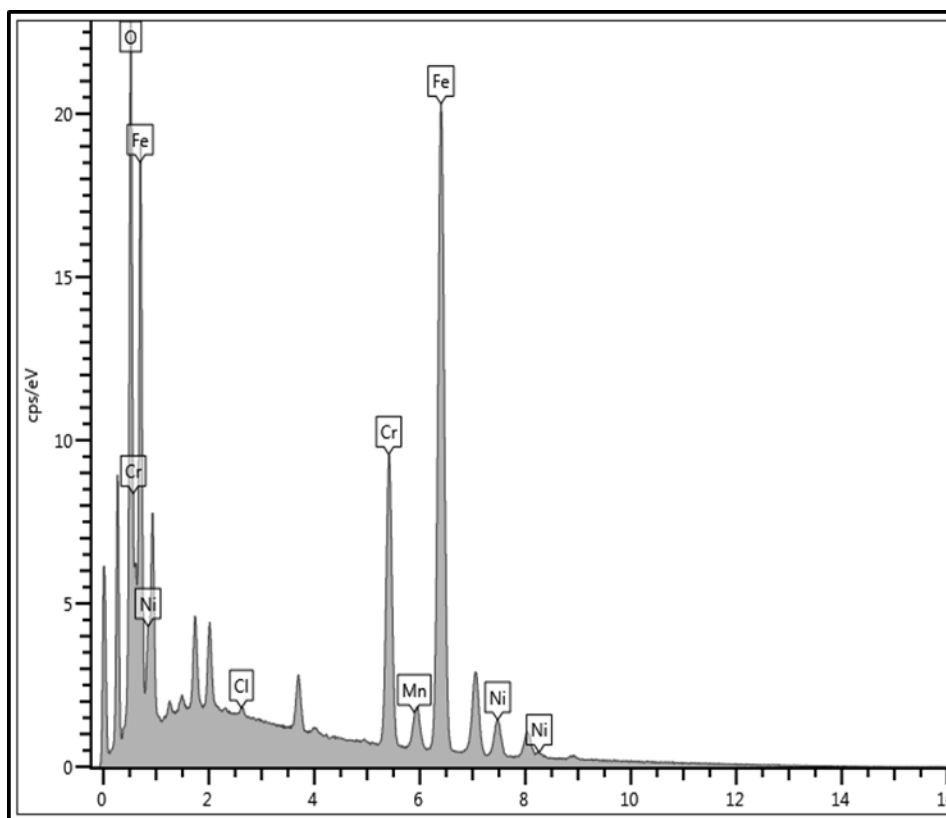
Figure 4-7. EDS elemental spectrum of the deposit on sample AVT-1 from the cross-sectional image shown that deposit is predominantly iron oxide. Test solution is $pH_{25\ °C} = 9.3$ $NH_4OH(aq)$ with magnetite.

Furthermore, neither the substrate (stainless steel) nor the epoxy had an oxygen peak in their EDS spectrum. In the case of the control experiment, the white specs showed high content of Mg, Zr and O, further indicating the ceramic used in the electrode assembly was contributing

small amounts of material. The other regions of the surface had Fe and Cr (from stainless steel) as dominant elements but significant amounts of oxygen were not detected.

Figure 4-8 shows the back scattered image of sample AVT-2 tested at $pH_{25°C} = 9.8$ and there are some particles on the surface of the steel. As it can be seen, the deposits were scattered all over unlike the surface images from the samples tested at $pH_{25°C} = 9.3$. The control case at $pH_{25°C} = 9.8$ was examined as well to see the possible source for the discoloration. Figure 4-9 shows the SEM image of the sample at 10000x. It can be seen that the surface is very clean indicating that there are no foreign particles on the surface.
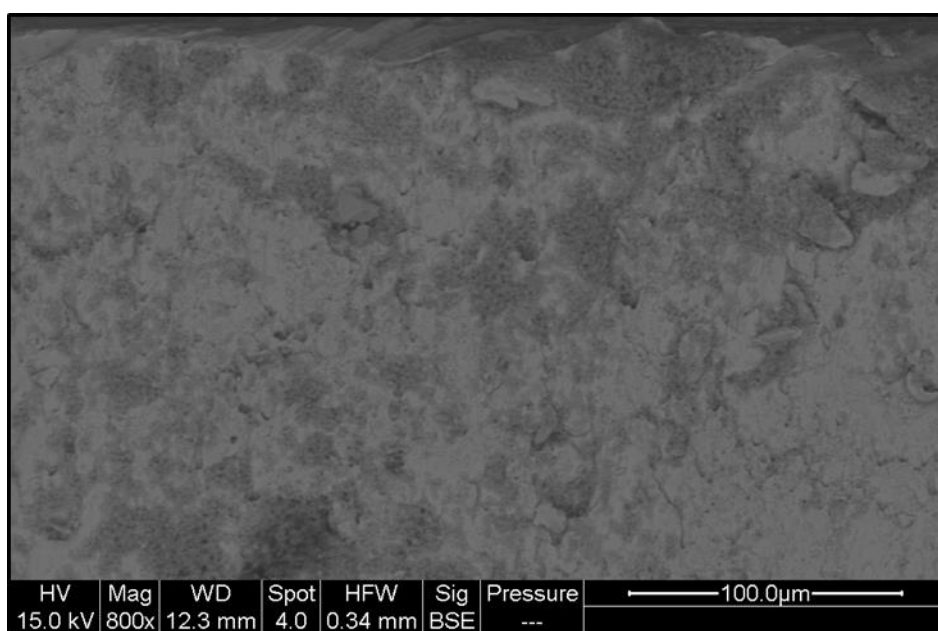
Figure 4-8. Secondary Electron Image (800x) showing poor surface coverage on sample AVT-2. Test solution is $pH_{25 °C} = 9.8$ NH_4OH(aq) with magnetite. Exposure time = 65 hours. Temperature 300 °C.
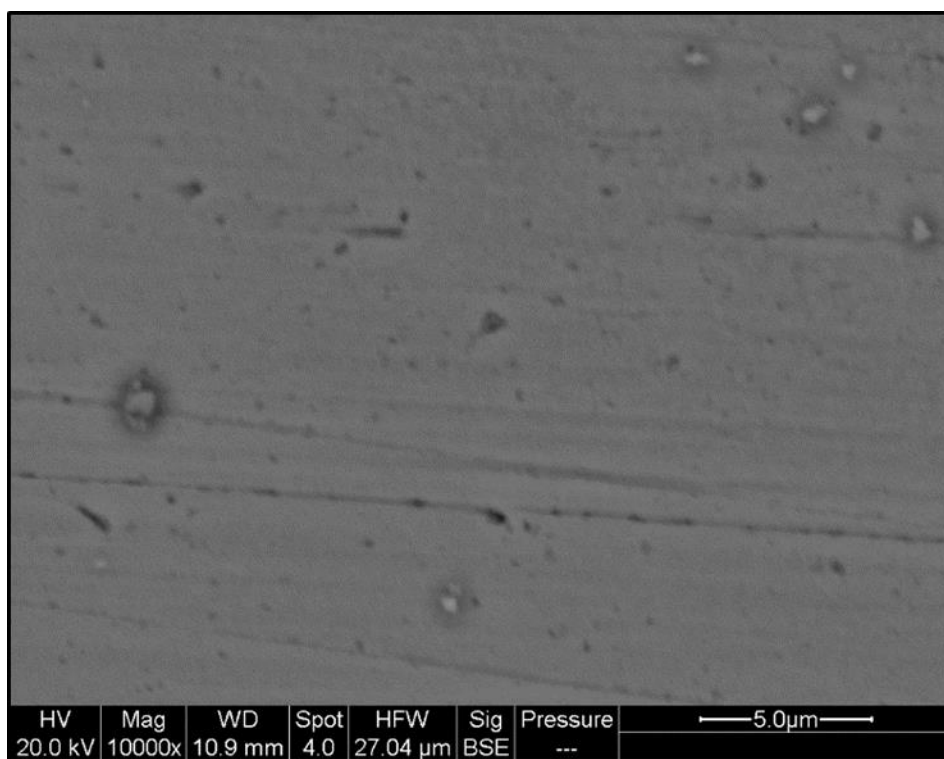
Figure 4-9. Secondary Electron Image (10000x) showing poor surface coverage on sample AVT-2C. Test solution is $pH_{25\,°C} = 9.8$ NH$_4$OH(aq) without magnetite. Exposure time = 65 hours. Temperature 300 °C.

The EDS analyses of sample AVT-2 tested at $pH_{25°C} = 9.8$ with magnetite indicate the presence of oxygen the particulates on the surface. However, the spectra, shown in Figure 4-10 also indicate the presence of iron, zirconium and magnesium. The significant elements on the deposit particles being iron, chromium, magnesium (peak between nickel and aluminum) and oxygen. The oxide contribution is from both the magnetite and the ceramic adhesive used in the electrode assembly. The surface image however, showed that any particles present are sparsely deposited on the surface.
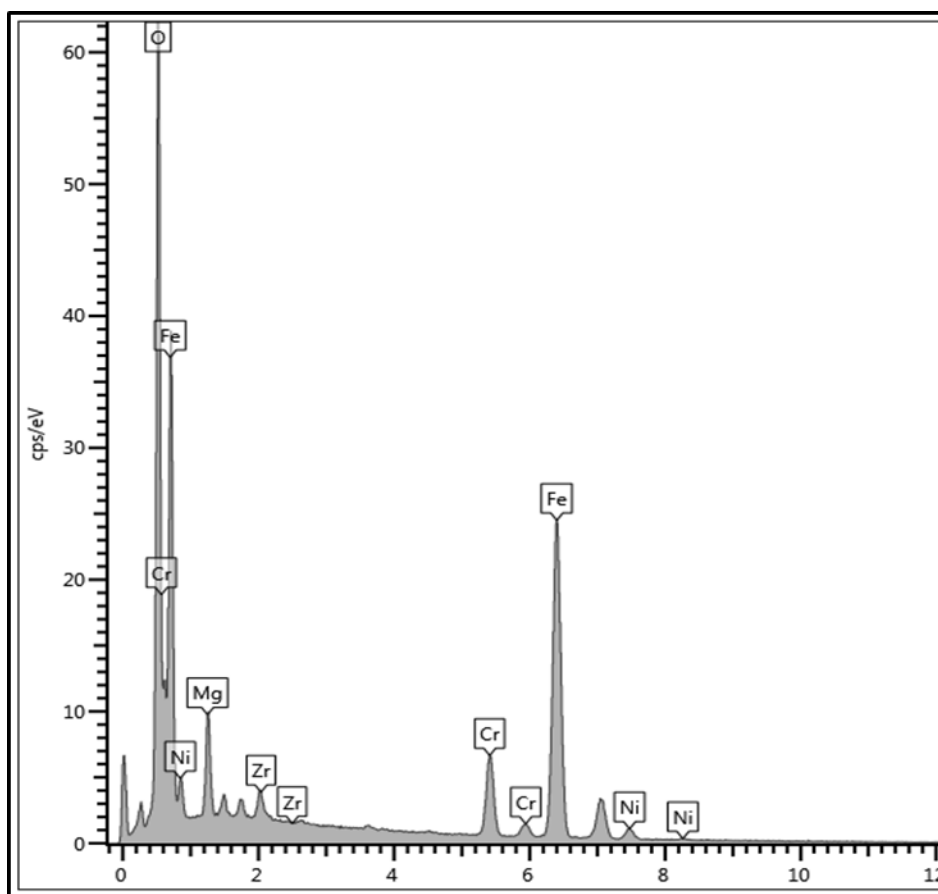
Figure 4-10. EDS spectrum of sample AVT-2 tested at $pH_{25°C} = 9.8$ indicating that the sparsely deposited particles on the surface are magnetite (iron oxides) and the ceramic adhesive (oxides of magnesium and zirconium).

AVT: EIS Results

EIS was carried out to monitor the impedance of the surface during the deposition process. In theory, the deposit, by causing a change in the metal-solution interface should alter the impedance of the system from a reference impedance of the metal–solution interface without deposits. As such, EIS was considered for monitoring the deposition process in-situ. Figure 4-11 shows the daily change in the impedance, in the form of a Bode plot, for sample AVT-1. Bode plot is one way of representing impedance data, where the magnitude of the impedance is plotted against the frequency[1]. Each impedance value is the impedance of system in the time frame for

---

[1] See Appendix for an overview of EIS.

which the potential perturbation is applied. At high frequencies when the time period is very short, only the quickest processes (mostly non-faradaic processes like double layer charging) contribute to the impedance. At lower frequencies, the signal is held for a longer time, giving sufficient time for processes like electrochemical reactions and diffusion to contribute to the impedance response. It should be noted that Bode plots are a cumulative in nature and hence, each value of impedance includes the processes occurring until that point. Therefore, the lowest frequencies include all the processes occurring at the interface and can be considered as the total impedance of the system.

It can be seen in Figure 4-11 that the impedance increased from Day 1 to Day 2 and dropped down to a constant value. For the control experiment, sample AVT-1C, Figure 4-12, the impedance modulus did not show any significant changes over the duration of the test when compared to the changes of the magnetite tests.
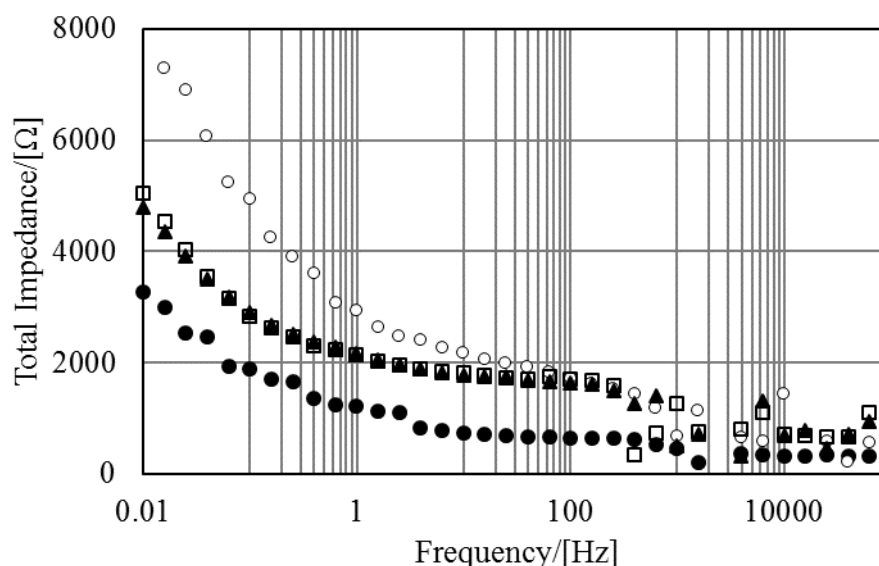
Figure 4-11. Modulus of total impedance as a function of frequency (Bode plot) over the duration of the test. Working Electrode: Sample AVT-1. Test solution of $pH_{25\,°C} = 9.3$ $NH_4OH(aq)$ with magnetite. [●] Day 1, [○] Day 2, [□] Day 3, [▲] Day 4.
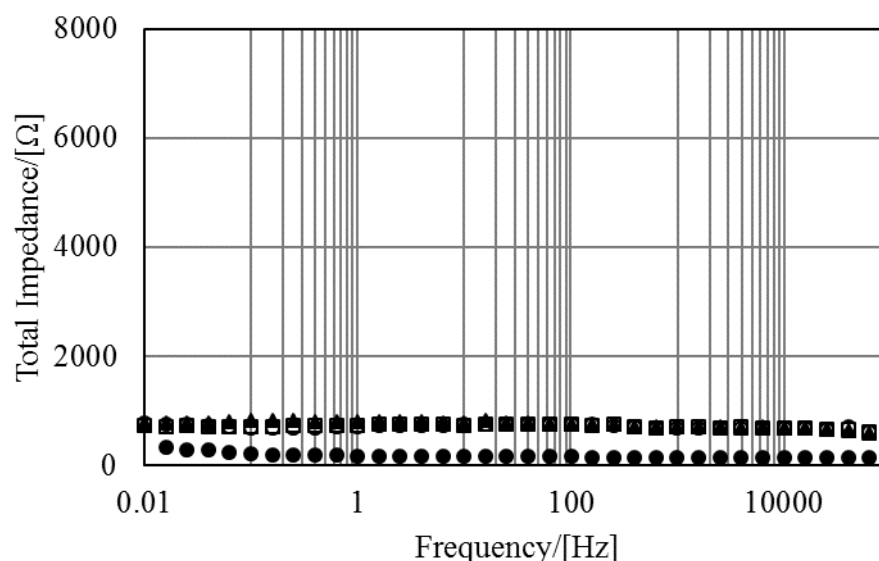
Figure 4-12. Modulus of total impedance as a function of frequency (Bode plot) over the duration of the test. Working Electrode: Sample AVT-C. Test solution of $pH_{25\,°C} = 9.3$ NH$_4$OH(aq) without magnetite. [●] Day 1, [○] Day 2, [□] Day 3, [▲] Day 4.

In contrast, the impedance measurements for sample AVT-2, tested at the high pH i.e. $pH_{25\,°C} = 9.8$ NH$_4$OH(aq), did not change much over the duration of the test regardless of whether magnetite was present or not. Figure 4-13 and Figure 4-14 show the Bode plots over time for the tests at $pH_{25\,°C} = 9.8$ NH$_4$OH(aq) with and without magnetite respectively.
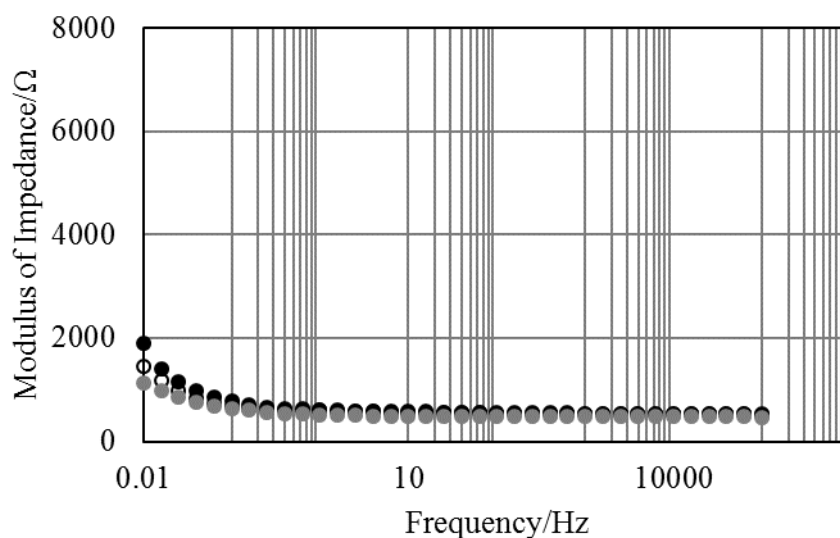
Figure 4-13. Bode plot showing the modulus of impedance as a function of frequency over the duration of the test. Working Electrode: Sample AVT-2. Test solution of $pH_{25\,°C} = 9.8$ NH$_4$OH(aq)with magnetite [●] Day 1, [○] Day 2, [●] Day 3
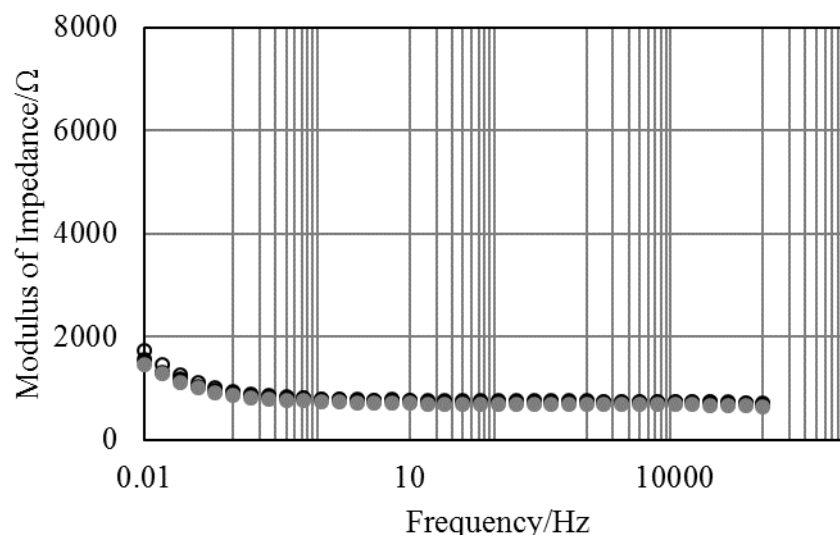
Figure 4-14. Bode plot showing the modulus of impedance as a function of frequency over the duration of the test. Working Electrode: Sample AVT-2C. Test solution of $pH_{25\ °C} = 9.8$ NH$_4$OH(aq)without magnetite [●] Day 1, [○] Day 2, [●] Day 3

The Bode plot has been plotted in the same scale as the $pH_{25\ °C} = 9.3$ case in order to better illustrate the contrast between observed impedances. Correlating with the visual observation, the impedance response in this case is similar to the control case for $pH_{25\ °C} = 9.3$, where no deposition was observed.

Caustic Treatment

The test solution in the low caustic case (0.5 ppm NaOH) has a $pH_{25°C} = 9.45$ and the high caustic case (1.2 ppm NaOH) has a $pH_{25°C} = 9.62$. At 300 ⁰C (572 ⁰F) and 100 bar, the pH values are 6.4 and 6.7 respectively for the low caustic and high caustic case.

Caustic Treatment: Visual Observations

In the case with low caustic concentrations, sample CT-2, no observable deposits were noticed on the surface of the sample. Closer examination of the low caustic sample revealed small quantities of magnetite on the surface. However, samples tested with the higher concentration of

caustic, sample CT-1, had black deposits on the surface. Although, the contrast is not as clear as the AVT case, the difference is visually observable between the samples. Figure 4-15 shows the stainless-steel samples, CT-1 and CT-2, tested at the caustic conditions.

Figure 4-15. Stainless steel samples post testing under caustic treatment. On the left: Sample CT-2 Test solution: $pH_{25°C}$ = 9.3 using NH_4OH + 0.5 ppm NaOH. On the right: Sample CT-1 Test solution: $pH_{25°C}$ = 9.3 using NH_4OH + 1.2 ppm NaOH. Exposure time = 65 hours. Temperature 300 °C.

Similar to the explanation for the reduced deposits at the high pH AVT test, the low caustic conditions had a predicted at temperature pH of 6.4, which is considerably higher than the pH_{IEP} of magnetite, which at 300°C is around 5.7. The low caustic condition pH is significantly higher than the pH of pure water at 300 °C, 5.66, and at-temperature pH for the lower end of the AVT tests, which is 5.8. Still, another important aspect of the zeta potential is that its magnitude depends on the ionic strength of the test solution. As the ionic strength of a solution increases, the electric double layer is compressed, which decreases the magnitude of the zeta potential. Results from the high caustic condition may indicate that the significantly increased ionic strength of the solution is mitigating the benefit of increasing the pH away from the pH_{IEP}. Hence, operating a very high caustic concentration should be avoided.

Caustic Treatment: Microscopy & Surface Analysis

Sample CT-2, with deposits on the surface was subjected to electron microscopy. The images clearly verified the presence of crystalline deposits of magnetite on the surface of the

steel. It can be seen from Figure 4-16 that the deposits are consistent in morphology. However, the surface of the steel is not uniformly covered. This can be observed even at high magnifications of 3200x. From Figure 4-17, it can be observed that the particles seem to agglomerate and then deposit on the substrate. There are multiple clusters of particles that can be noticed on the surface. In the tests with low caustic concentrations, there were no visually observable deposits on the surface. Therefore, these samples were not subjected to electron microscopy.
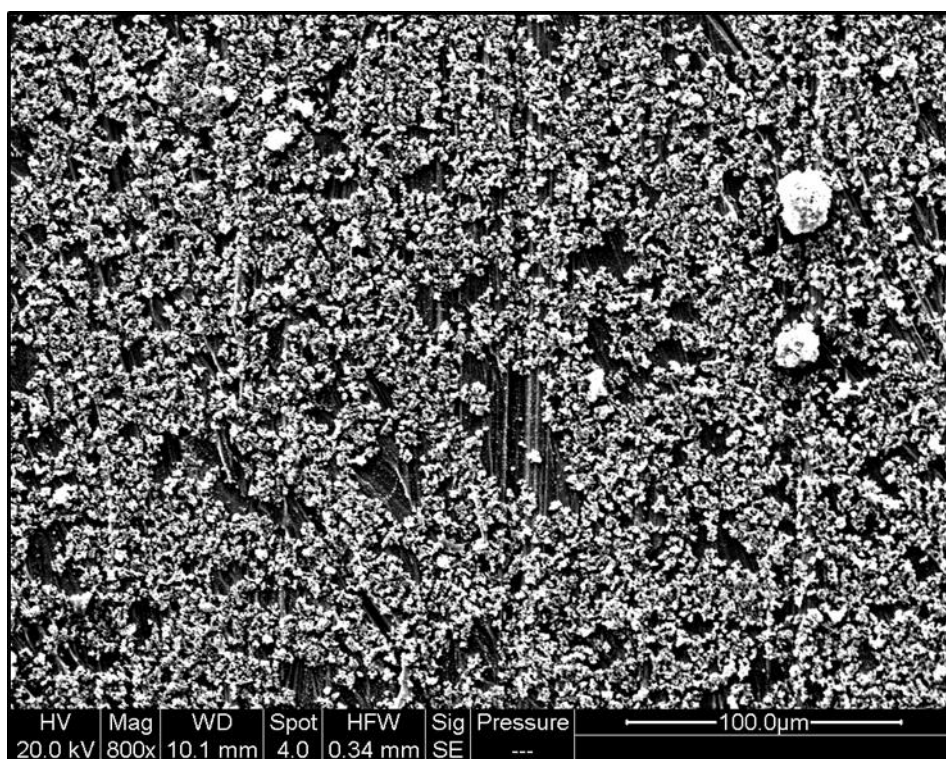
Figure 4-16. SEM image (800x) showing partial crystalline deposits on the surface of sample CT-2. Test solution is $pH_{25 °C} = 9.3$ $NH_4OH(aq)$ + 1.2 ppm NaOH with magnetite. Exposure time = 65 hours. Temperature 300 °C.
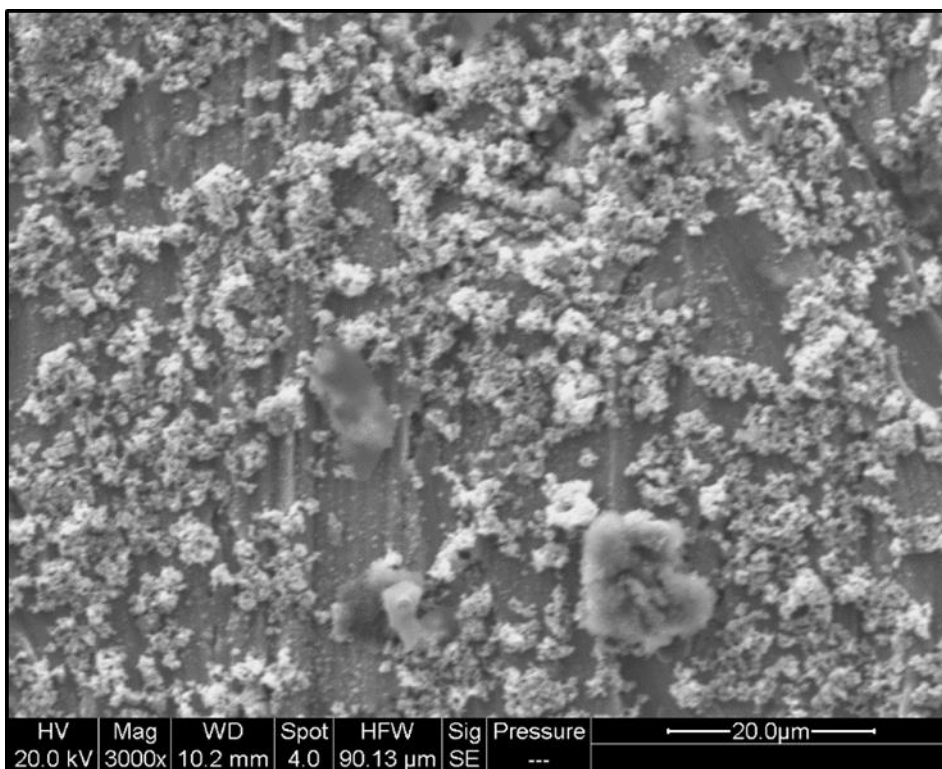
Figure 4-17. SEM image (3000x) showing partial surface coverage by crystals. Sample CT-2. Test solution is $pH_{25\,°C}$ = 9.3 $NH_4OH(aq)$ + 1.2 ppm NaOH with magnetite. Exposure time = 65 hours. Temperature 300 °C.

EDS analyses were carried out to verify the elemental composition of the deposits on the surface. Figure 4-18 shows the elemental composition of the deposits. The high counts of iron and oxygen confirmed that the deposits were oxides of iron.
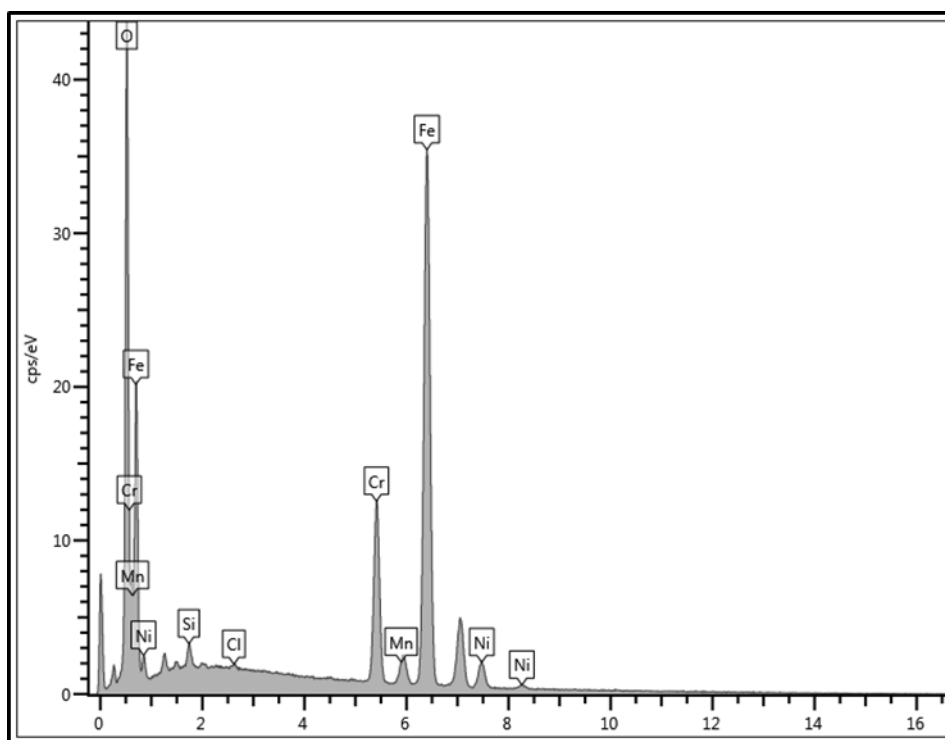
Figure 4-18. EDS spectrum showing elemental composition of the deposits on the surface of the Sample CT-2. The dominant iron and oxygen peaks indicate that the deposit is iron oxide. Test solution is $pH_{25\,°C} = 9.3$ $NH_4OH(aq)$ + 1.2 ppm NaOH with magnetite.

Caustic Treatment: EIS Results

Figure 4-19 shows the Bode plots of sample CT-1 under the low caustic environment. It can be noticed that the magnitude of the system impedance is within approximately 500 Ω of the initial value. The impedance towards the end of the test has a slightly lower value. The steady impedance response along with the lower values compared to the high caustic condition could be correlated to the lack of deposition on the surface. Figure 4-20 is the Bode plot of the system with sample CT-2 as the working electrode, tested under the high caustic environment. Representative data of the caustic treatment are shown in these plots. In this case, where deposition was observed on the surface, the magnitude of the impedance is markedly high. It can be seen that there is a much larger spread in the impedance values in the low frequency region. The low frequency spread in the impedance values could be due to the magnetite deposits influencing the diffusion of ions to and from the surface.
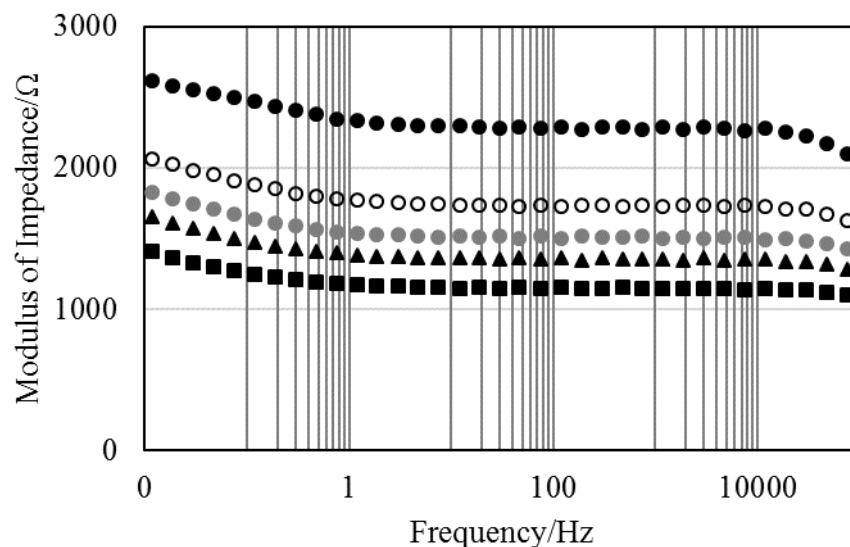
Figure 4-19. Bode plot showing the impedance magnitude behavior over time. Working Electrode: Sample CT-1. Test Solution: $pH_{25°C}$ = 9.3 equivalent $NH_4OH(aq)$ + 0.5 ppm NaOH(aq), [●] 0 hours, [○] 15 hours, [●] 24 hours, [▲] 34 hours, [■] 44 hours.
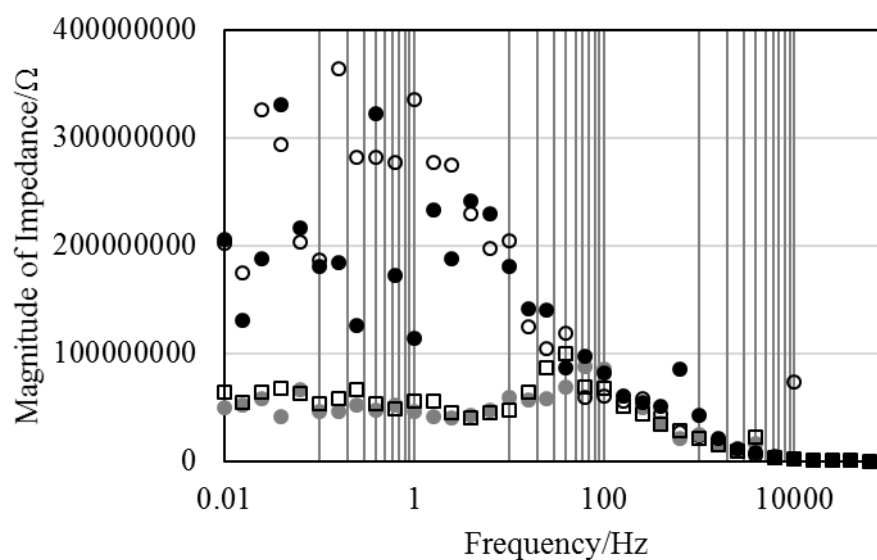
Figure 4-20. Bode plot showing the varying impedance magnitude over time. Working Electrode: Sample CT-2. Test Solution: $pH_{25°C}$ = 9.3 equivalent $NH_4OH(aq)$ + 1.2 ppm NaOH(aq), [●] 0 hours, [○] 16 hours, [●] 37 hours, [□] 62 hours.

Phosphate Treatment

The test solution in the low phosphate case (0.3 ppm Na_3PO_4) has a $pH_{25°C} = 9.32$ and the high phosphate case (3 ppm Na_3PO_4) has a $pH_{25°C} = 9.51$. At 300 °C (572 °F) the pH values are 6.0 and 6.8 respectively for the low phosphate and high phosphate case.

Phosphate Treatment: Visual Observations

Sodium phosphate was added as trisodium phosphate. In the case with low phosphate concentrations, no observable deposits were noticed on the surface of sample PT-2. However, sample PT-1, tested with the higher concentration of phosphate had black colored deposits on the surface. The observations in this case are similar to that of the caustic conditions. Figure 4-21 shows the stainless-steel samples tested under phosphate treatment.
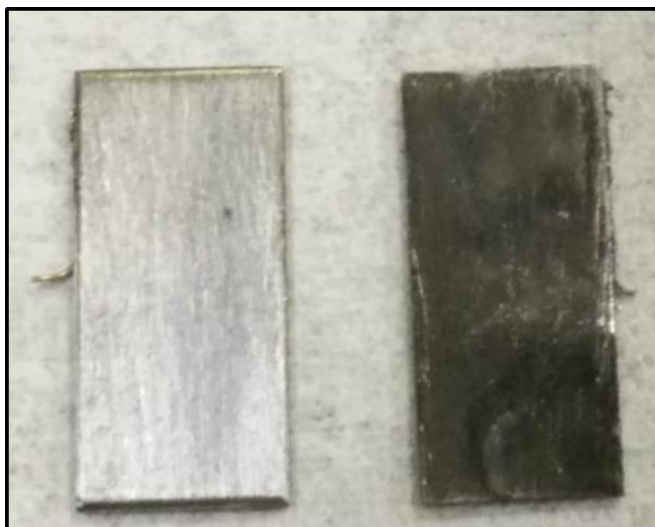
Figure 4-21. Stainless steel samples post testing under phosphate treatment. On the left: Sample PT-2 Test solution: $pH_{25°C} = 9.3$ using $NH_4OH + 0.3$ ppm Na_3PO_4. On the right: Sample PT-1 Test solution: $pH_{25°C} = 9.3$ using $NH_4OH + 3$ ppm Na_3PO_4. Exposure time = 65 hours. Temperature 300 °C.

Phosphate Treatment: Microscopy & Surface Analysis

The visual observations were validated with surface analyses. It was verified that there were crystalline deposits on the surface of sample PT-1. However, the deposits were very much unlike the clusters of deposits observed in the caustic tests. Under a magnification of 3200x, clusters of oxide deposits with exposed steel surface was noticed under the caustic environment. However, with phosphate treatment, the surface is uniformly covered with oxide crystals as shown in Figure 4-22. The glowing white regions are the ceramic adhesive used in the electrode assembly. EDS (Figure 4-24) was used to verify that the surface is covered with iron oxide. Figure 4-23 is a magnified image of the surface focused inside the red colored rectangle in Figure 4-22. The octahedral crystals, commonly attributed to magnetite can be clearly seen on the surface in Figure 4-23. The surface is covered predominantly with 0.5 – 1.0 micron sized particles.
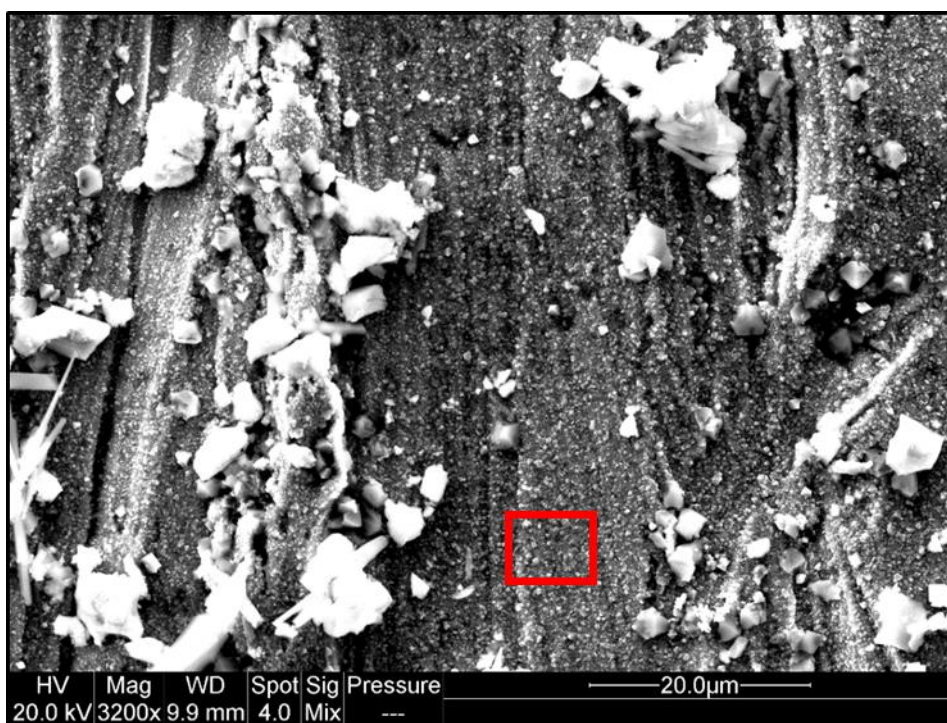
Figure 4-22. SEM image (3200x) showing crystalline deposits on the surface of the sample PT-1. Test solution is $pH_{25\,°C} = 9.3$ $NH_4OH(aq)$ + 3 ppm Na_3PO_4 with magnetite. Exposure time = 65 hours. Temperature 300 °C.
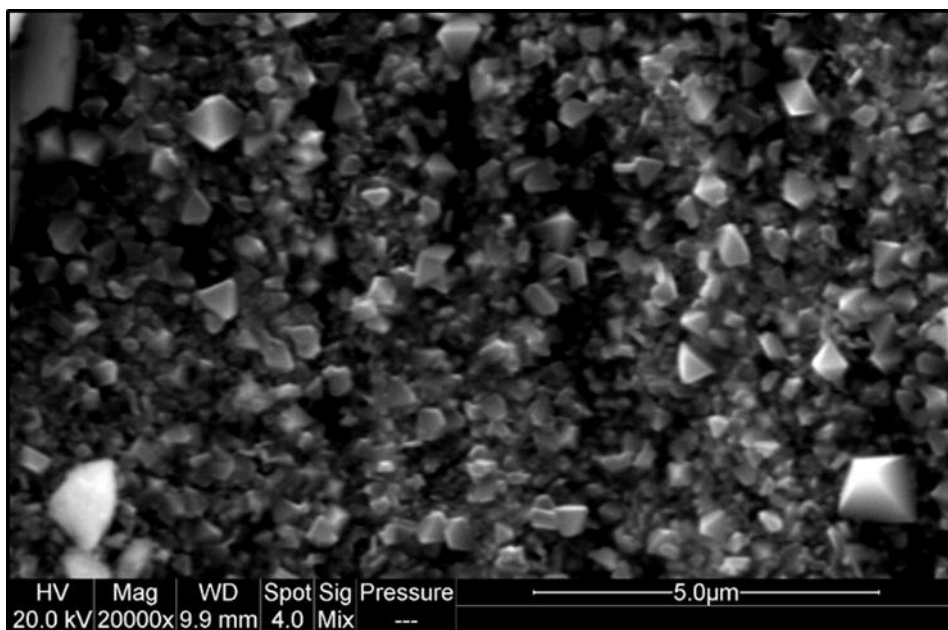
Figure 4-23. SEM image (20000x) showing tightly packed crystalline deposits on the surface of sample PT-1. Test solution is $pH_{25\,°C}$ = 9.3 $NH_4OH(aq)$ + 3 ppm Na_3PO_4 with magnetite. Exposure time = 65 hours. Temperature 300 °C.
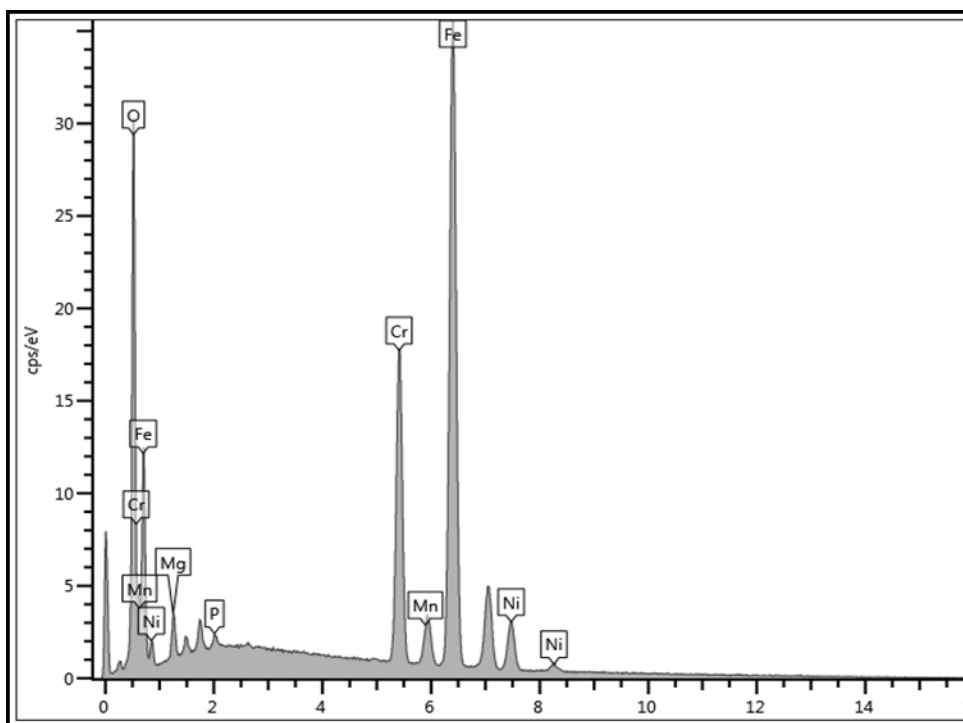
Figure 4-24. EDS spectrum showing elemental composition of the deposits on the surface of sample PT-1. Iron and oxygen are the predominant elements. Test solution is $pH_{25\,°C}$ = 9.3 $NH_4OH(aq)$ + 3 ppm Na_3PO_4 with magnetite

Phosphate Treatment: EIS Results

Figure 4-25 and Figure 4-26 show the Bode plots over the duration of the test for the low phosphate, sample PT-2, and high phosphate, sample PT-1, concentration respectively. As it was determined with caustic treatment, the low phosphate condition, where no deposition was observed, has impedance values within 400 Ω of each other. This is relatively constant compared to the spread of impedance magnitudes observed in the high phosphate case, where deposition was observed. The spread in the impedance values was observed at low frequency as can be seen in Figure 4-26. This could be due to the magnetite deposits influencing the diffusion of ions to and from the surface.
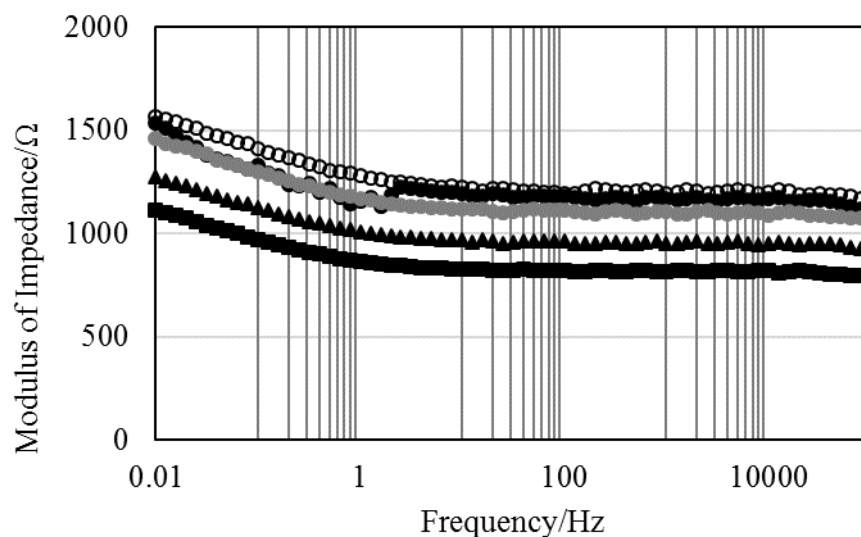
Figure 4-25. Bode plot showing constant impedance magnitude over time. Working Electrode: Sample PT-2. Test Solution: $pH_{25°C}$ = 9.3 equivalent $NH_4OH(aq)$ + 0.3 ppm Na_3PO_4 (aq), [●] 0 hours, [○] 14 hours, [●] 28 hours, [▲] 42 hours, [■] 61 hours.
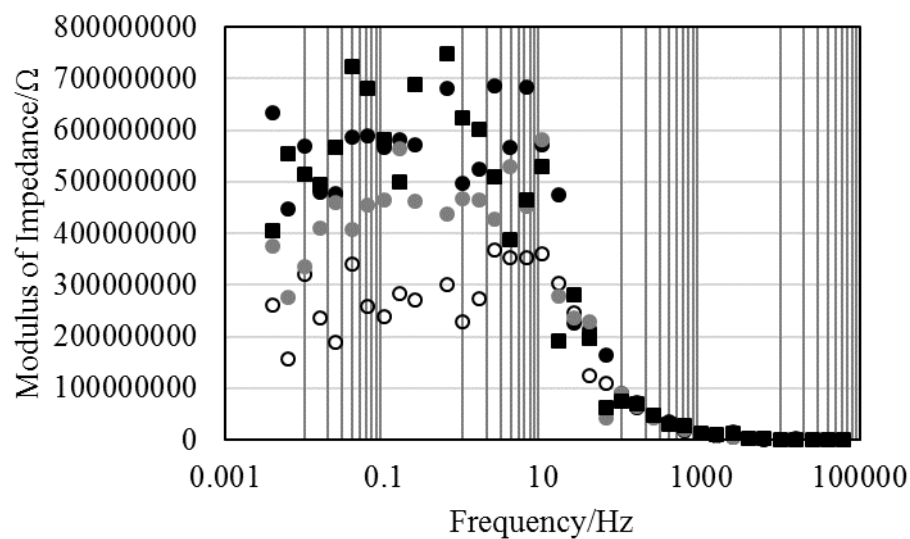
Figure 4-26. Bode plot showing the impedance magnitude behavior over time. Working Electrode: Sample PT-1. Test Solution: $pH_{25°C} = 9.3$ equivalent $NH_4OH(aq) + 3$ ppm Na_3PO_4 (aq), [●] 5 hours, [○] 26 hours, [●] 48 hours, [■] 60 hours.

Effect of Addition of Hydrazine

Addition of Hydrazine: Visual Observations

In both the high and low hydrazine residuals conditions, visual observations of the samples showed considerable deposition. In both cases the stainless-steel sample was covered with black deposits and no visually observable differences on the surface of the sample. Figure 4-27 shows the photographs of the stainless-steel samples tests with 30 ppb, sample AVTH-1 and 90 ppb, sample AVTH-2, hydrazine residuals. The photographs appear different due to differences in lighting at the time of capturing the picture.
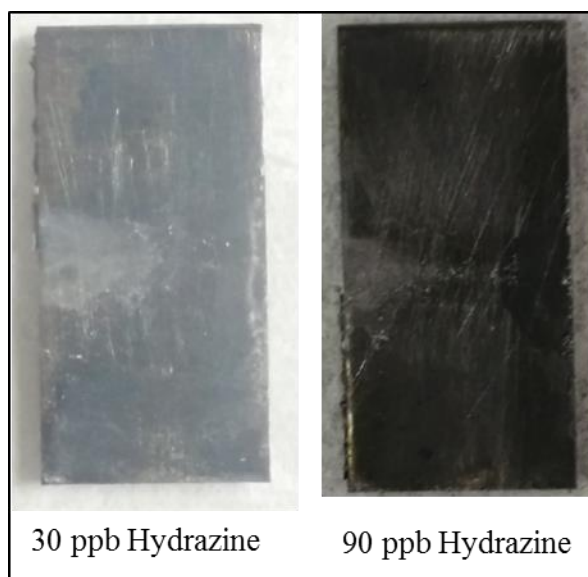
Figure 4-27. Photographs of the 304 SS substrates tested with hydrazine residuals. On the left side: Sample AVTH-1 with 4.4 10^{-5} mol kg^{-1} + 30 ppb N_2H_4. On the right: Sample AVTH-2 with 4.4 10^{-5} mol kg^{-1} + 90 ppb N_2H_4. Exposure time = 65 hours. Temperature 300 °C.

The consistent presence of black colored deposits may indicate that hydrazine does not significantly alter the deposition mechanism.

Addition of Hydrazine: Microscopy & Surface Analysis

Surface analyses was carried out to study the topography and the nature of the deposits to corroborate the visual observations. Sample AVTH-1, exposed to 30 ppb of hydrazine residual showed uniform coverage with particles. The particles have the characteristic octahedral shape of magnetite. Figure 4-28 is a SEM image of the surface at 5000x showing uniform surface coverage. The presence of crystalline deposits on the surface can be noticed. The substrate, a darker shade of grey, can be seen in the image. This could indicate impaction was the reason for the presence of particles on the surface.
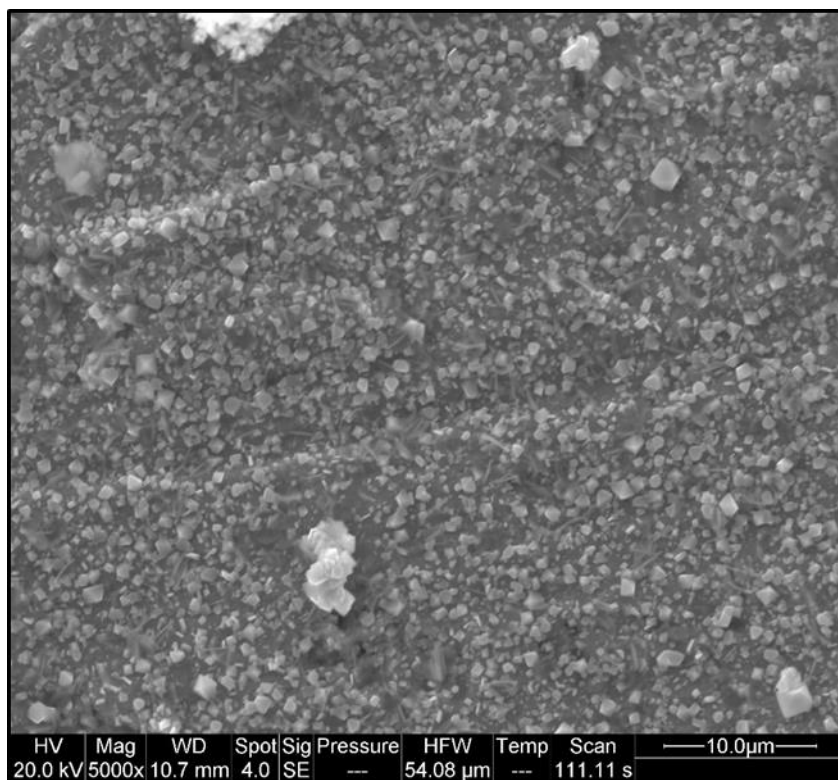
Figure 4-28. Secondary Electron Image (5000x) showing magnetite particles on the surface of sample AVTH-1. Test solution is $pH_{25 °C}$ = 9.3 $NH_4OH(aq)$ + 30 ppb N_2H_4 residuals with magnetite. Exposure time = 65 hours. Temperature 300 °C.

Figure 4-29 is an SEM image of the surface of sample AVTH-1 at 10000x. The higher magnification shows more closely packed crystalline particles. Even at such a high magnification some areas of the substrate are visible. It can also be observed that the deposit particles are not aligned in the same direction. Here again, the octahedral shape of the magnetite crystals on the substrate can clearly be identified. The size of the particles Figure 4-29 is 1.0 – 2.0 microns.
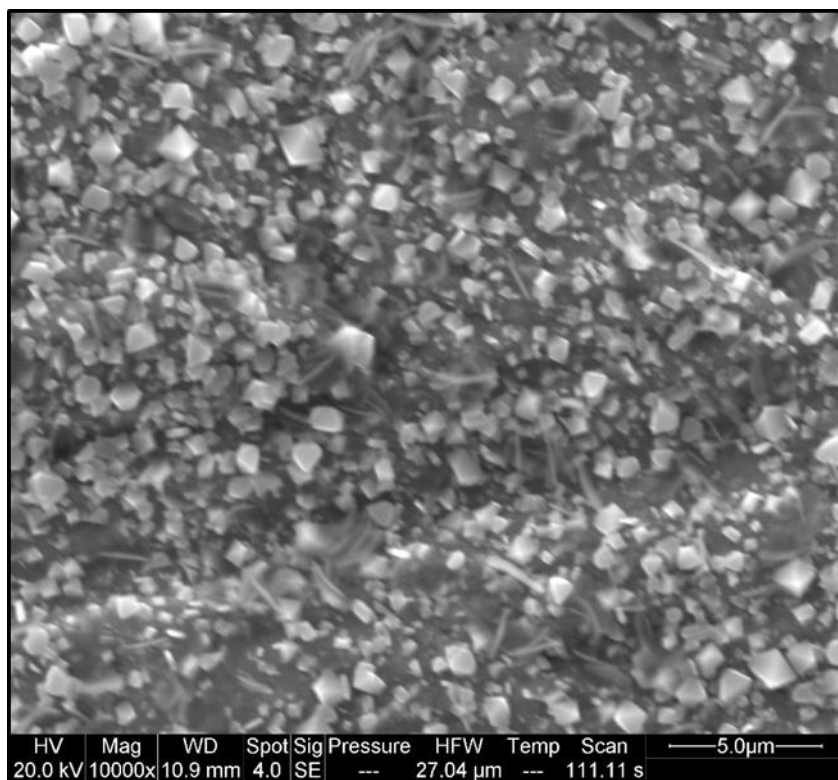
Figure 4-29. Secondary Electron Image (10000x) showing octahedral magnetite particles uniformly covering the surface of sample AVTH-1. Test solution is $pH_{25\ °C} = 9.3$ $NH_4OH(aq)$ + 30 ppb N_2H_4 residuals with magnetite. Exposure time = 65 hours. Temperature 300 °C.

Surface imaging of sample AVTH-2, tested at 90 ppb hydrazine residuals showed remarkable similarity to the 30 ppb hydrazine case. The substrate showed uniform surface coverage with crystalline particles. At 5000x, as shown in Figure 4-30, by eyeballing the SEM images, it could be argued that there are less particles as compared to the 30 ppb case, but there is no contrasting difference in the surface coverage between samples AVTH-1 and AVTH-2. Further magnification to 10000x, Figure 4-31 showed the octahedral crystals of magnetite on the surface similar to what was observed in the 30 ppb hydrazine case. Energy dispersive spectroscopy (EDS) was used to verify that the deposits were iron oxides.

Macroscopically, both cases exhibited uniform surface coverage on the 304 SS substrates. The surface analyses corroborate the observations and prove that there are no significant differences in the nature of type of the deposits between the two cases. The similarity of the at temperature pH & ionic strength for the 30 ppb hydrazine and 90 ppb hydrazine residuals shows that the two conditions offer the same aqueous environment for the suspended magnetite. At the test conditions, residual hydrazine will break down to ammonia and the only

effect on the suspended magnetite particles is the development of surface charge. Being close to the pH_{IEP} of magnetite at 300 °C, both cases exhibit significant deposition on the substrate.

HV	Mag	WD	Spot	Sig	Pressure	HFW	Temp	Scan	——10.0µm——
20.0 kV	5000x	9.4 mm	4.0	SE	---	54.08 µm	---	56.80 s	
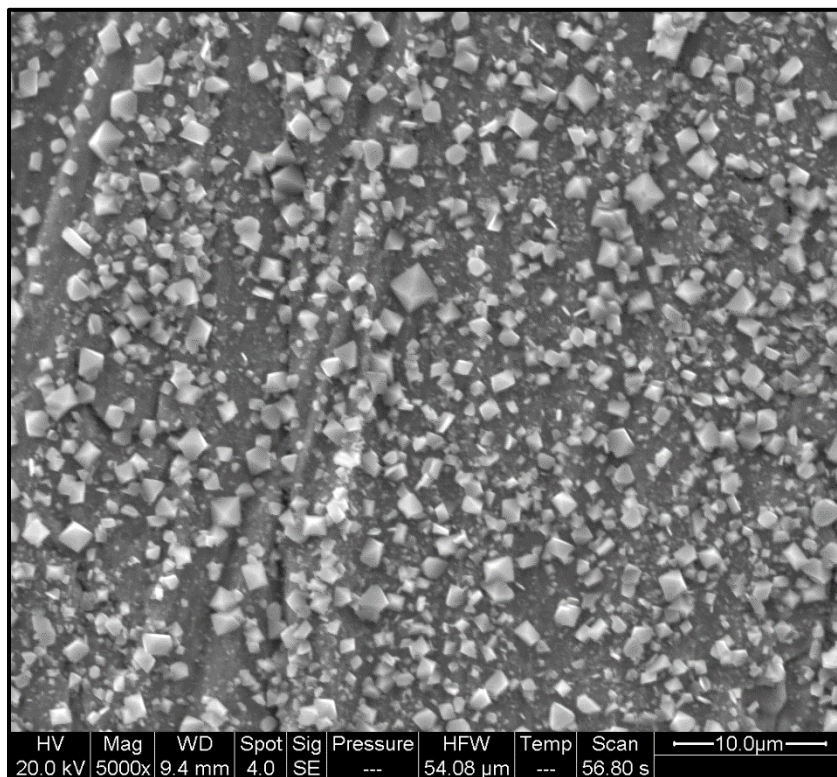
Figure 4-30. Secondary Electron Image (5000x) showing octahedral magnetite particles uniformly covering the surface of sample AVTH-2. Test solution is $pH_{25\ °C}$ = 9.3 $NH_4OH(aq)$ + 90 ppb N_2H_4 residuals with magnetite. Exposure time = 65 hours. Temperature 300 °C.
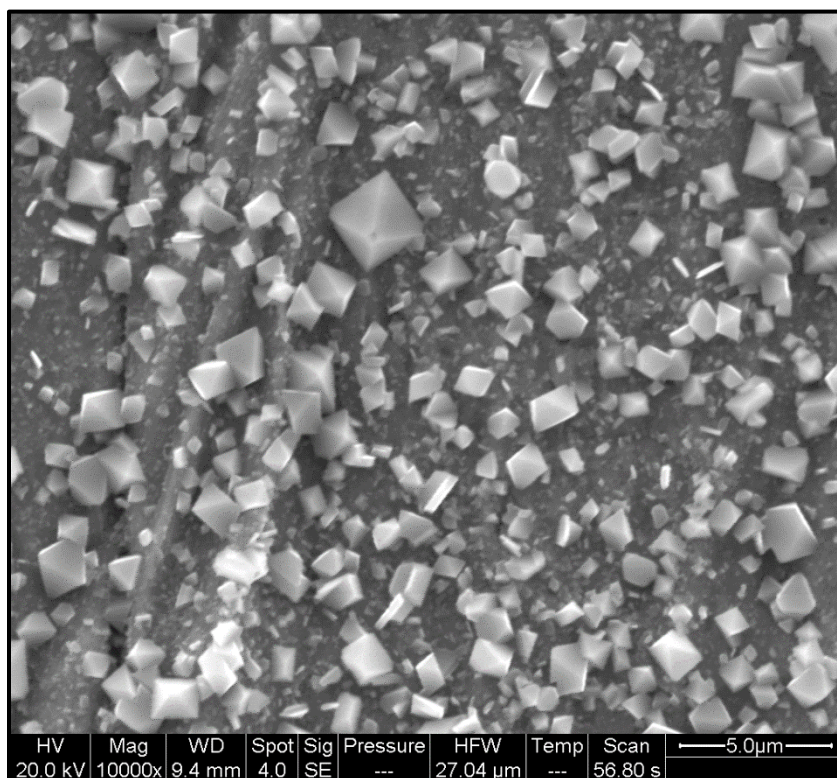
Figure 4-31. Secondary Electron Image (10000x) of sample AVTH-2 showing uniformly deposited octahedral magnetite particles covering the surface. Test solution is $pH_{25\,°C} = 9.3$ $NH_4OH(aq) + 90$ ppb N_2H_4 residuals with magnetite. Exposure time = 65 hours. Temperature 300 °C.

Of the three tests performed at 30 ppb hydrazine residuals, there was an interesting observation in one of the samples. Under the SEM, certain regions of the samples showed different kinds of deposits compared to what was seen in general across the samples. This region, shown in Figure 4-32, exhibited clusters of small crystalline deposits interspersed with larger particles. This region appears to have a mixed morphology of small and large octahedral particles along with some shapes which appear to be plate like structures. Such types of deposits were not consistently found across the surface of the sample. It is possible that these could be aggregates of smaller particles forming in solution prior to deposition. EDS analysis of this region confirmed that the deposits were iron oxides. It was not possible to identify these regions visually, macroscopically the surface looks uniformly covered.
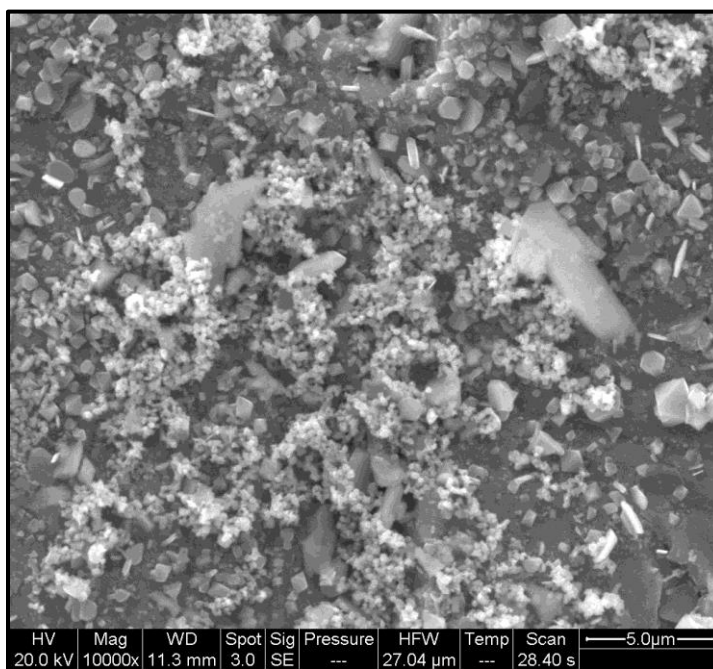
Figure 4-32. Secondary Electron Image (10000x) of the sample showing clusters of magnetite particles covering the surface. Test solution is $pH_{25\,°C} = 9.3$ NH$_4$OH(aq) + 90 ppb N$_2$H$_4$ residuals with magnetite. Exposure time = 65 hours. Temperature 300 °C.

Addition of Hydrazine: EIS Results

EIS was used to monitor the substrate solution interface in situ. As was observed in the previous tests with the phosphate and caustic treatment conditions, very high impedance values (order of MΩ) were observed when there was a deposit on the surface. Figure 4-33 shows the Bode plot for the 30 ppb residual hydrazine tests. The plot shows high values of impedance and on the log scale, the impedance is independent of the frequency. These observations are similar to what was observed in the high caustic and high phosphate concentrations, where magnetite deposition was found to occur on the substrate.

Figure 4-33. Modulus of total impedance as a function of frequency (Bode plot) over the duration of the test. Working Electrode: AVTH-1. Test solution: $pH_{25°C} = 9.3 + 30$ ppb N_2H_4 residual ($\circ$) 10 hours, ($\bullet$) 25 hours, ($\square$) 35 hours, (Δ) 48 hours, ($\Diamond$) 58 hours.

Figure 4-34 is the Bode plot for the test with 90 ppb residual hydrazine in solution. The impedance response for the system is similar to the 30 ppb hydrazine residual case, both in terms of the values of the impedance and the dependence on frequency.

Figure 4-34. Modulus of total impedance as a function of frequency (Bode plot) over the duration of the test. Working Electrode: AVTH-2. Test solution: $pH_{25°C} = 9.3 + 90$ ppb N_2H_4 residual (○) 6 hours, (●) 20 hours, (□) 31 hours, (Δ) 46 hours, (◊) 52 hours.

The phase angle plots are good indicators of mechanistic changes and this is usually identified by different time constants. Figure 4-35 shows the phase angle plots for sample AVTH-1 and sample AVTH-2 from the different tests. It can be seen that both early in the exposure and towards the end of tests, the phase angle vs. frequency plots are similar. There are no additional time constants (local maxima or minima) and the phase angle values are comparable. This could be construed as further proof that there is no significant mechanistic impact on the two residual concentrations of hydrazine on the interface.
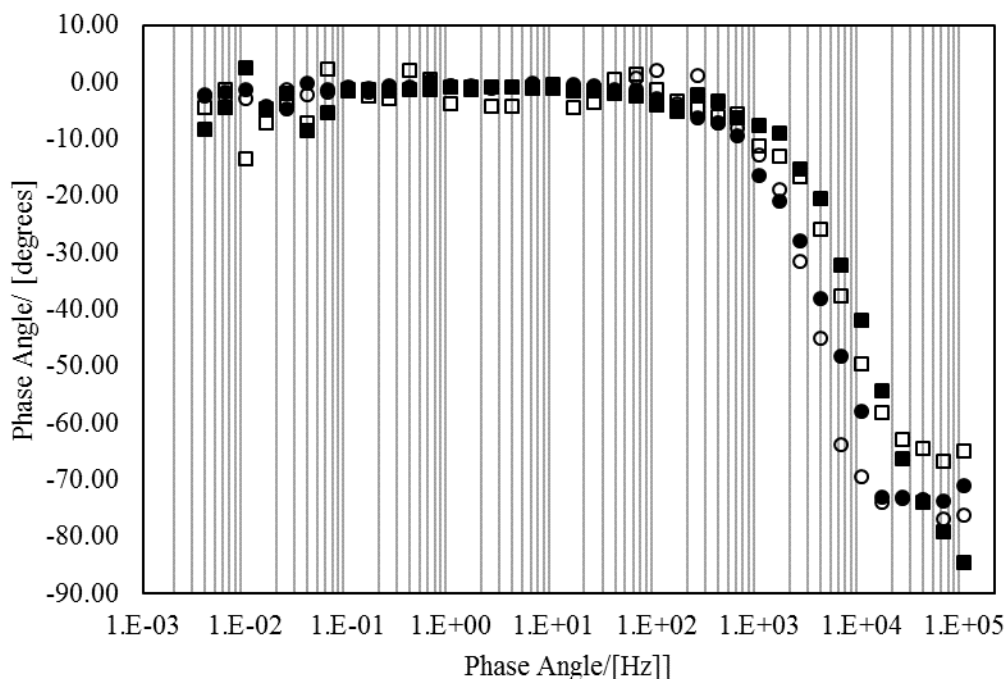
Figure 4-35. Phase Angle as a function of frequency for both residual concentrations of hydrazine. (■) Working Electrode: AVTH-1, Solution: 30 ppb N_2H_4, 6 hours, (●) Working Electrode: AVTH-1, Solution: 30 ppb N_2H_4, 58 hours, (□) Working Electrode: AVTH-2, Solution: 90 ppb N_2H_4, 6 hours, (○) Working Electrode: AVTH-2, Solution: 90 ppb N_2H_4, 52 hours.

Based on the aqueous solution speciation at 300 °C (572 °F) and 10 MPa (1450 psi), we can see that the hydrazine does not alter the pH much at the concentrations tested here. In these tests, based on the fact that $pH_{300 °C}$ is close to the pH_{IEP} of magnetite at 300 °C, we can conclude that this is an environment conducive for deposition of magnetite. The results from the AVT $pH_{25°C} = 9.3$ tests show that deposition occurs when the $pH_{300 °C}$ is close to the pH_{IEP} of magnetite at 300 °C. The change in $pH_{300 °C}$ due to the addition of hydrazine, both 30 ppb and 90 ppb, is not sufficient to significantly alter the surface charge developed on the surface of magnetite. Therefore, addition of hydrazine would not affect the interaction between the particles and substrates.

Filming Amine Chemistry: HRSG-02

In all the tests with filming amines, only HRSG-02 was used to condition the pH of the boiler water. The amine was used as per instructions from the manufacturer.

HRSG-02: Visual Observations

The tests with the filming amines did not show an obvious mitigation of the deposition like sample AVT-2 in the AVT pH_{25^oC} 9.8 case. Figure 4-36 shows the stainless-steel coupons tested at 2.5 ppm HRSG-02, sample FFA-1 and 5 ppm HRSG-02, sample FFA-2. Visual observations did not reveal any macroscopic differences between the samples. Both the samples showed regions which were darker than others and some regions which looked uncovered with magnetite. This could be an indicator of different types of deposits on the surface. It was however clear that neither test condition completely mitigated deposition.
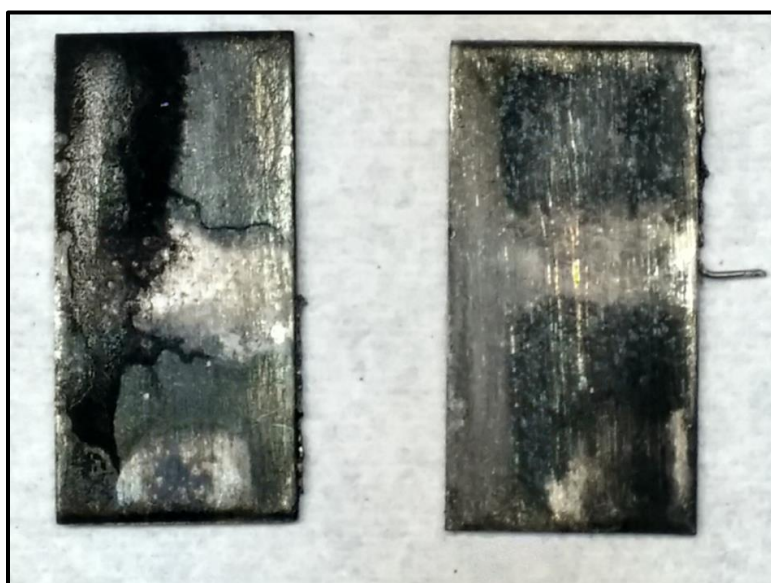
Figure 4-36. Optical photograph of the samples tested in HRSG-02 poly amine treatment. Three distinct types of deposits seen visually. Left: Sample FFA-1, Solution: 2.5 ppm HRSG-02, Right: Sample FFA-1, Solution: 5 ppm HRSG-02. Exposure time = 65 hours. Temperature 300 °C.

HRSG-02: Microscopy & Surface Analysis

Visual observations indicated that there could be different types of deposits on the surface. SEM and EDS were used to further analyze the nature of the deposits and corroborate the visual observations. In sample FFA-1, the visual observations indicated regions of contrast on the substrate. These were further analyzed under an SEM. Surface analyses revealed, 3 distinct surface features on the substrate. Firstly, there were regions where no deposits were observed on the surface. The only features on the surface were the streaks from roughening up the surface as a

part of the electrode preparation before the test. Figure 4-37 shows the SEM image of this region at 5000x. The substrate looked free of any crystalline particles. However, there are also no obvious signs of an amine coating present on the surface. This was determined by the lack of any nitrogen in the EDS spectra.
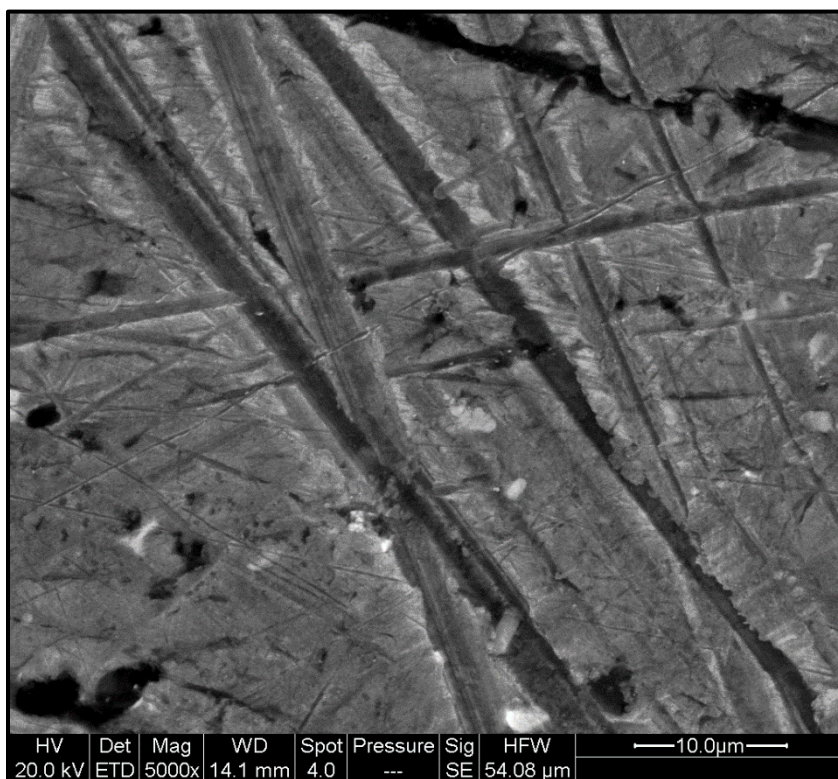
Figure 4-37. Secondary Electron Image (5000x) of the sample showing region with no surface coverage. Sample: FFA- 1. Test solution is 2.5 ppm HRSG-02. Exposure time = 65 hours. Temperature 300 °C.

Secondly, there were regions on the substrate where deposition was noticed and the nature of the deposits were similar to what was observed previously with the hydrazine tests. The particles can be seen to be adhering to the substrate. Figure 4-38 is an SEM image of one such region on sample FFA-1 at a magnification of 5000x. The similarity to the type of deposition observed in the previous tests is very clear. The individual particles are adhered to the substrate and some regions of the substrate are visible.
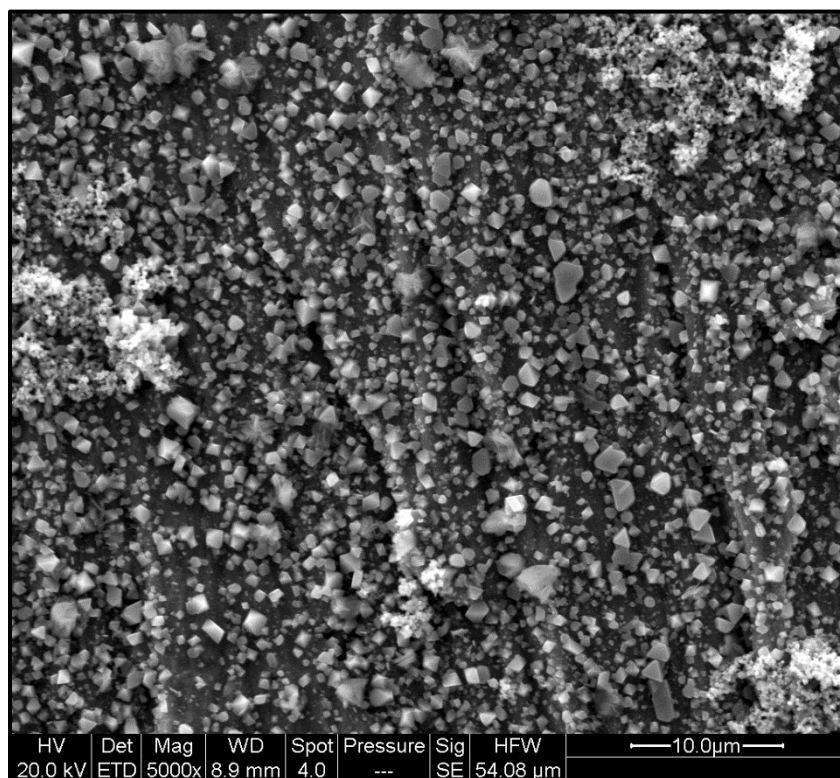
Figure 4-38. Secondary Electron Image (5000x) of the sample showing magnetite particles uniformly covering the surface. Octahedral shaped crystals uniformly deposited on the surface. Sample: FFA-1. Test solution is 2.5 ppm HRSG-02. Exposure time = 65 hours. Temperature 300 °C.

A higher magnification at 10000x, as shown in Figure 4-39, showed the characteristic octahedral shape of the magnetite nanoparticles. These images clearly established that there is magnetite deposition in these regions and uniform surface coverage.
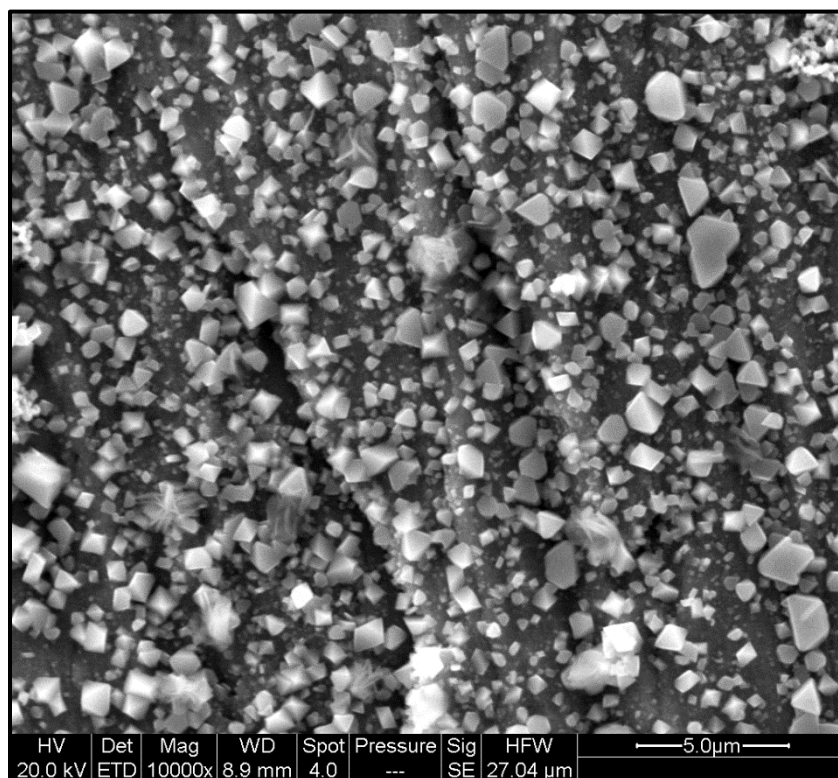
Figure 4-39. Secondary Electron Image (10000x) of the sample showing octahedral magnetite particles uniformly covering the surface. Sample: FFA-1. Test solution is 2.5 ppm HRSG-02. Exposure time = 65 hours. Temperature 300 °C.

Lastly, a third feature was observed on the substrate and this region showed very high deposition with the deposits having features different from the previously observed deposits. The deposits appear to be very closely packed with smaller particles. These regions showed very high aggregation and clustering of particles. Figure 4-40 is an SEM image at 2500x showing the region with very high deposit adjacent to a region with moderate deposition. The contrast between two regions is immediate. On the left-hand side of the image is the region with closely packed particles on the surface and on the right is a region similar to what was observed in previous tests under different conditions. Macroscopically, both these regions appear to be coated with magnetite. However, there are regions on the substrate which appear darker and those could be correlated to the closely packed deposit layer.
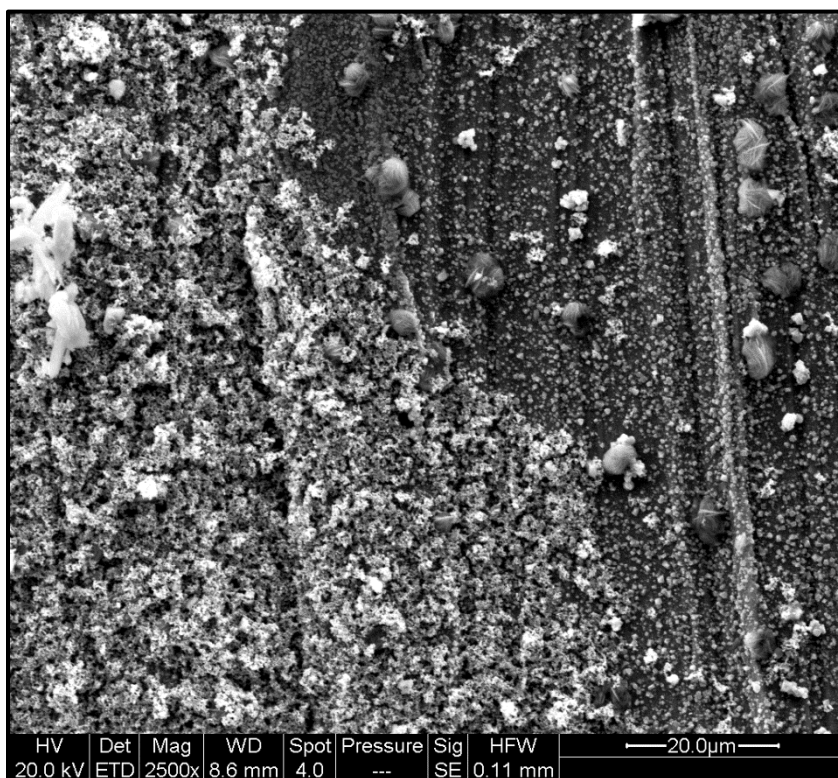
Figure 4-40. Secondary Electron Image (2500x) of Sample FFA-1 showing regions exhibiting different types of deposits. Left hand side of the image shows densely packed aggregate deposits. Right hand side shows individual particles on the substrate. Test solution is 2.5 ppm HRSG-02. Exposure time = 65 hours. Temperature 300 °C.

Further magnification of this region, Figure 4-41, enhances the contrast between the two types of deposition features. At 10000x, the small particles of the aggregate clusters could be identified. The densely-packed deposit layer does indeed appear to be made of aggregated particles.
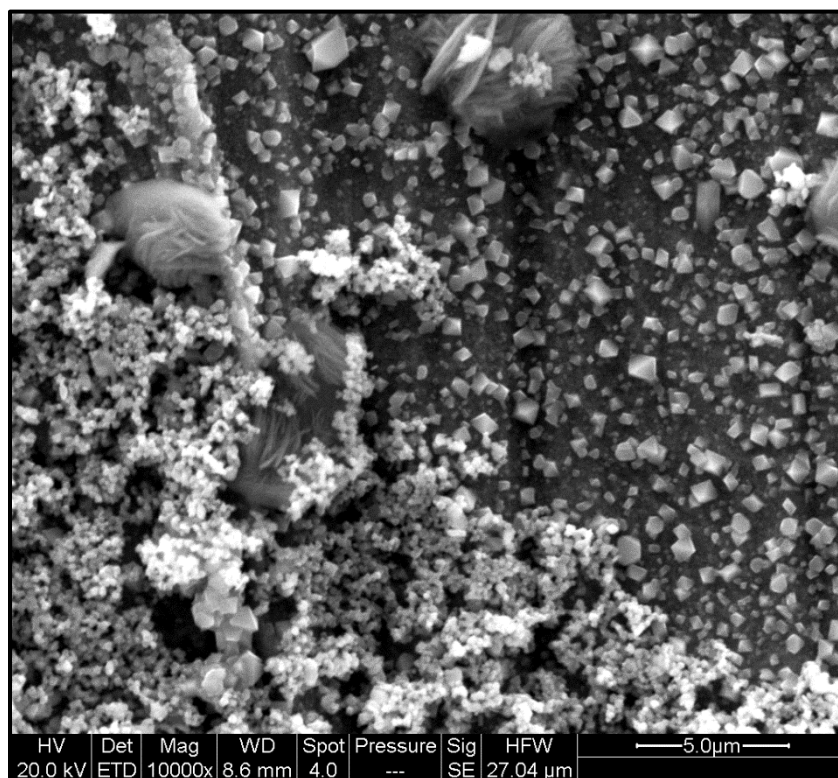
Figure 4-41. Secondary Electron Image (10000x) of the Sample FFA-1 showing regions exhibiting different types of deposits. Left hand side of the image shows densely packed aggregate deposits. Right hand side shows individual particles on the substrate. Test solution is 2.5 ppm HRSG-02. Exposure time = 65 hours. Temperature 300 °C.

EDS was used to qualitatively assess the elemental composition of the deposit layer. Both types of deposits were predominantly iron oxide. Interestingly, the regions which showed no presence of particles, Figure 4-37, also emitted signals corresponding to oxides. However, lack of any features on the surface implies that this is either a very thin layer or stray signals from the surrounding regions with deposits.

As with the samples from the 2.5 ppm HRSG-02 tests, the sample FFA-2 tested at the higher concentration, 5 ppm HRSG-02, also exhibited three different types of deposits. Regions with no deposits, regions with moderate deposition where individual particles were observable and finally regions with densely packed deposits were observed. In all the cases, there were similarities in the nature of the deposits compared to the 2.5 ppm HRSG-02 tests.

Figure 4-42 shows a region the surface of substrate FFA-2 at 5000x, where the surface coverage is very poor. There are a few stray particles on the surface and some surface coverage

can be seen at the bottom left corner of the image. Similar regions were observed on the sample tested with the 2.5 ppm HRSG-02 test solution as well.
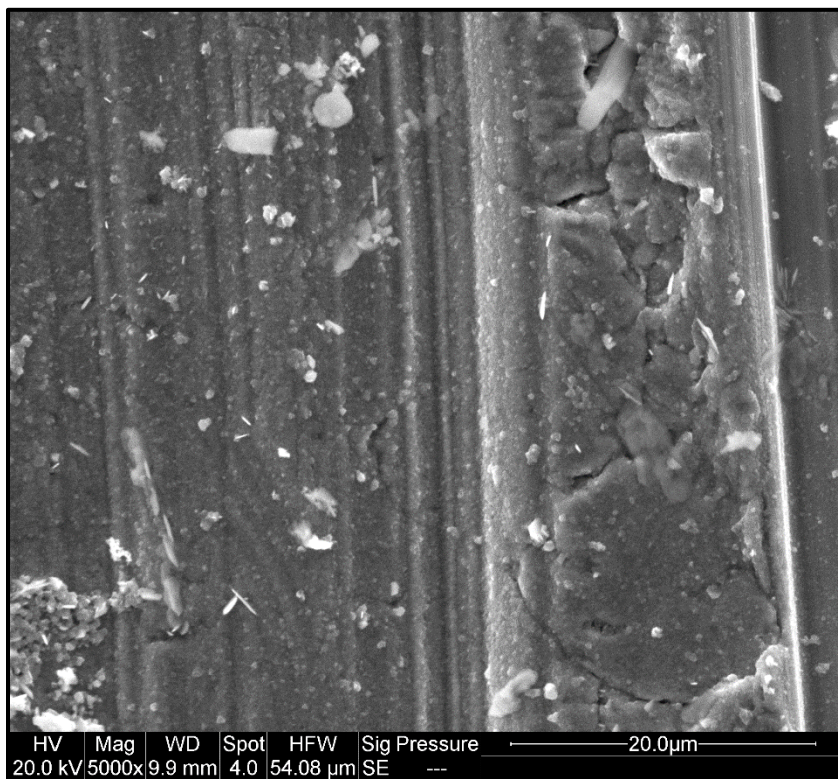
Figure 4-42. Secondary Electron Image (5000x) of the Sample FFA-2 showing a region with no surface coverage. Lack of any crystalline particles on the surface. Test solution is 5 ppm HRSG-02. Exposure time = 65 hours. Temperature 300 °C.

In Figure 4-43 at 5000x, the particles can be seen covering the surface. The surface coverage is uniform, even if not complete. This type of deposition was observed in the previous tests with hydrazine and increased particle size. Macroscopically, these regions look like they are completely covered with magnetite. Under the SEM, the substrate is visible in some regions and there is a uniform surface coverage with particles. However, the surface coverage, appears to be higher than what was observed in the 2.5 ppm HRSG-02 tests.
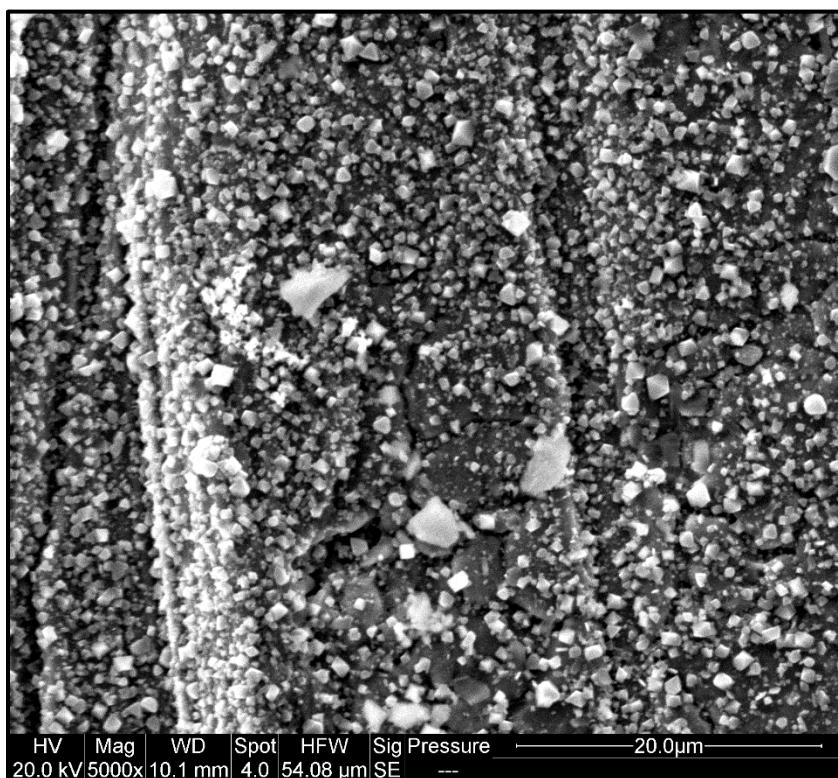
Figure 4-43. Secondary Electron Image (5000x) of the Sample FFA-2 showing magnetite particles uniformly covering the surface. Test solution is 5 ppm HRSG-02. Exposure time = 65 hours. Temperature 300 °C.

Further magnification to 10000x, clearly shows the octahedral shape of magnetite crystals. In addition to this, portions of the substrate are also visible. This is shown in Figure 4-44.
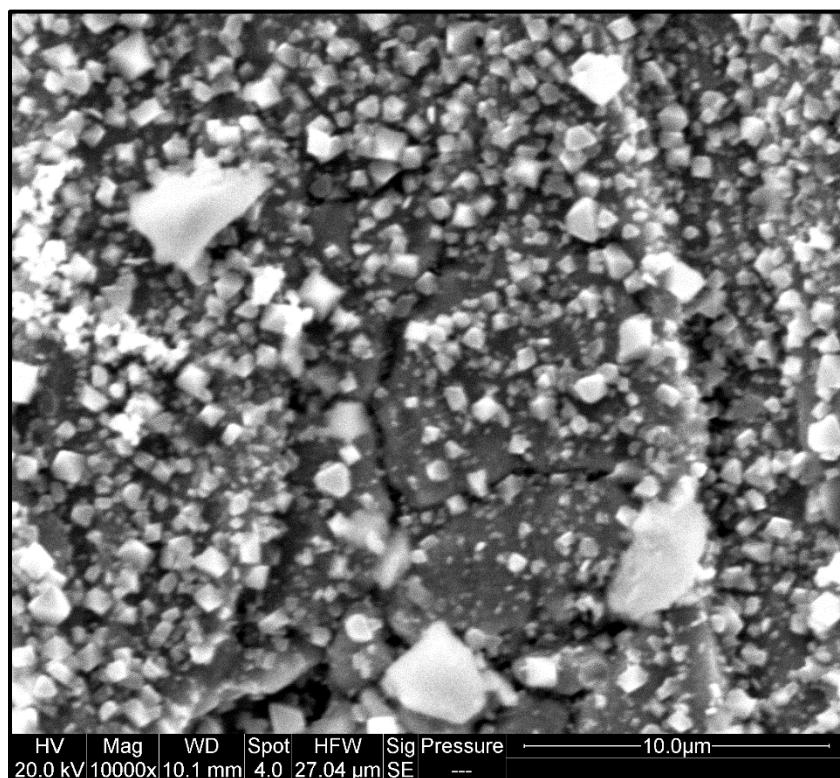
Figure 4-44. Secondary Electron Image (10000x) of the Sample FFA-2 showing octahedral magnetite particles uniformly covering the surface. Test solution is 5 ppm HRSG-02. Exposure time = 65 hours. Temperature 300 °C.

Lastly, regions with close densely packed deposits were also observed on the substrate. In such regions, it was not possible to point out individual particles and the steel substrate was not distinctly visible. The surface coverage was much higher than other regions of the substrate and the deposits were more densely packed. Figure 4-45 is an SEM image of one such portion of the substrate. The nature of the deposit observed here was very close to what was observed in Sample FFA-1 (2.5 ppm HRSG-02). Scanning the sample under the SEM indicated that the sample FFA-2 had more regions of dense tightly packed deposits as compared to the sample FFA-1.
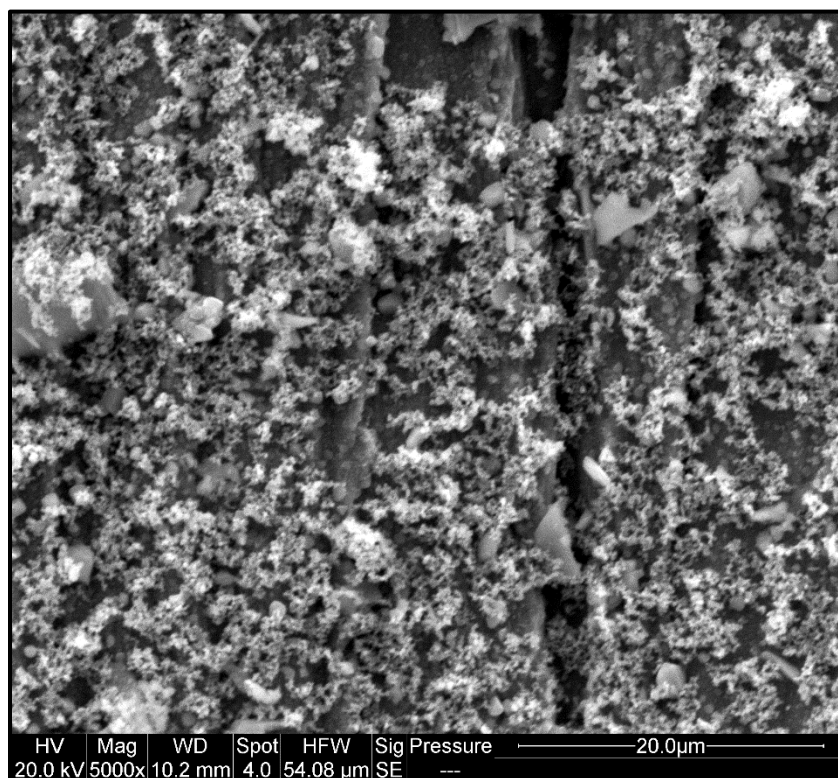
Figure 4-45. Secondary Electron Image (5000x) of the Sample FFA-2 showing regions with dense, closely packed aggregates on the substrate. Test solution is 5 ppm HRSG-02. Exposure time = 65 hours. Temperature 300 °C.

As with all the previous tests, EDS was used to confirm that the deposits were iron oxides. However, EDS was unable to detect nitrogen (from the amines) in any of the analyses performed here. This could be because the surface was covered with oxides, whose signal completely masked the nitrogen or the EDS probe was unable to detect the small quantity of nitrogen present on the surface.

The surface analyses of the samples tested with the filming amines revealed some interesting observations. Although, these did not reveal any obvious differences in the rate of deposition or amount of deposits on the surface, three different types of deposits or lack thereof were observed in the same substrate for the first time. Regions of no deposition and the moderate deposition have been observed before. Conditions not favoring deposition, like pH 9.8 AVT (Sample AVT-2), have surfaces similar to the regions without any deposition. The regions of moderate surface coverage are similar to what has been observed in the hydrazine tests and the particle size test under pH =9.3 AVT (Sample AVT-1). General observations indicated that the

sample exposed to 5 ppm HRSG-02 was more crowded, higher number of particles on the surface, but more tests and analyses will be required to provide a quantitative estimate.

However, the third type of deposition observed, the dense, closely packed deposits have been a characteristic of the tests with HRSG-02 in the test solution. This type of deposition could be a result of the interaction between the HRSG-02 and magnetite particles. From the tests conducted here, it is not possible to identify the mechanism that results in such deposits being formed. These could be a result of the interaction between the amine chains and the magnetite or a result of the aqueous chemistry at 300 °C. However, such deposition has been consistent with all the tests with HRSG-02 and can be attributed to the presence of the filming amine in boiler water solution. The dense, closely packed aggregate deposits were observed in both in Sample FFA-1 and sample FFA-2.

HRSG-02: EIS Results

The impedance response was similar to the cases where there was deposition on the substrate. The magnitude of the impedance for both Sample FFA-1 and FFA-2 was roughly 10 times higher than the previous tests with hydrazine and the particle size. Considering that the approximate calculated ionic strength of the HRSG-02 test solutions is close to the ionic strength of the test solution in the hydrazine tests and increased particle size tests, the increase in impedance could be attributed to the filming compounds present in HRSG-02. It is also plausible that the nature of the magnetite deposits observed in the tests with the filming amine, especially the densely packed aggregate deposits could also have caused the increase in impedance.

Figure 4-46 is a Bode plot showing the modulus of impedance for the sample FFA-1. As mentioned earlier the impedance response is similar to what was observed previously, but the impedance values are higher. Also noticeable here is the trend of the impedance values over time. The impedance is higher initially and then settles down to a lower, near constant value towards the end of the test. This was observed previously in the AVT $pH_{25^\circ C}$ = 9.3 test with sample AVT-1, which showed very high magnetite deposition. This is also in contrast to the AVT $pH_{25^\circ C}$ = 9.8 test, where the impedance was more or less constant over the duration of the test.
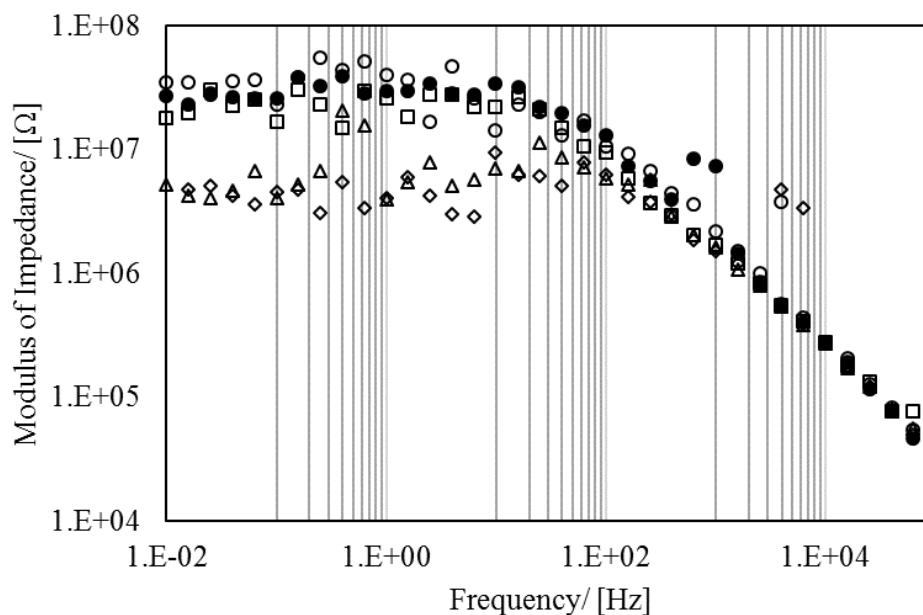
Figure 4-46. Modulus of total impedance as a function of frequency (Bode plot) over the duration of the test. Working Electrode: Sample FFA-1. Test solution: 2.5 ppm HRSG-02 (○) 0 hours, (●) 15 hours, (□) 25 hours, (Δ) 45 hours, (◊) 65 hours.

Figure 4-47 is the Bode plot for the sample FFA-2 tested at the 5 ppm HRSG-02 test solution. The impedance values are higher than the hydrazine (AVTH-1 and AVTH-2), but not drastically different from the 2.5 ppm HRSG-02 case. Also, the impedance response at 5 ppm does not show any clear trend as displayed by the 2.5 ppm HRSG-02 case. Although, it could be speculated that the sticking mechanism could be different and that there was much lesser erosion after the deposits were formed, the tests conducted here do not confirm these speculations. The increased surface coverage observed in the SEM images could be used to say that the particle removal from the surface was lower than in sample FFA-1.
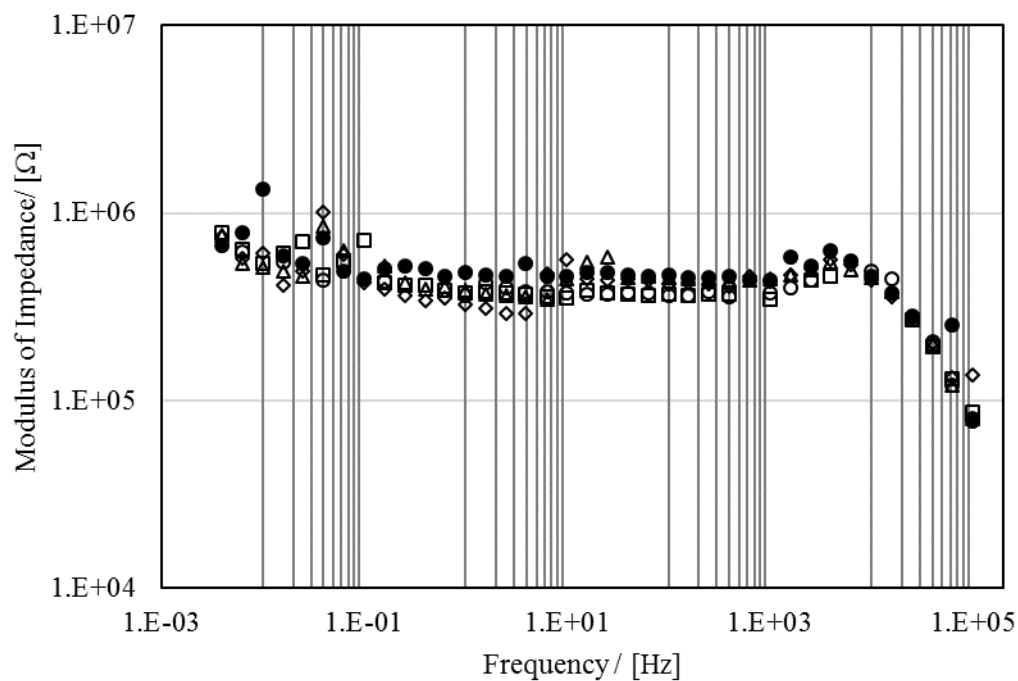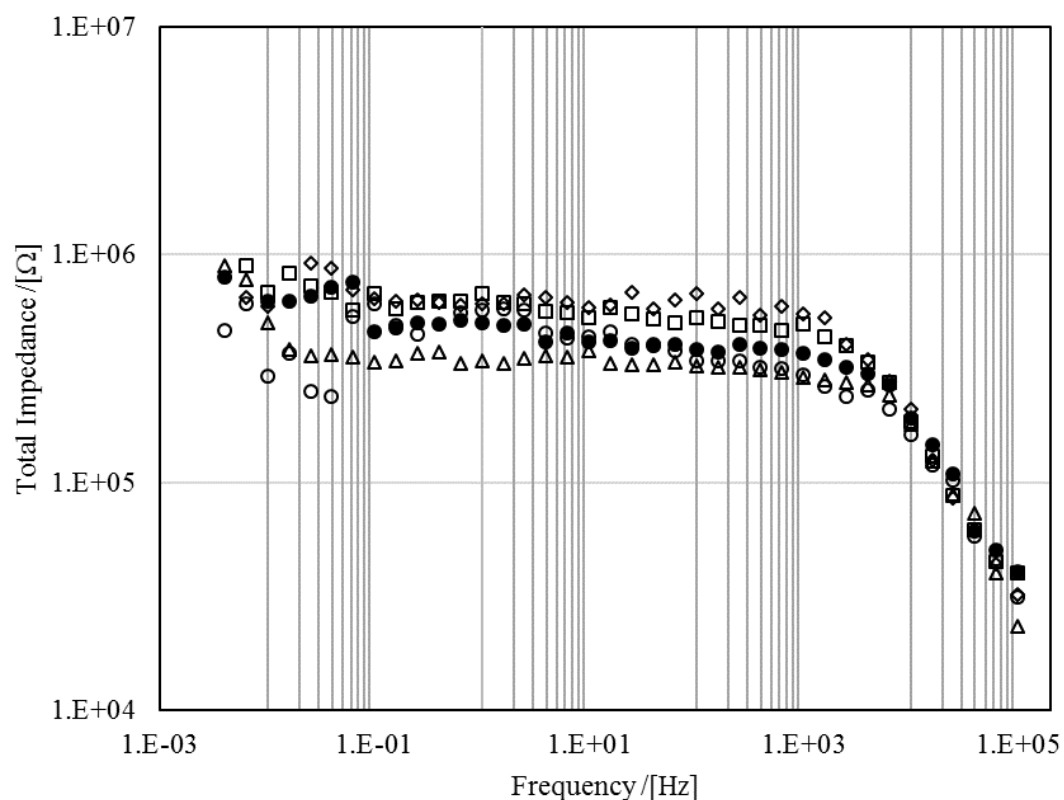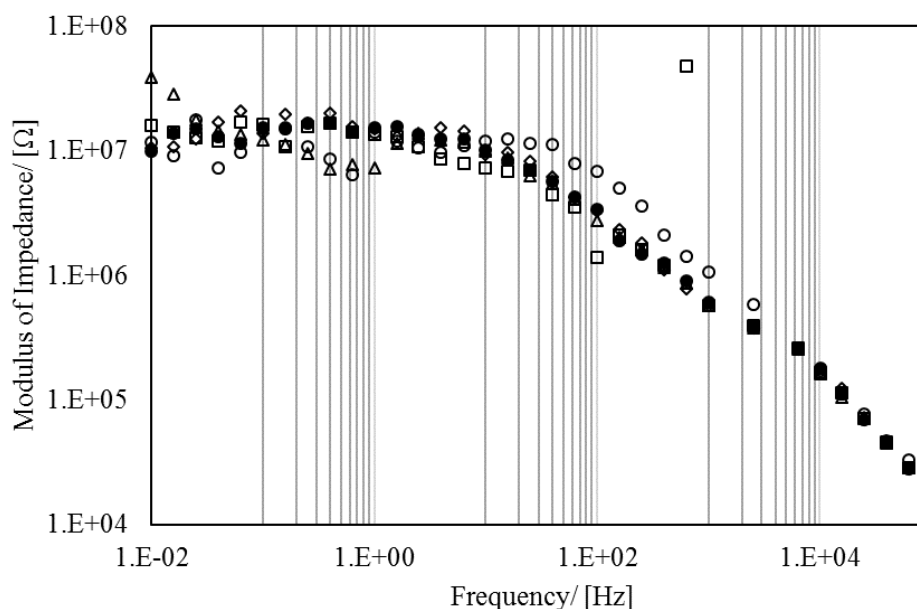
Figure 4-47. Modulus of total impedance as a function of frequency (Bode plot) over the duration of the test. Working Electrode: Sample FFA-2. Test solution: 5 ppm HRSG-02 (○) 5 hours, (●) 15 hours, (□) 35 hours, (△) 50 hours, (◊) 60 hours.

Although in both the tests, SEM images revealed that there were regions without any deposit or surface coverage, the impedance behavior was not similar to a partially covered electrode. The impedance response indicated the presence of surface coatings or layers. This could be due to the presence of an organic film in the surface altering the impedance response of the substrate.

Identifying the Offline Protection Offered by HRSG-02

In addition to monitoring the interface at 300 °C, *in situ* EIS was also used to monitor the metal solution interface in the 'filming amine + magnetite' environment over a range of temperatures. Impedance measurements were made at 100 °C and 200 °C during the ramp up to 300 °C and also during the cool down after the 65-hour exposure. This data provides information about the metal solution interface before and after the exposure at 300 °C. In both the 2.5 ppm HRSG-02 and the 5 ppm HRSG-02 tests, the magnitude of the impedance at 100 °C and 200 °C after the exposure at 300 °C was multiple orders of magnitude higher than what was measured at the temperature before the exposure at 300 °C.

Figure 4-48 is a Bode plot showing the impedance magnitude at 100 °C and 200 °C during ramp up to and ramp down from 300 °C for Sample FFA-1. The impedance magnitudes at 100 °C and 200 °C, are in hundreds of ohms before exposure at 300 °C and range between 1 MΩ and 100 MΩ after the exposure. This indicates a change occurring at the interface between 200 °C and 300 °C, which is not reversible by simply reducing the temperature.
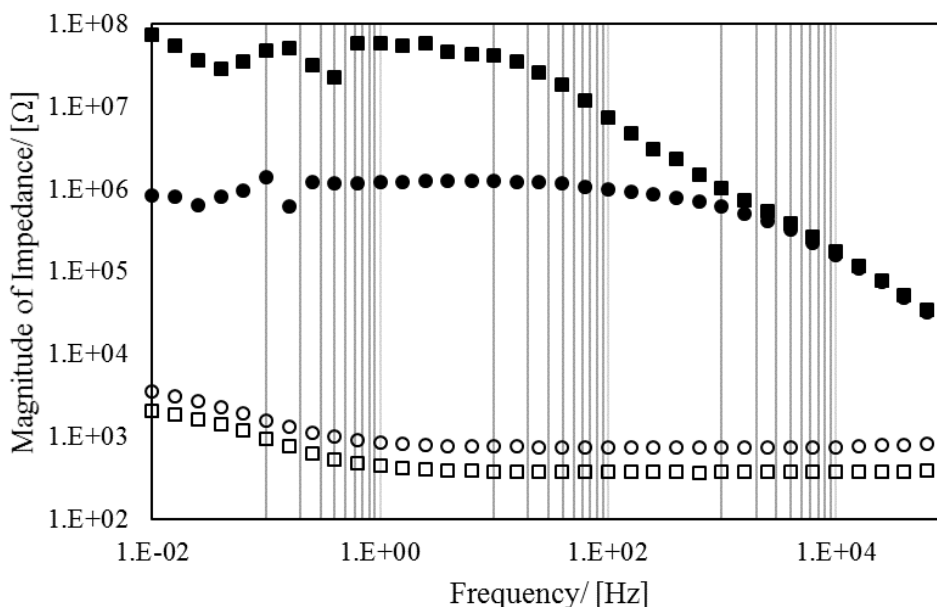
Figure 4-48. Modulus of total impedance as a function of frequency (Bode plot) at 100 °C and 200 °C during ramp up to and ramp down from 300 °C. The effect of the filming amine at different temperatures, before and after exposure at 300 °C is clearly identified. Time of exposure at 300 °C: 65 hours. Working Electrode: FFA-1. Test solution: 2.5 ppm HRSG-02, (○)100 °C Ramp up, (●) 100 °C Ramp down, (□) 200 °C Ramp up, (■) 200 °C Ramp down.

A similar behavior was observed for Sample FFA-2. The Bode plots are shown in Figure 4-49. Even with some noise in the measurements post exposure, it can be seen that after exposure at 300 °C, the impedance of the surface is in the order of mega ohms at 100 °C and 200 °C. The impedance response clearly enables us to identify the action of the magnetite and/or HRSG 02 filming amine at the interface. It can be said that the deposition and film formation occur at some temperature between 250 °C and 300 °C. It has previously been shown that magnetite deposits do not detach at lower temperatures. If there is a contribution from the amine film to the impedance, then these results would suggest that the amine film forms above a particular temperature but once formed, will stay on the surface. This could offer valuable corrosion protection when the boiler is offline.
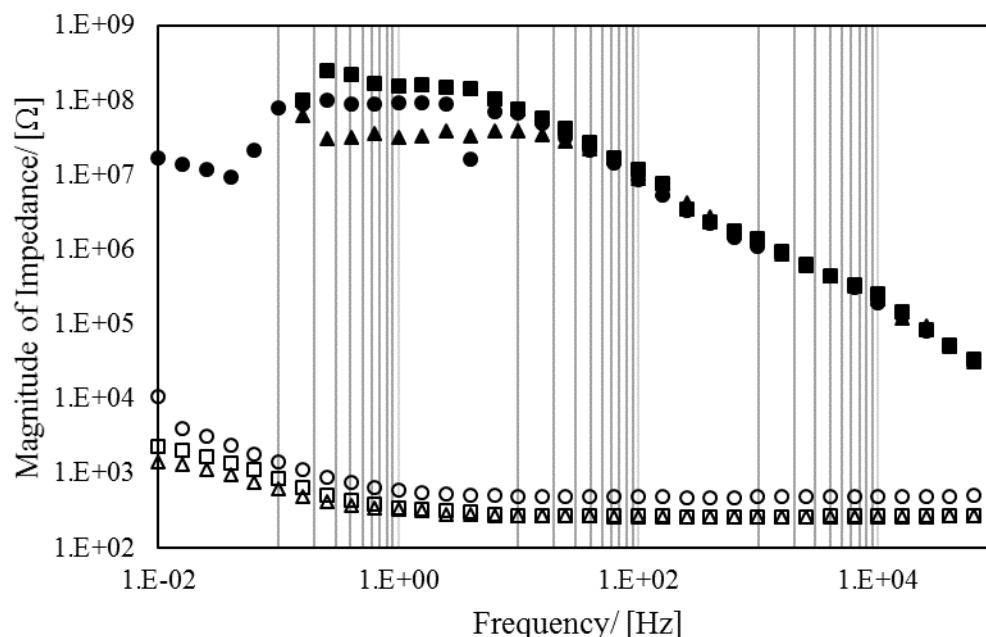
Figure 4-49. Modulus of total impedance as a function of frequency (Bode plot) at 100 °C and 200 °C during ramp up to and ramp down from 300 °C. The effect of the filming amine at different temperatures, before and after exposure at 300 °C is clearly identified. Time of exposure at 300 °C: 65 hours. Working Electrode: FFA-2. Test solution: 5 ppm HRSG-02, (○)100 °C Ramp up, (●) 100 °C Ramp down, (□) 200 °C Ramp up, (■) 200 °C Ramp down.

In situ EIS offers an easy way of monitoring the interface in the HRSG-02 + magnetite environment. However, there are caveats in these inferences. These tests were performed in an environment with both HRSG-02 product and suspended magnetite. Considering there is deposition on the surface, a part of the high impedance could be a contribution of the magnetite coating on the surface in addition to a protective film. Also, the solution chemistry of HRSG-02 at high temperatures is unclear. If the product breaks down or decomposes irreversibly into compounds which make the conductivity of the solution very low, then the impedances in a Bode plot would be high.

Effect of Increased Particle Size on Deposition

In the following sections, Test A and Test B are defined as follows,

- Test A: AVT $pH_{25°C}$=9.3 using $NH_4OH(aq)$, magnetite particle size 50-100 nm. Sample AVT-1.
- Test B: AVT $pH_{25°C}$=9.3 using $NH_4OH(aq)$, magnetite particle size < 5 μm. Sample AVTPS.

Tests with different particle size provide insight into the deposition mechanism as particle-particle interaction forces are also dependent on the size or the interacting particles. Test B, as defined here, provides a contrasting condition compared to Test A. It can also be said that Test B, with a wider particle size distribution presents a more realistic picture of the boiler environment where particle sizes are not controlled.

Increased Particle Size: Visual Observations

The tests showed that a greater particle size reduced the deposition on the surface of the substrates. Figure 4-50 is an optical photograph of the sample AVTPS tested in Test B in comparison with the sample AVT-1 from Test A. It can be seen from the image that conditions in Test A resulted in complete surface coverage with magnetite. When the particle size was increased to a distribution of <5 μm, Test B, the substrate was only partially covered with magnetite deposits indicating a reduction in deposition. Visual observations show regions of good (high deposition) and poor (no deposition) surface coverage on the substrate and surface analyses can provide more evidence. Given that the solution chemistry and the exposure time was the same in Test A and Test B, the partial coverage can be construed as reduced deposition or lower rate of deposition and can be considered as an effect of the increased particle size in suspension.
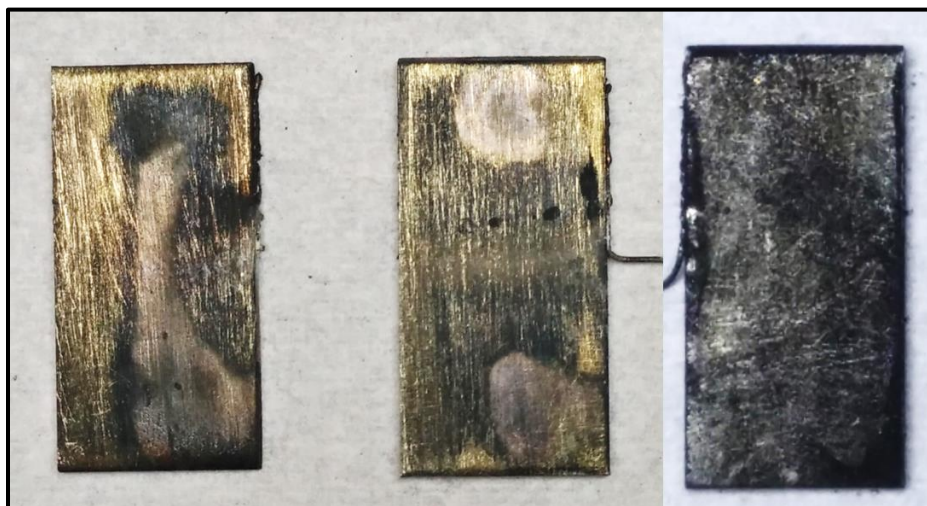
Figure 4-50. Optical Photograph of the samples from Test B and Test A: Left and middle: sample AVTPS (from Test B) and right: Sample AVT-1(from Test A). Exposure time = 65 hours. Temperature 300 °C.

Increased Particle Size: Microscopy & Surface Analysis

As with the earlier tests, surface analyses with SEM and EDS were carried out to corroborate the visual observations. All the SEM images shown here are of sample AVTPS, from Test B, with the higher particle size suspension of magnetite. Visual observations indicated partial deposition on the surface-regions with and without magnetite deposits on the surface. Both these regions were examined under the SEM. Figure 4-51 shows the surface of the sample AVTPS imaged at 5000x in a region where deposition was observed. The image shows high surface coverage with magnetite particles. The characteristic octahedral shape of magnetite crystals can be observed at a higher magnification, as shown in Figure 4-52.
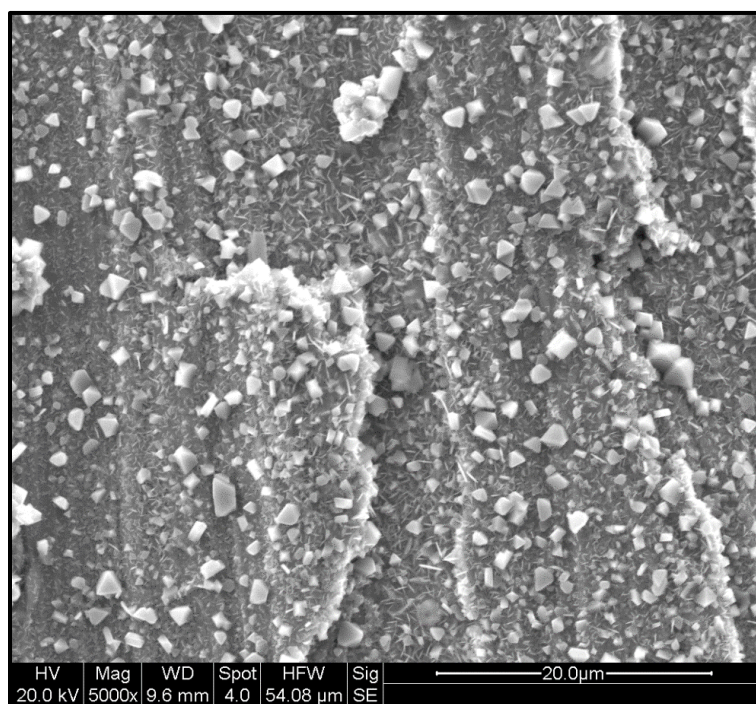
Figure 4-51. Secondary Electron Image (5000x) of sample AVTPS showing octahedral magnetite particles covering the surface. Test solution is $pH_{25\,°C} = 9.3$ $NH_4OH(aq)$. Test B: Particle size distribution < 5µm. Exposure time = 65 hours. Temperature 300 °C.
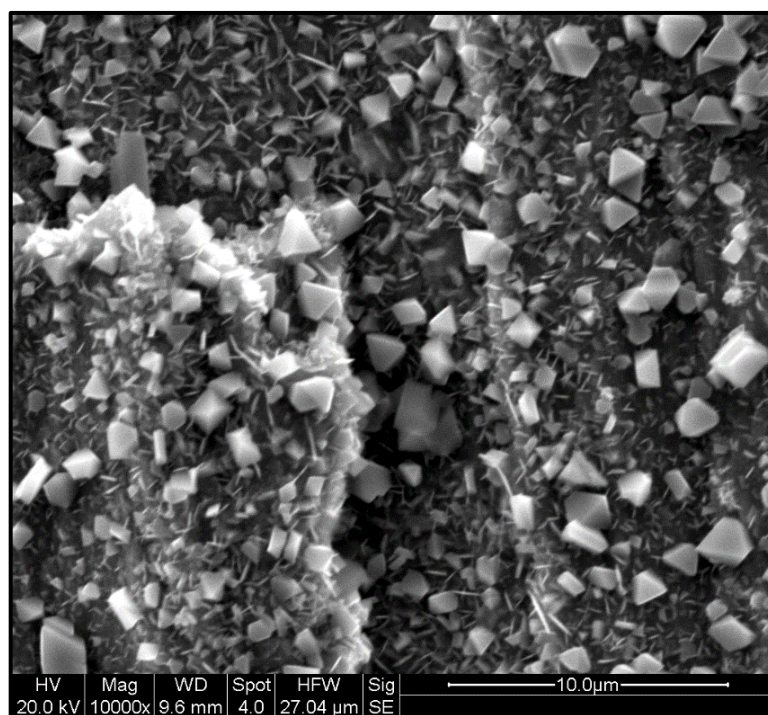
Figure 4-52. Secondary Electron Image (10000x) of sample AVTPS showing magnetite particles covering the surface. Test solution is $pH_{25\ °C} = 9.3$ NH$_4$OH(aq). Test B: Particle size distribution < 5μm. Exposure time = 65 hours. Temperature 300 °C.

Figure 4-53 shows the surface at 5000x in a region of the substrate where no deposition was observed. It can be observed that the surface coverage in this region is very poor. A few particles can be seen on the surface, however there is big contrast in the appearance when compared to Figure 4-51. Doubling the magnification to 10000x, as shown in Figure 4-54, also showed no hints of deposition or high surface coverage. The rod like particle on the surface of sample AVTPS in Figure 4-54 can be attributed to the purity of the magnetite powder used (95% pure commercial magnetite). These images corroborate with visual observation that the substrates showed regions of high and poor surface coverage.
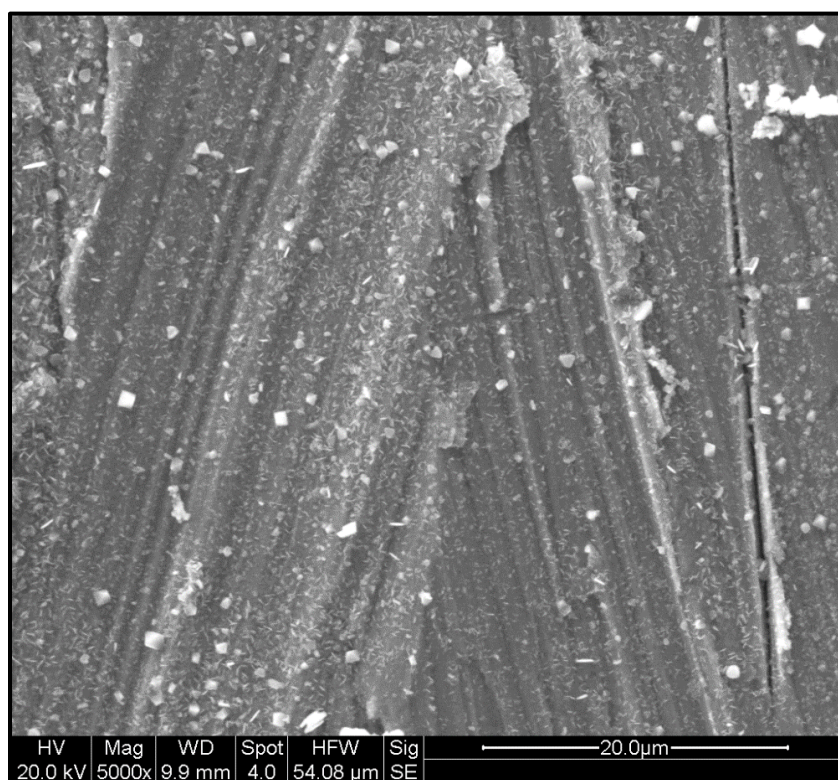
Figure 4-53. Secondary Electron Image (5000x) of the sample AVTPS showing negligible or sparse surface coverage. Region corresponding to little or poor coverage on the sample. Test solution is $pH_{25\ °C}$ = 9.3 NH4OH(aq). Test B: Particle size distribution < 5μm. Exposure time = 65 hours. Temperature 300 °C.
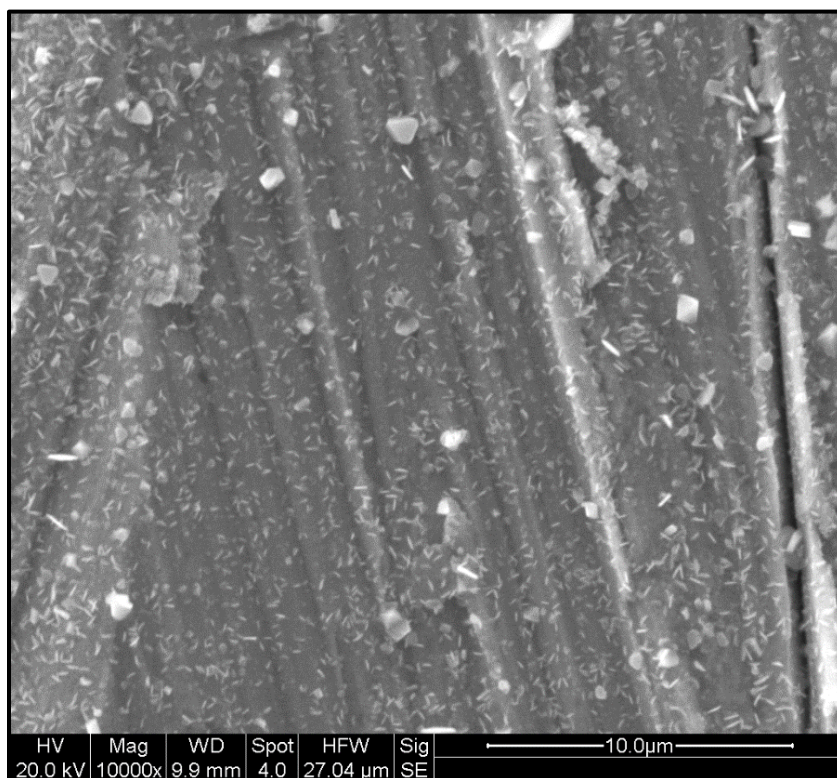
Figure 4-54. Secondary Electron Image (10000x) of the sample AVTPS showing negligible or sparse surface coverage. Test solution is $pH_{25\,°C} = 9.3$ NH$_4$OH(aq). Test B: Particle size distribution < 5μm. Exposure time = 65 hours. Temperature 300 °C.

Formation of Clusters/Aggregates on the Substrate

Surface analyses of the substrate (sample AVTPS) revealed the presence of multiple clusters on the surface. These clusters were observed in both regions of high surface coverage and poor surface coverage. Figure 4-55 and Figure 4-56 are examples of both cases showed particle aggregates on the surface in different regions. The presence of these aggregates can be explained by the increased particle size in the system. Such aggregates were not observed on the surface in the initial tests, where the magnetite particle size was 50-100 nm. Based on the theories of particle aggregation, the rate of aggregation or agglomeration increases as the particle size increases. Hence, the increased particle size will increase the aggregation rate thereby leading to the formation of clusters and aggregates of particles in the system.

Figure 4-55. Secondary Electron Image (3000x) of the sample AVTPS showing a cluster of particles in a region with deposits. The clusters are agglomerates of smaller particles. Test solution is $pH_{25 °C} = 9.3$ $NH_4OH(aq)$. Test B: Particle size distribution $< 5\mu m$. Exposure time = 65 hours. Temperature 300 °C.
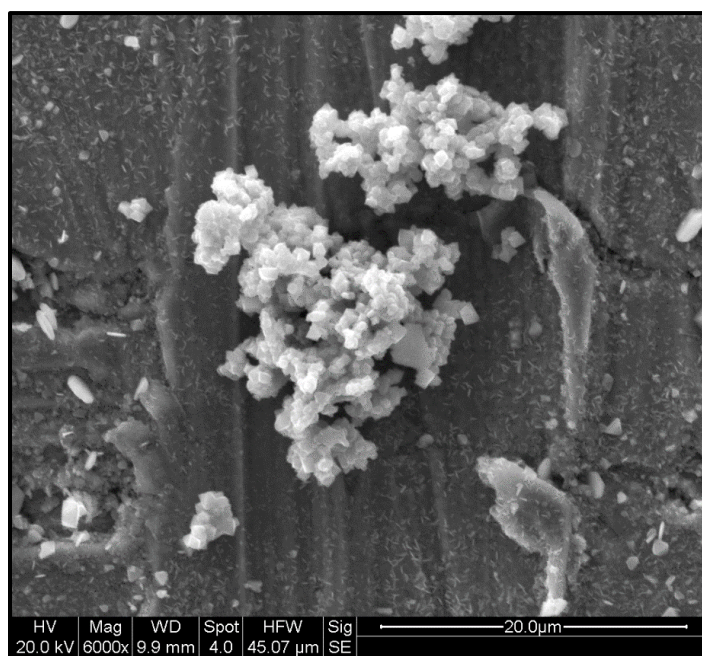
Figure 4-56. Secondary Electron Image (6000x) of sample AVTPS showing a cluster of particles in a region of the sample where deposition was sparse. Test solution is $pH_{25 °C} = 9.3$ $NH_4OH(aq)$. Test B: Particle size distribution $< 5\mu m$. Exposure time = 65 hours. Temperature 300 °C.

Energy dispersive spectroscopy was used in all cases to verify that the deposits were primarily iron oxides. Considering the controlled environment and the shape of the crystals observed under high magnifications, it can be concluded that the iron oxide deposits are of magnetite.

Increased Particle Size: EIS Results

As with the previous tests electrochemical impedance spectroscopy was used to monitor the substrate solution interface. The magnitude of the impedance values was ~ 200 kΩ lesser than the hydrazine residual tests. This can be correlated to the incomplete surface coverage by the magnetite particles resulting in more of the metal surface exposed to the solution. Figure **4-57** is the Bode plot for the Test B with sample AVTPS as the working electrode. Unlike the hydrazine tests, the bode plots show a distinct dependency on the frequency at the low frequency regions. This could be indicative of a diffusion type behavior at the exposed metal substrate.
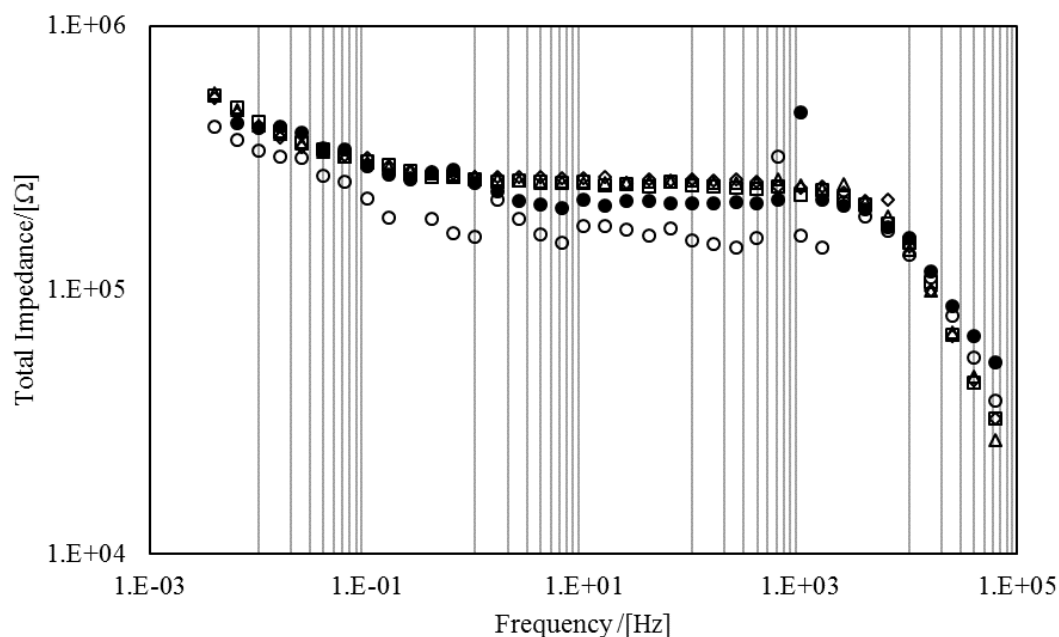
Figure 4-57. Modulus of total impedance as a function of frequency (Bode plot) over the duration of Test B. Working Electrode: Sample AVTPS. Test solution: $pH_{25°C} = 9.3$, Magnetite Particles: < 5μm, (○) 10 hours, (●) 28 hours, (□) 50 hours, (Δ) 55 hours, (◊) 60 hours.

It can be noted that the impedance measurements towards the end of the exposure test are less noisy and closer to a steady state value. Further examination of these points is provided in Figure 4-58 in the form of a Nyquist plot. The shape of the Nyquist plot here resembles the impedance response expected in the case of a partially covered electrode. In the conditions tested here, this would translate to a case where the 304 SS substrate is partially covered with magnetite deposits.
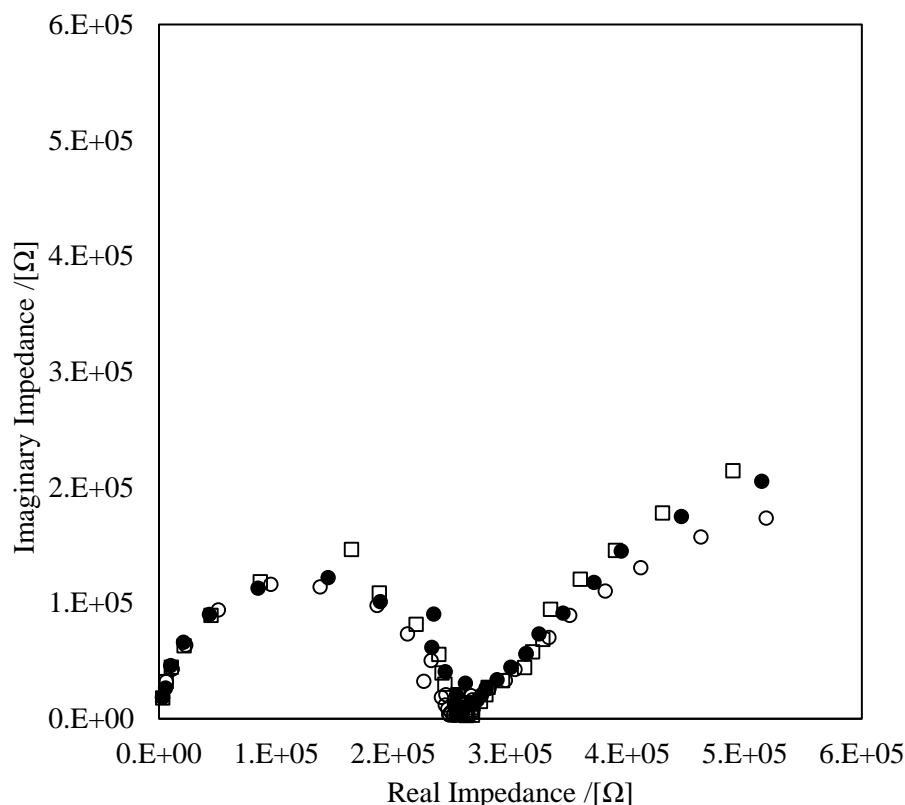
Figure 4-58. Nyquist plot of the impedance response towards the end of Test B. Nyquist plots indicative of partially covered surface. Working Electrode: Sample AVTPS. Test solution: $pH_{25°C}$ = 9.3, Magnetite Particles: < 5μm, (○) 50 hours, (●) 55 hours, (□) 60 hours

Considering the increased rate of aggregation due to high particle size, it is possible that all the particles settled at the bottom of the autoclave, leaving a negligible number of particles in suspension. This can have two significant effects. Firstly, removing the source of the particles, i.e. lack of suspended particles, will prevent further deposition on the 304 SS substrate. Secondly, if the suspended magnetite particles were affecting the impedance response by interfering with the electric field, the lack of any such particles will lead to a less noisy response. The EIS results shown here corroborate the visual observations and surface analyses.

Chapter 5

Interaction Energy Calculations for Quantifying Magnetite Deposition on 304 Stainless Steel in Boilers

Introduction

The Deraguin-Landau-Verwey-Overbeek (DLVO) theory of colloidal stability is frequently used to predict the colloidal stability of particle suspensions in aqueous solutions [1–4]. The DLVO theory states that the total interaction energy of the suspended particles is equal to the sum of attractive van der Waals and repulsive electrostatic interactions in a system [1,5,6]. Deposition in boilers occurs due to the presence of suspended oxide nanoparticles in the boiler water [7,8]. Boilers and steam generators are interesting physicochemical environments in terms of their varying water treatment chemistry, temperature and nature of the suspended particles. Although well established, DLVO interaction energy calculations have not been extended to boiler environments to understand the deposition and fouling issues that occur frequently. The goal here is to use the DLVO theory to quantify and understand the particle-particle and particle substrate interactions which govern the aggregation and deposition of oxide nanoparticles in different boiler water treatment chemistries. This is an extension to the experimental work presented in the previous sections. The focus of this work is the deposition of magnetite on 304 stainless steel in boiler water subject to the all-volatile treatment (AVT) regime [7]. The interaction energy calculations provide information regarding the stability of the magnetite particles in boiler water and their affinity to deposit or agglomerate. This information enhances the ability to identify the ranges within the operating limits of boiler water treatment chemistry, where deposition is expected. This data in addition to experimental results will provide valuable information to boiler operators on tuning the boiler water chemistry to minimize and mitigate deposition.

Methodology

DLVO Theory and Equations

DLVO theory stipulates that the stability of a suspended nanoparticle depends on the balance between the attractive and repulsive forces. The attractive van der Waals forces are a result of the interactions between fluctuating or permanent dipoles for molecular and macroscopic bodies close to each other [5,6]. The magnitude of the attractive van der Waals (vdW) interaction energy depends on the Hamaker constant, A, and the distance between the two bodies in consideration. The vdW interaction energy decreases as separation distance between particles increases [5]. The Hamaker constant depends on the particle and solvent properties like dielectric constant and refractive index, for a given nanoparticle suspension [1,2,5]. vdW forces between similar particles in a medium is always attractive and this attractive interaction dominates when the suspended particles are uncharged [5]. Particles suspended in polar media are often charged and because of the surface charges, a repulsive interaction exists. When attractive van der Waals forces dominate at short distances, and the suspension is not colloidally stable. When there is sufficient contribution from the repulsive interactions, a high enough energy barrier to agglomeration is created. Based on DLVO theory of colloidal stability, ~15 kT is considered to be a high enough interaction energy barrier to keep the colloid stable and prevent agglomeration [3].

The vdW interaction energy was calculated using the following expression [5],

$$W_A = -\frac{A}{12D}\left(\frac{d_1 d_2}{d_1 + d_2}\right)$$ (1)

W_A, is the attractive interaction energy due to vdW forces in J, A is Hamaker constant in J, d_1 and d_2 are the diameters of particle 1 and particle 2 respectively in nm. D, is the distance of separation between the two bodies in nm.

When studying magnetite deposition in boilers, both magnetite-magnetite particle interactions and magnetite-substrate interactions come into play. The vdW attractive interaction energy for two similar particles breaks down into,

$$W_A = -\frac{Ad}{24D}$$ (2)

d, is the diameter of the particles in nm.

When calculating the particle-substrate interaction energy, the flat substrate is considered to be a spherical particle with very large diameter. In Eq. (1), $d_1 << d_2$, and Eq. (1) can be approximated to,

$$W_A = -\frac{A d_1}{24 D} \tag{3}$$

The Hamaker constant depends on the materials (magnetite and steel) and the medium (aqueous electrolyte) in the system. The Hamaker constant for the magnetite-water-magnetite system is denoted as A_{131}. Similarly, the Hamaker constant for the stainless steel-water-stainless steel system is denoted as A_{232}. To obtain the Hamaker constant for the magnetite-water-stainless steel system the following combining relationship was used [5],

$$A_{132} = \sqrt{A_{131} A_{232}} \tag{4}$$

The electrostatic repulsive interaction energy for particle-substrate interaction was calculated using the following expression [9],

$$W_R = \frac{\pi \varepsilon_o \varepsilon_3 d_1 d_2}{2(d_1 + d_2)} \left[(\psi_1^2 + \psi_2^2) \ln(1 - e^{-2\kappa D}) + 2\psi_1 \psi_2 \ln\left(\frac{1 + e^{-\kappa D}}{1 - e^{-\kappa D}}\right) \right] \tag{5}$$

W_R, is the electrostatic repulsive interaction energy in J, d_1 and d_2 are the diameters of particle and substrate respectively in nm. Since the substrate is assumed to be a very large spherical particle, $d_1 << d_2$. D, is the distance of separation between the two bodies in nm. ε_o, is the dielectric permittivity of vacuum, $8.854 \ 10^{-12}$ F/m. ε_r, is the dielectric constant of water at a given temperature. ψ_1 is the zeta potential of magnetite in V. ψ_2 is the zeta potential of stainless steel in V. κ, is the inverse Debye length for the given physicochemical environment in m^{-1}, calculated using the following equation,

$$\kappa = \sqrt{\frac{2 N_A e^2 I}{\varepsilon_0 \varepsilon_3 k T}} \tag{6}$$

I, is the ionic strength of the aqueous medium in mol m^{-3}.N_A, is the Avagadro's number 6.023 10^{23} mol^{-1}. *e*, is the elementary charge 1.602 10^{-19} C. *k*, is the Boltzmann constant 1.380 10^{-23} J K^{-1}. *T*, is the absoute temperature in K.

Key physiochemical parameters like pH, ionic strength and temperature are tied into Eq. (5) via the ψ and κ values.

For the magnetite-magnetite particles interactions, $d_1 = d_2 = d$ and $\psi_1 = \psi_2 = \psi$. Eq. (5) now becomes,

$$W_R = \pi d \varepsilon_o \varepsilon_3 \psi^2 \left[ln(1 - e^{-2\kappa D}) + ln\left(\frac{1+e^{-\kappa D}}{1-e^{-\kappa D}}\right) \right] \tag{7}$$

The total interaction energy is the sum of the attractive and repulsive interaction energies,

$$W_T = W_A + W_R \tag{8}$$

Suspended metal oxides develop surface charges based on the pH, ionic strength and composition of the boiler water. The change in the physicochemical environment will affect the magnetite-magnetite particle interactions as well as magnetite-steel interactions. This will be reflected in W_T through changes in W_R.

The agglomeration probability, α, for the different cases was calculated using the following expression [10],

$$\alpha = \frac{\left(\int_2^\infty \left(\frac{\exp\left[\frac{W_A}{kT}\right]}{s^2} \right) ds \right)}{\left(\int_2^\infty \left(\frac{\exp\left[\frac{W_T}{kT}\right]}{s^2} \right) ds \right)} \tag{9}$$

Where, $s = 2D/d$, *D* being the distance between the bodies and *d* being the diameter of the particles.

The DLVO interaction energy calculation were carried out in Excel spreadsheets used for similar purposes by Tabakovic (2015) [1] and Tang (2016) [2]. Numerical integration was used to compute the numerator and denominator terms for Eq. [9].

Input values for interaction energy calculations

The physicochemical conditions considered for the DLVO calculations closely match the test conditions in the experimental part of this research. The size range of the magnetite particles used in the experimental study was 50-100 nm. Staying within the particle size range, the interaction energy calculations were made for particle sizes of 50 nm, 75 nm and 100 nm. The boiler water treatment chemistry considered in this study was the traditional all volatile treatment (AVT), where the boiler water pH is controlled using ammonium hydroxide. Typically, in the AVT regime, the pH of the boiler water is maintained between 9.3 – 10.0, measured at 25 °C. The experiments were run at a temperature of 300 °C and a pressure of 100 bar (10 MPa) closely simulating a boiler environment. Raman et al. (2016) experimentally investigated the deposition of magnetite on 304 stainless steel in the lower end of the AVT operating range, $pH_{25°C} = 9.3$ [7]. For the interaction energy calculations, the lower and upper operating limits of the AVT regime were considered. Table 5-1 summarizes the aqueous parameters of the AVT regime at 25 °C and 300 °C. The ionic strength, I, of the boiler water and $pH_{300°C}$ were calculated using OLI Analyzer. The calculations are described in Chapter 2.

Table 5-1 Summary of the AVT aqueous environment

Test Condition	Chemical Used	$pH_{25°C}$	$pH_{300°C}$	$I_{25°C}$ [mol/kg]	$I_{300°C}$ [mol/kg]
AVT-Low	NH_4OH (4.4 10^{-5} mol kg^{-1})	9.3	5.8	2.050 10^{-5}	3.660 10^{-6}
AVT-High	NH_4OH (32 10^{-5} mol kg^{-1})	9.8	6.2	6.740 10^{-5}	1.002 10^{-5}

The ionic strength values listed in Table 5-1 were used in the calculation of κ at the respective temperatures. The zeta potentials for magnetite and steel at the corresponding pH values were obtained either directly from literature or by extrapolating data from literature. Table 5-2 lists the values of physical constants and other parameters used for the DLVO calculations.

Table 5-2 List of parameters and physical constants used for DLVO calculations.

Parameter	Value	Source
A_{131}	30 X 10^{-20} J	[11]
A_{232}	2.88 x 10^{-19} J	[12]
A_{132}	2.93 x 10^{-19} J	Eq. [4]
ε_3 at 298.15 K	78	NIST Database
ε_3 at 573.15 K	21	
ε_o	8.854 x 10^{-12} F/m	
k_B	1.38 x 10^{-23} J K^{-1}	
e	1.6021 x 10^{-19} C	
$\psi_{magneite}$ (AVT Low and AVT High at 25 °C)	~-40 mV	[13] [14]
ψ_{steel} (AVT Low and AVT High at 25 °C)	~-43mV	[15]
$\psi_{magneite}$ (AVT Low 300 °C)	0 ± 5 mV	Close to IEP [16,17]
$\psi_{magneite}$ (AVT High 300 °C)	-113 mV	Values extrapolated from [16,17]
ψ_{steel} (AVT High 300 °C)	Range of ZP values from 0 mV to -110 mV tested	

The zeta potential values listed in Table 5-2 were obtained from literature for corresponding pH values at given temperatures. Although the different studies used different background electrolytes, all the electrolytes were indifferent electrolytes and there was not specific adsorption. Vidojkovic et al. (2011) [16] experimentally measured the zeta potential of magnetite particles as function of pH at different temperatures up to 200 °C. The study showed that the zeta potential of magnetite increases with temperature. For obtaining the zeta potential of magnetite at 300 °C, the results from this study were linearly extrapolated up to 300 °C. Due to the lack of experimental zeta potential values at 300 °C, the extrapolation is the closest approximation of zeta potential values that can be obtained at 300 °C. It must also be pointed out that the ionic strength of the background electrolyte used by Vidojkovic et al. (2011) [16] is higher than the ionic strength of the boiler water subject to AVT chemistry. The reduction in

ionic strength will increase the zeta potential of magnetite leading to greater repulsive interaction. So, the values obtained via extrapolation are very conservative estimates of the zeta potential of magnetite at 300 °C. For the zeta potential values of stainless steel at 300 °C, due to lack of experimental data, a range of zeta potential values from 0 mV to -100 mV was used.

Results & Discussion

The DLVO interaction energy calculations were performed for two different AVT chemistries, AVT-Low, with 4.4×10^{-5} mol kg^{-1} of NH$_4$OH(aq) and AVT-High, with 32×10^{-5} mol kg^{-1} of NH$_4$OH(aq). For each chemistry, both magnetite-magnetite interactions and magnetite-steel interactions were investigated. The interaction energies are represented in units of kT and are plotted versus distance of separation between the two bodies. Staying within the 50-100 nm particle size used in the experiments, all the calculations were performed for particle diameters of 50 nm, 75 nm and 100 nm.

AVT-Low: 4.4×10^{-5} mol kg^{-1} of NH$_4$OH(aq), pH$_{25°C}$ = 9.3

Magnetite-Magnetite Particle Interactions

The magnetite-magnetite particle interaction energies were calculated using Eq. [1], Eq. [7] and Eq. [8]. Figure 5-1 is a plot of the total interaction energy versus separation for magnetite-magnetite particle interactions at 25 °C for the AVT-Low water chemistry. There is an energy barrier greater than 15 kT for the particle size range investigated here. The particles will have to surmount this energy barrier to agglomerate. The plot indicates that this condition is not suitable for particle-particle agglomeration. The attachment efficiency for all the particle diameters is 0%.
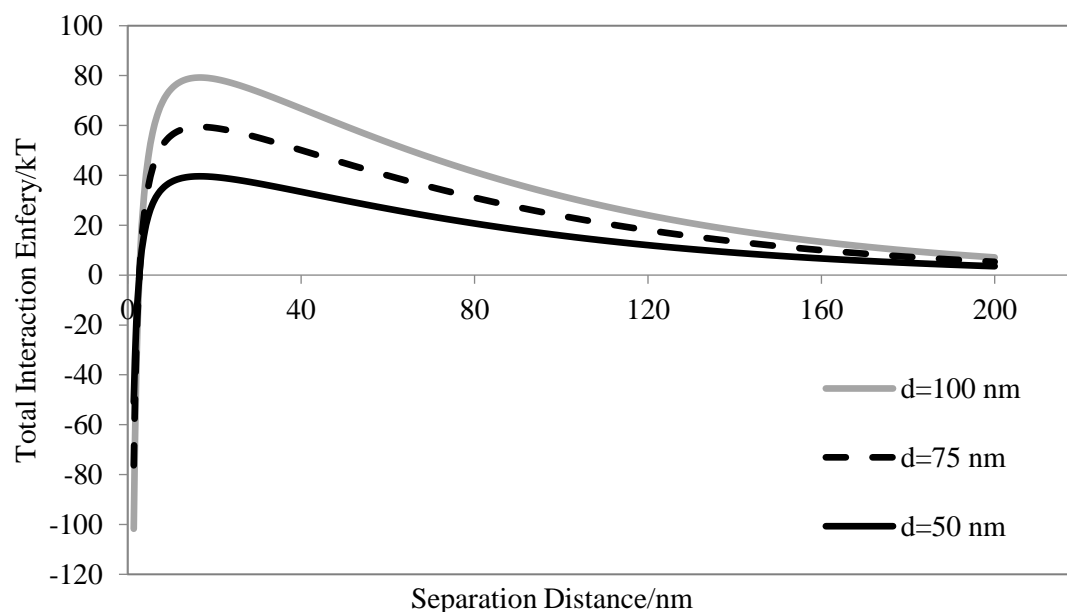
Figure 5-1. Total interaction energy versus separation distance for magnetite-magnetite particle interactions at 25 °C and AVT-Low water chemistry. d is the diameter of the particles in nm. There is an energy barrier to agglomeration for the entire particle size range. The attachment probability is 0 % for all three particle diameters.

This result can be explained by the fact that at ambient conditions at a pH of 9.3, all the magnetite particles have a negative surface charge and as a result a negative zeta potential [17–20]. This will maintain a strong repulsive interaction between the particles, preventing agglomeration.

However, the temperature of interest here is the boiler operating temperature of 300 °C. The pH of the boiler water at 300 °C is very different from the pH at 25 °C. In the AVT Low case, a $pH_{25°C}$ = 9.3 using $NH_4OH(aq)$ corresponds to a pH of 5.8 at 300 °C [7]. This is very close to iso-electric point (IEP) of magnetite at 300 °C [16,17]. At the IEP, the zeta potential of the material is 0 mV. Figure 5-2 is a plot of the total interaction energy versus separation distance for magnetite-magnetite interactions at 300 °C for the AVT Low chemistry, taking the zeta potential of the magnetite particles to be 0 mV. In contrast to Figure 5-1, all the curves drop down below the x-axis, with insignificant energy barrier against agglomeration. For all values of separation between the particles, the interaction energy strongly favors agglomeration.
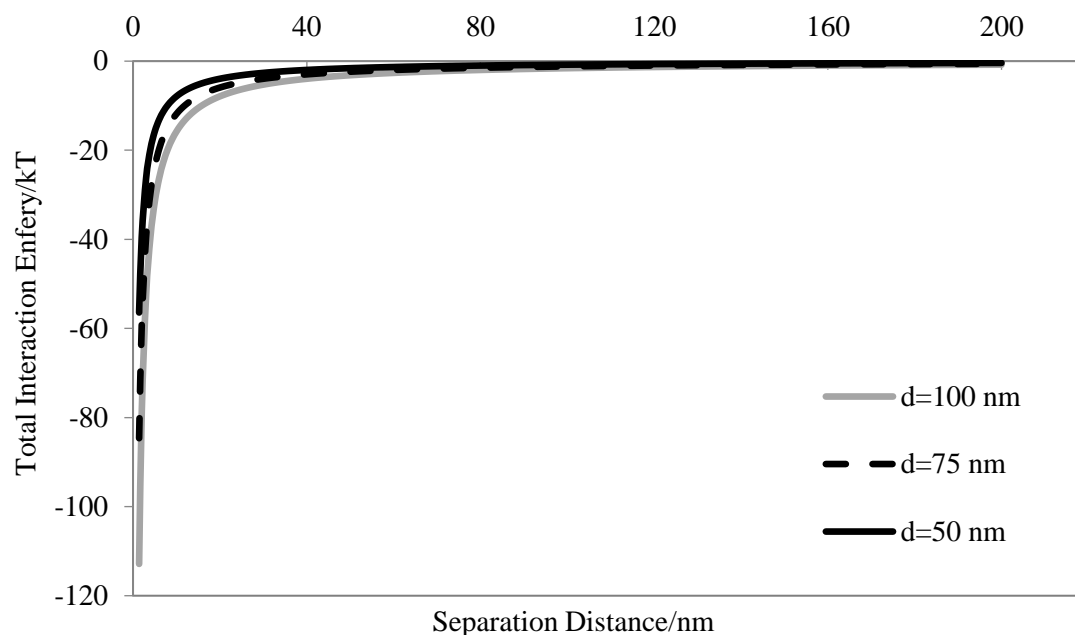
Figure 5-2. Total interaction energy versus separation distance for magnetite-magnetite particle interactions at 300 °C and AVT-Low water chemistry. There is no energy barrier to agglomeration for the entire particle size range. *d* is the diameter of the particles in nm.

At the IEP, since the zeta potential is 0, there is a lack of electrostatic repulsion keeping the particles from agglomerating. This is clearly a condition which favors particle agglomeration as illustrated by Figure 5-2.

Due to uncertainties in experimental data, the agglomeration probability for this case was calculated for a range of zeta potential values of magnetite. The agglomeration probability calculations were performed using 0 ± 5 mV as the zeta potential of magnetite. Figure 5-3 shows the calculated agglomeration probability (as percentage) values for magnetite-magnetite interactions for different values of magnetite zeta potential for the AVT Low treatment chemistry at 300 °C.
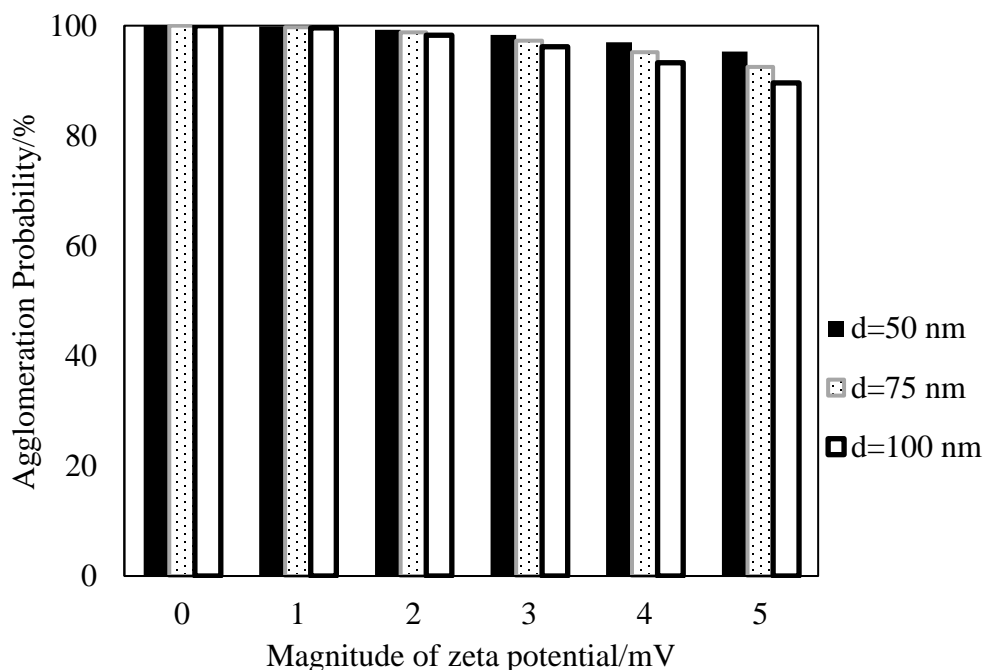
Figure 5-3. Calculated agglomeration probability values for magnetite-magnetite interactions for different values of magnetite zeta potential. AVT Low water treatment chemistry at 300 °C. High value of the agglomeration probability indicates that the environment favors magnetite particle agglomeration.

All the probability values shown in Figure 5-3 are greater than 90%. This shows that being closer to IEP at a given temperature makes the physicochemical environment conducive for agglomeration. In a boiler environment, this would imply that magnetite particles will agglomerate in the bulk solution (boiler water) and that magnetite particles from bulk can deposit on existing magnetite deposits. The results also show how drastically the increase in temperature affects the behavior of suspended particles and emphasizes the importance of studying the phenomena at the temperature of interest.

Magnetite-Steel Interactions

The DLVO interaction energy calculations for magnetite-steel interactions were also carried out for two different temperatures, 25 °C and 300 °C, under the AVT Low chemistry regime. The flat steel substrate was assumed to be a spherical particle with very large diameter and the diameter of the steel substrate was set to be much greater than the diameter of the magnetite particles.

Much like the magnetite-magnetite interactions, at 25 °C, the DLVO interaction energy calculations indicate that there is an energy barrier greater than 15 kT for the deposition of magnetite on steel. This is illustrated in Figure 5-4. Although not as high as the energy barrier in magnetite-magnetite interactions (Figure 5-1), the energy barrier is high enough to keep the magnetite particles suspended and prevent deposition. The data from electrokinetic experiments in literature suggests that at a pH of 9.3, both magnetite and steel have a zeta potential of around -40 mV (Table 5-2). This explains the lack of any attractive interactions and supports the inferences from the DLVO interaction energy curves in Figure 5-4. The calculated agglomeration probability for this condition was 0 % for all the particle sizes.
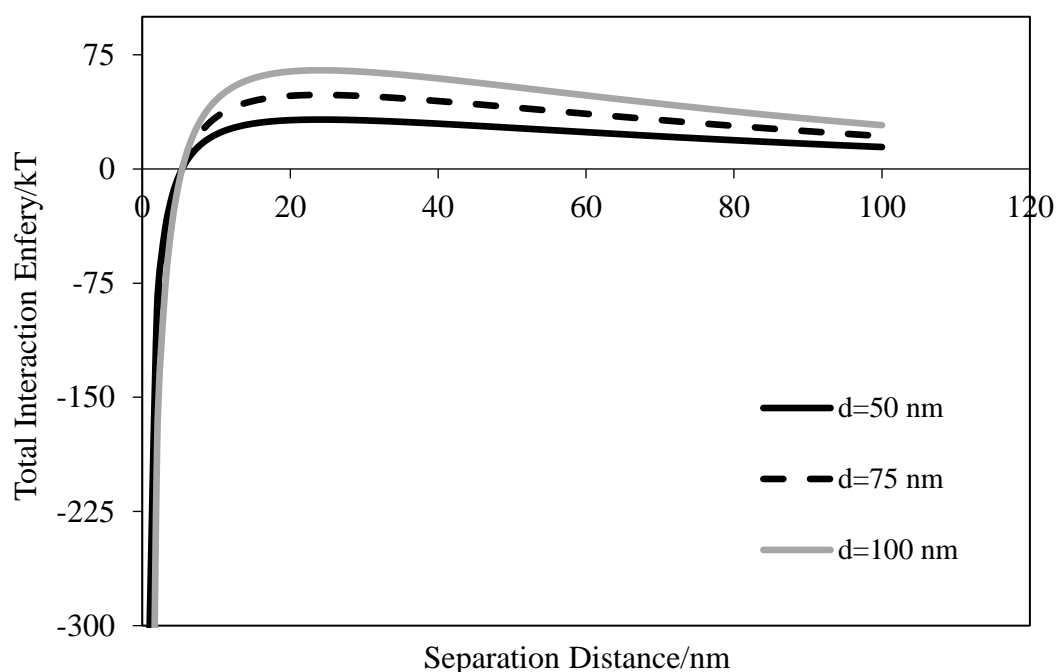
Figure 5-4. Total interaction energy versus separation distance for magnetite-steel interactions at 25 °C and AVT-Low water chemistry. There is an energy barrier to agglomeration for the entire particle size range. *d* is the diameter of the particles in nm.

At 300 °C, the pH of the boiler water corresponds to the IEP of magnetite at 300 °C. For the magnetite-steel DLVO interaction energy calculations, the zeta potential of magnetite was assumed to be 0 mV. Due to the lack of experimental data on the zeta potential of steel at high temperatures, a range of zeta potential values from 0 mV – 100 mV was considered for the steel substrate. Figure 5-5 is a plot of the interaction energy curves versus the separation distance of magnetite-steel interactions at 300 °C under the AVT Low treatment chemistry regime. The

graph is plotted for a magnetite particle diameter of 50 nm and zeta potential of steel ranging from 0 mV to - 100 mV.
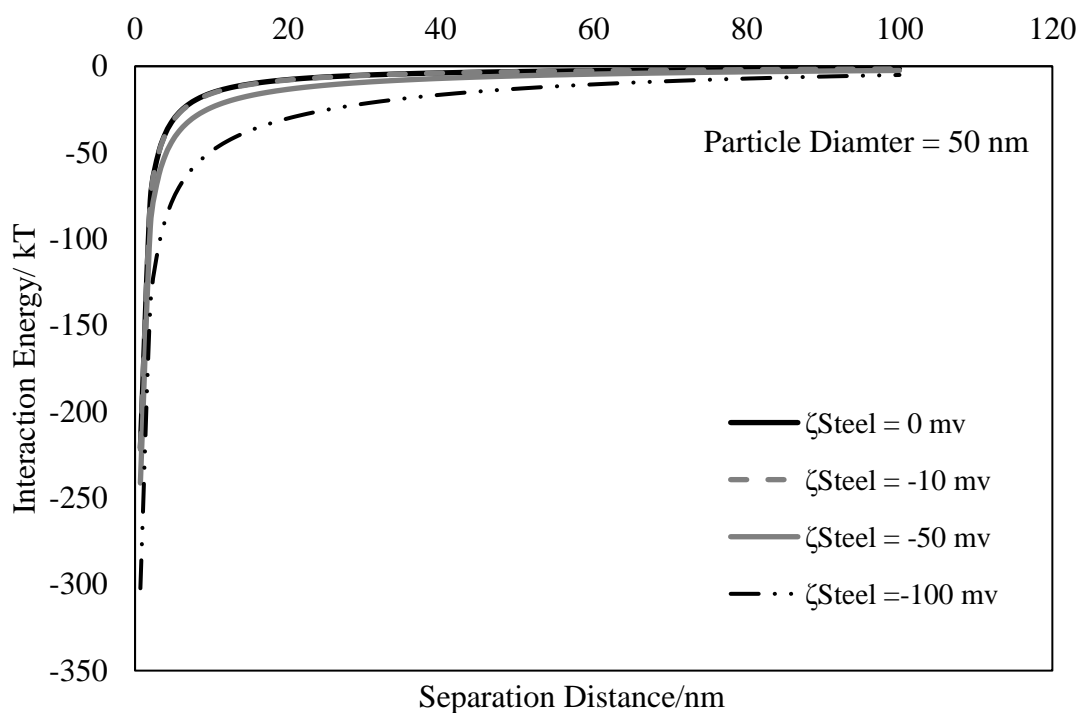
Figure 5-5. Total interaction energy versus separation distance for magnetite-steel interactions at 300 °C and AVT-Low water chemistry. Magnetite particle size = 50 nm. There is an energy no barrier to agglomeration for the entire particle size and zeta potential ranges

The interaction energy curves in Figure 5 indicate that at this condition, there is no barrier to magnetite deposition on the steel substrate. The DLVO interaction energy curves for magnetite particle diameters of 75 nm and 100 nm were similar to the curves in Figure 5. The same range of zeta potential values of steel was used for all particle diameters. None of the cases showed an energy barrier to agglomeration or deposition. Up to a separation distance of 100 nm, the interaction energy between magnetite and steel is negative, implying that adhesion or deposition is favored. The adhesion percentages for all the cases was 100 %. This aligns with the observations from the magnetite-magnetite particle interaction energies. When the zeta potential of magnetite is very close to 0, agglomeration and deposition is favored. The DLVO calculations show that in the AVT Low case at 300 °C, both agglomeration of magnetite and deposition of magnetite on stainless steel will be favored. This inferences from the DLVO interaction energy calculations are in agreement with the results from experiments carried out under the AVT Low regime. The stainless-steel substrate was completely covered with magnetite. The pH of the boiler water under the AVT Low chemistry is close to the IEP of magnetite at 300 °C and as a result

there are repulsive interactions in the system. This causes the agglomeration and deposition of magnetite.

The DLVO calculations for magnetite-steel interactions at 25 °C show that a stable suspension in boiler water at ambient conditions can favor agglomeration and deposition at the operating temperature of 300 °C. This reiterates the need to study such systems, experimentally and theoretically at the operating temperatures, rather than attempt to extrapolate the results from ambient conditions.

AVT-High: 32 x 10^{-5} mol kg^{-1} of NH$_4$OH(aq), pH$_{25°C}$ = 9.8

For the sake of brevity, the DLVO calculations for magnetite-magnetite particle interaction and magnetite-steel interactions under the AVT High chemistry regime at 25 °C are not shown here. The DLVO interaction energies at 25 °C for the AVT High chemistry were similar to the AVT Low chemistry at 25 °C. This is primarily because there is no appreciable change in the zeta potential of magnetite or stainless steel from a pH of 9.3 to a pH of 9.8. The negative zeta potential ensured the presence of repulsive forces between the particles and the particle and the substrate preventing any agglomeration or deposition. Based on these results, it can be extrapolated that the entire AVT regime does not favor agglomeration or deposition at ambient conditions.

Magnetite-Magnetite Particle Interactions

Figure 5-6 is a plot of the total interaction energy [kT] as a function of separation distance [nm] for particle diameters 50 nm, 75 nm and 100 nm under the AVT High water chemistry at 300 °C. The value of zeta potential of magnetite is listed in Table 2 along with the other parameters used. Unlike the AVT Low chemistry, the total interaction energy curves show an energy barrier to agglomeration at 300 °C and does not favor agglomeration even at close range. The agglomeration probability or attachment efficiency for this system was calculated to be 0.
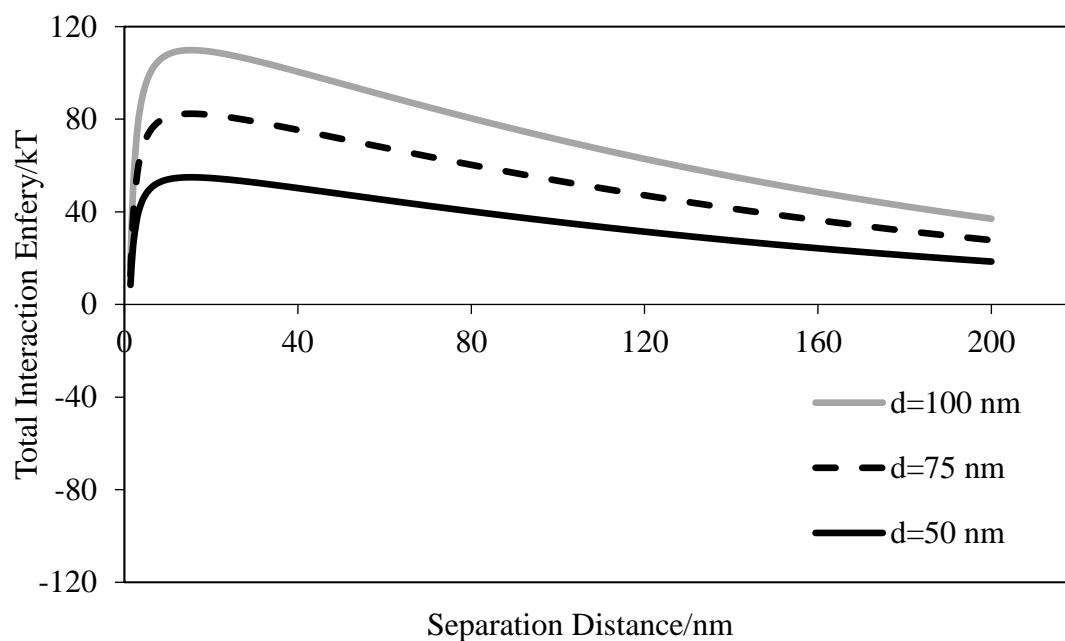
Figure 5-6. Total interaction energy versus separation distance for magnetite-magnetite particle interactions at 300 °C and AVT-High water chemistry. There is a large energy barrier to agglomeration. *d* is the diameter of the particles in nm.

Both the interaction energy curves and the agglomeration probabilities indicate that when the boiler water is condition to the upper end of the AVT operating range (AVT High), there will be no agglomeration of suspended magnetite particles.

Magnetite-Steel Interactions

The approach to quantifying the DLVO interactions between the magnetite and steel was the same as the AVT Low case. Figure 5-7 is a plot of the total DLVO interaction energy as a function of separation distance for 50 nm magnetite particles under the AVT High water chemistry regime. Due to the lack of experimental data regarding zeta potential of steel at high temperatures, a range of zeta potential values from 0 mV to -100 mV was investigated.
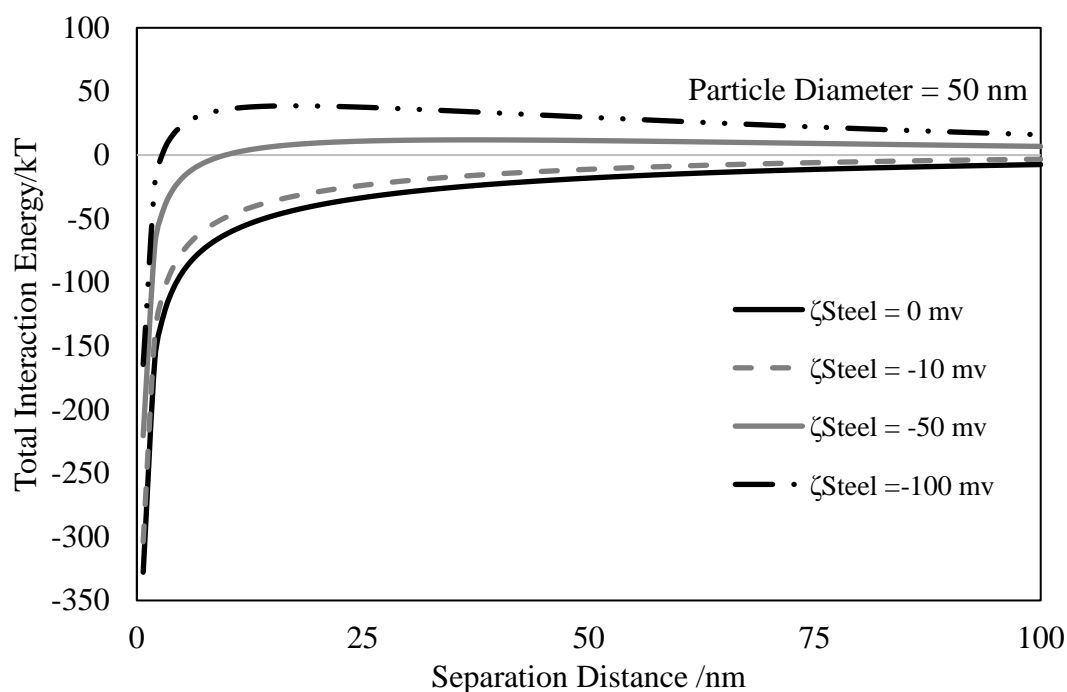
Figure 5-7. Total interaction energy versus separation distance for magnetite-steel interactions at 300 °C for AVT-High water chemistry. Magnetite particle size = 50 nm. Adhesion is favored when the zeta potential magnitude of steel is below ~ 10 mV.

From Figure 5-7, one can see that attractive forces dominate when the zeta potential of steel is close to 0 mV. As the zeta potential of steel increases, the repulsive interactions increase and the interaction energy curves develop a barrier to attraction, in this case adhesion of magnetite on steel. The DLVO interaction energy curves for magnetite particle diameters of 75 nm and 100 nm were similar to the curves in Figure 5-7 and are not shown here.

The agglomeration probabilities were calculated for all the above cases, three different particle sizes and four different zeta potential values of steel. Figure 5-8 is a plot of the agglomeration probabilities (as percentages) for magnetite adhesion on steel for the different zeta potential values of steel considered in this study. This representation paints a more complete summary of the system than the individual interaction energy curves. For zeta potential values of -50 mV and -100 mV, the agglomeration probability is 0 % indicating lack of deposition of magnetite on steel. If the steel is at its IEP, a zeta potential of 0 mV, the environment favors deposition of magnetite on steel. At zeta potential values close to IEP, ~ -10 mV, the agglomeration probability varies between 50-90 % based on the particle size. This indicates that at zeta potential values of -10 mV deposition will not be completely mitigated.
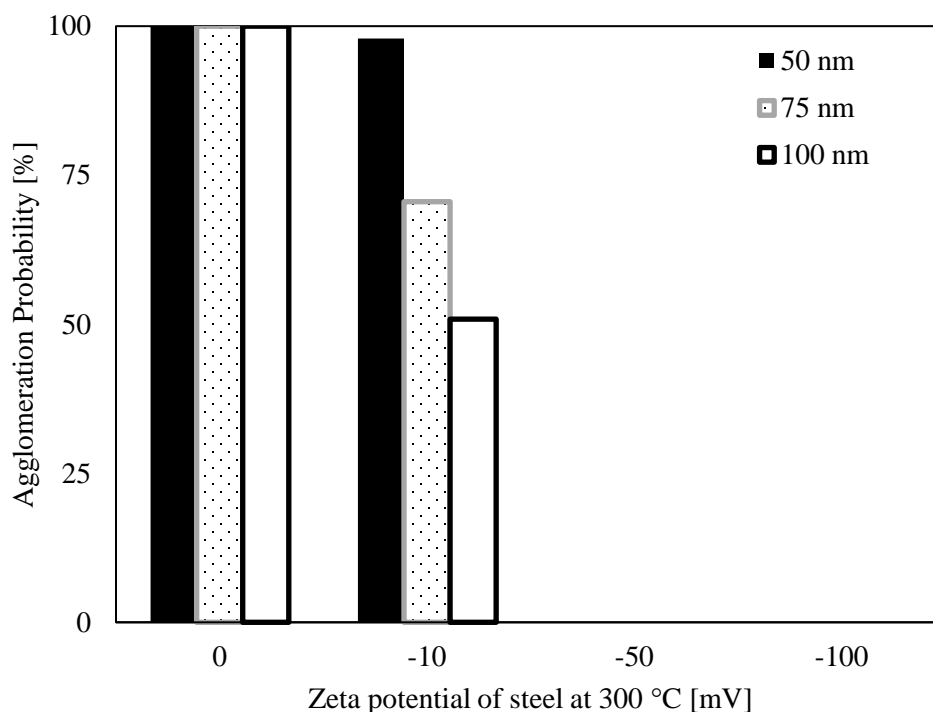
Figure 5-8. Calculated agglomeration probability (as percentage) for different values of zeta potential of steel at 300 °C. Zeta potential of magnetite =-113 mV (Table 2). AVT High water treatment chemistry at 300 °C. The probability of deposition is reduced to 0 % between -10 mV and -50 mV.

For the AVT High water chemistry, higher values of zeta potential of steel completely mitigate deposition. With respect to the magnetite particles, the pH of the solution is away from the IEP of magnetite at 300 °C (Table 5-2) [16]. The zeta potentials of magnetite and stainless steel in this case are both negative and significantly larger than 0 and -10 mV. This will maintain a repulsive interaction in the system and prevent deposition of magnetite on the steel substrate. This argument is supported by the interaction energy plots and the agglomeration probabilities. Experiments under the AVT High regime showed there was no magnetite deposition on the stainless-steel substrate. Combining the experimental results with the DLVO calculations, we can predict that the zeta potential of 304 stainless steel at 300 °C is not close to the IEP at 300 °C.

Beyond just the deposition of magnetite on stainless-steel, the inferences from the interaction energy calculations can be extended to cases where the substrate is already covered with magnetite. Based on the magnetite-magnetite particle interaction energy calculations, one can predict that there will be no deposition over the existing magnetite layer.

The DLVO interaction energy calculations can be extended beyond the AVT chemistry to other boiler water treatment chemistries like the phosphate treatment or the caustic treatment provided zeta potential values are available. In theory, for each type of boiler water treatment chemistry, regions which favor deposition can be identified based on DLVO calculations and can be avoided in order to mitigate deposition in boilers. DLVO interaction energy calculations can also serve as precursors to experimental studies and aid in designing suitable test conditions. Such calculations can be a valuable addition to experimental studies and can enhance the understanding of the deposition phenomena in boiler like environments.

References

[1] A. Tabakovic, Investigation of laundering and dispersion approaches for silica and calcium phosphosilicate composite nanoparticles synthesized in reverse micelles. The Pennsylvania State University, 2015.

[2] X. Tang, Dye-Doped Calcium Phosphosilicate Nanoparticles for the Early Detection of Human Cancers. The Pennsylvania State University, 2016.

[3] E.J.W. Verwey,, J.T.G. Overbeek, Theory of the stability of lyophobic colloids, Elsevier Publishing Company, Amsterdam, 1948.

[4] B. V Derjaguin,, L.D. Landau, Acta Physicochim. USSR 14 (1941) 633–62.

[5] J.N. Israelachvili, Intermolecular and surface forces, Academic press, 2011.

[6] R. Hunter, Foundations of Colloid Science, Oxford University Press, 2001.

[7] B. Raman,, D.M. Hall,, S.J. Shulder,, M.F. Caravaggio,, S.N. Lvov, Colloids Surfaces A Physicochem. Eng. Asp. (2016).

[8] EPRI, Deposition Mechanism of Lower Header Orifice Fouling in Forced Circulation Units. Available at: http://www.epri.com/abstracts/Pages/ProductAbstract.aspx?ProductId=000000000001025597. Accessed February 10, 2016.

[9] R. Hogg,, T.W. Healy,, D.W. Fuerstenau, Trans. Faraday Soc. 62 (1966) 1638–51.

[10] D.N.L. McGown,, G.D. Parfitt, J. Phys. Chem. 71(2) (1967) 449–50.

[11] B. Faure,, G. Salazar-Alvarez,, L. Bergström, Langmuir 27(14) (2011) 8659–64. 10.1021/la201387d.

[12] Y.Y. Song,, H.K.D.H. Bhadeshia,, D.W. Suh, Powder Technol. 272 (2015) 34–44. 10.1016/j.powtec.2014.11.026.

[13] M. Erdemoğlu,, M. Sarikaya, J. Colloid Interface Sci. 300(2) (2006) 795–804. 10.1016/j.jcis.2006.04.004.

[14] C.W. Turner,, D. Guzonas,, S.J. Klimas,, P. Frattini, Surface chemistry interventions to control boiler tube fouling, Heat Exchanger Technology Branch, Chalk River Laboratories, 2000.

[15] L. Boulangé-Petermann,, A. Doren,, B. Baroux,, M.N. Bellon-Fontaine, J. Colloid Interface Sci. (1995) 179–86.

[16] S. Vidojkovic,, V. Rodriguez-Santiago,, M. V. Fedkin,, D.J. Wesolowski,, S.N. Lvov, Chem. Eng. Sci. 66(18) (2011) 4029–35. 10.1016/j.ces.2011.05.021.

[17] S.M. Vidojkovic,, M.P. Rakin, Adv. Colloid Interface Sci. (2016).

[18] M.A. Blesa,, N.M. Figliolia,, A.J.. Maroto,, A.E. Regazzoni, J. Colloid Interface Sci. 101(2) (1984) 410–8. 10.1016/0021-9797(84)90052-3.

[19] M. Erdemoğlu,, M. Sarıkaya, J. Colloid Interface Sci. 300(2) (2006) 795–804. 10.1016/j.jcis.2006.04.004.

[20] M. Barale,, C. Mansour,, F. Carrette,, E.M. Pavageau,, H. Catalette,, G. Lefèvre,, M. Fedoroff,, G. Cote, J. Nucl. Mater. 381(3) (2008) 302–8. 10.1016/j.jnucmat.2008.09.003.

[21] B. Buecker, Power Plant Water Chemistry: A Practical Guide, PennWell Publishing Company, 1997.

Chapter 6

Discussion

The visual observations across the different conditions confirmed that suspended magnetite could readily deposit forming a sizable layer on the surface of stainless steel for some simulated boiler water treatments. This was concluded by comparing the surface of samples exposed to solutions that contained added magnetite particles to samples exposed to identical conditions excluding the addition of magnetite. This established that any deposits found in the tests with added magnetite was primarily due to the added magnetite rather than corrosion of the steel electrode. The friable nature of the surface coverage indicated that the deposit was not a densely-packed layer.

Testing results indicated that when boiler water was conditioned to a $pH_{25°C} = 9.3$ under AVT conditions, the environment at 300 °C favored significant deposition of magnetite particles onto stainless steel surfaces. Contrastingly, tests at $pH_{25°C} = 9.8$ did not show any observable magnetite deposits on the surface of the substrate. This indicated that the deposition at high pH was hindered when compared to the $pH_{25°C} = 9.3$ case.

The visual observations of samples exposed to different pH values with magnetite appear to be consistent with a deposition influenced by the zeta potential. According to the general principles of particle aggregation within colloids, particle aggregation is more likely as the magnitude of the zeta potential decreases [1]. The pH where the zeta potential of a suspended particle is zero can be referred to as isoelectric point pH_{IEP}. From literature, it was found that the pH_{IEP} at 300 °C for magnetite is between pH of 5.6 to 5.9 [2]. As such, it would be expected that samples exposed to solutions with pH values closer to the pH_{IEP} should exhibit more deposition than those further away. This was verified from the observations in the AVT tests. The largest extent of deposition occurred on the sample exposed to the test condition AVT $pH_{25c} = 9.3$, which had a pH at 300 °C of 5.8. As the pH was increased away from the pH_{IEP}, the zeta potential of the suspended magnetite particles would then be expected to increase, adding an electrostatic repulsion between magnetite surfaces. The decrease in deposition at the high pH AVT condition tested could be attributed to the hindrances of a larger zeta potential.

These inferences are also supported by the DLVO interaction energy calculations in the AVT regime, which take into account the zeta potential of magnetite and stainless steel. In the AVT Low case, at 300 °C, the total interaction energy curves do no present any energy barrier

against magnetite-magnetite particle agglomeration. The calculated agglomeration probabilities are greater than 0.9, indicating that the physicochemical environment suits magnetite-magnetite agglomeration. The same can be said about the magnetite-steel interactions. Operating at the AVT Low treatment chemistry favors aggregation of magnetite in bulk solution as well as deposition of magnetite on stainless steel substrates. This behavior is explained by the fact that, at 300 °C, the solution chemistry is such that magnetite is at its IEP and hence there are no repulsive interactions in the system. As the condition is changed to AVT High, the upper operating limit of the AVT regime, the interaction energy calculations do not favor magnetite-magnetite particle agglomeration. Regarding the magnetite-steel interactions, the DLVO calculation indicate that as long as the steel is not at its iso-electric point at 300 °C, when operating under the AVT High regime, there will be no deposition of magnetite on the steel substrate.

The results from the experiments and the inferences from the DLVO calculation corroborate one another. Both experimental results and theoretical calculations establish the effect of zeta potential and colloidal interaction in driving the deposition of magnetite from bulk solution on to stainless steel. The agglomeration/adhesion probabilities (shown as percentages) are an excellent indicator of the stability of the suspended particles. The samples tested experimentally and the agglomeration probabilities, both indicate that operating close to iso-electric point of magnetite leads to high amounts of deposition. Although there has been information on iso-electric points and high temperature solution pH, the two have been combined and comprehensively tested to establish this in a boiler like environment.

In the case of the caustic conditions, the low concentration (0.5 ppm) did not result in any noticeable deposition on the surface whereas the higher concentration (1.2 ppm) caused deposition of the magnetite particles on the surface. This could be attributed to the phenomenon of double layer compression. The hydroxyl ion is a potential determining ion as it directly influences the surface charge and zeta potential on the particle. The sodium and the phosphate ions can be considered indifferent ions. At high enough concentrations, the oppositely charged ions, in this case the positive ions, can play role in reducing the length of the double layer. This phenomenon is called double layer compression [1]. High ionic strength solutions will a greater concentration of the oppositely charged ions surrounding the negatively charged oxide surface, thereby reducing the net effect of the surface charge on the particle and reducing the zeta potential. At 300 °C, the conductivity and hence, the ionic strength of the test solution with 1.2 ppm NaOH is more than twice as much as the conductivity of the solution with 0.5 ppm NaOH at

300 ˚C. The oxide particles bearing a surface charge will attract the oppositely charged ions, in the caustic case, the sodium ions. In conditions with high ionic strength, the double layer compression reduces the effect of the surface charge, thereby possibly reducing the electrostatic repulsion between the particles. This could be a reason to cause agglomeration or deposition. Based on just the pH at 300 ˚C, deposition is not expected in the high caustic environment, similar to $pH_{25°C} = 9.8$. However, the visually observable deposits on the surface can be explained using the double layer compression theory. In the case of lower concentration of caustic (0.5 ppm), the pH at condition is higher than $pH_{25°C} = 9.8$ condition, so that the electrostatic repulsion between the particles is high enough to keep them in suspension. Considering that there were no noticeable deposits on the surface of the sample, it could be proposed that the ionic strength was not high enough for double layer compression to negate the repulsive forces. A similar explanation can be offered for the phosphate environment. The high phosphate concentration (3 ppm) resulted in observable deposits on the surface whereas the low concentration of phosphate did not result in any observable deposits. Differences in conductivity values, (κ), can be used to qualitatively indicate large differences in ionic strength between the various test solutions.

The presence of excess magnetite in the autoclave ensured that the quantity of magnetite was not the limiting step in the deposition process. Under this condition, whether a particle adheres to the surface to form a deposit or not will depend on the properties of the suspended particle, the suspension hydrodynamics and surface. The observations indicate that zeta potential is a driving factor in the deposition of suspended oxide particles in boiler environments. The zeta potential however, is strongly influenced by the pH and the ionic strength of the solution i.e. the water chemistry properties. The closer the zeta potential is to the iso-electric point of the oxide at the conditions, the greater that chance of deposition. Table 6-1 summarizes the finding of the tests with AVT and the solid alkali chemistry.

Table 6-1 Summary of Deposition Results from AVT and solid alkali tests

Test Condition	$pH_{25°C}$	$pH_{300°C}$	$\kappa_{300°C}$, [mS/m]	Deposition
AVT $pH_{25°C}$ 9.3	9.30	5.8	0.54	high
AVT $pH_{25°C}$ 9.6	9.60	6.0	0.81	moderate
AVT $pH_{25°C}$ 9.8	9.80	6.2	1.20	negligible
AVT + low Na_3PO_4	9.32	6.0	0.85	negligible
AVT + high Na_3PO_4	9.51	6.8	5.30	moderate
AVT + low NaOH	9.45	6.4	1.50	negligible
AVT + high NaOH	9.62	6.7	3.40	moderate

Conductivity values at 300 ^{o}C ($\kappa300°C$) were obtained from OLI Analyzer.
As a reference for pH values at given temperatures, the pH of pure water at 300 ^{o}C is 5.66. The deposition tests were not carried out in pure water.

The secondary electron images showed the crystalline morphology of the deposits on the surface. The images show a stark difference in the surface coverage for the AVT range. The test at $pH_{25°C}$ = 9.3 showed nearly full surface coverage whereas the sample tested at $pH_{25°C}$ = 9.8 showed negligible deposits on the surface. This validates the visual observation about the deposits. EDS analyses consistently showed that the iron and oxygen were the main elements of the deposits. Considering the test environment, the only source of iron oxides in the system is the added magnetite. The control experiments showed no surface coverage, establishing that the possible anaerobic oxidation reaction of iron does not form any noticeable amounts of oxide over the time duration the test was run. The surface analyses acted as a verification tool to corroborate the visual observations.

Under AVT conditions, impedance spectroscopy results were used qualitatively to indicate that the presence of magnetite caused some changes on the surface and also the effect of the pH on the deposition. As shown in Figure 4-11 significant changes in the impedance of the system were observed over the duration of the test, which was not the case in the control experiment. An increase followed by a decrease in the impedance was correlated to the buildup of deposits on the surface followed by removal until a steady state was reached. There were no significant changes in the impedance values for the control experiment over the duration of the test. The difference in the impedance value between two tests (with and without magnetite) was correlated to the visual observations and surface imaging, where the presence of suspended magnetite in the autoclave caused magnetite deposits to form on the surface on the samples at

$pH_{25°C} = 9.3$. The impedance data obtained at $pH_{25°C} = 9.8$ was very similar to the control experiment at $pH_{25°C} = 9.3$. There were no significant changes in the impedance magnitude over the duration of the test. With designed control experiments, it is possible to differentiate the contribution of the deposition process in the impedance spectra.

In the case of the caustic and phosphate tests, the absence of control experiments prevented direct isolation of contributing processes from the impedance spectra. Still, it was established earlier that, in the duration for which the tests were run, all the deposition was due to the added magnetite. The decreasing impedance values observed in the low caustic and low phosphate conditions could be an effect of a corrosion process occurring on the surface. In cases with the magnetite deposits, it appears as though these samples have a markedly higher impedance, as expected. Correlating with the visual observations, it can be established that for a given electrode assembly, the magnitude of impedance is orders of magnitude ($> 10^5$ Ω) higher when there is deposition on the substrate compared to the case without deposition on the surface. Across all the EIS tests, there is also the possibility that the magnetic nature of the suspended magnetite affects the alternating current measurements or that the ac potential applied influences the movement of the particles in the environments.

The results of the tests with the two hydrazine residuals established that there is no influence of hydrazine in the deposition mechanism and there were no noticeable differences between the two concentrations tested. Table 6-2 provides the data on the calculated pH and ionic strength for both tests at 25 °C and 300 °C. The concentrations of hydrazine in the residuals maintained do not significantly alter the pH or ionic strength at room temperature or at 300 °C. At ambient conditions, the role of hydrazine will be to remove the dissolved oxygen from the test solution. At higher temperatures, hydrazine will decompose to form ammonia, thereby contributing to the pH. However, at the concentrations tested here, pH calculations using OLI Analyzer indicated that there are no significant differences in the at-temperature pH between the 30 ppb and 90 ppb cases.

Table 6-2. Calculated pH and ionic strength for 30 ppb N_2H_4 and 90 ppb N_2H_4 residuals at 25 °C and 300 °C.

	pH		Ionic Strength [mol kg^{-1}]		Specific Conductivity [mho m^{-1}]	
	25 °C	300 °C	25 °C	300 °C	25 °C	300 °C
AVT	9.30	5.88	2.05 10^{-5}	3.66 10^{-6}	5.52 10^{-4}	4.26 10^{-4}
AVT + 30 ppb N_2H_4	9.30	5.89	2.05 10^{-5}	3.72 10^{-6}	5.53 10^{-4}	4.32 10^{-4}
AVT + 90 ppb N_2H_4	9.30	5.91	2.06 10^{-5}	3.83 10^{-6}	5.54 10^{-4}	4.43 10^{-4}

It can be seen that the solution chemistry, especially at 300 °C in the hydrazine tests is not very different from the AVT(R) pH = 9.3 case where the deposition was the highest. This can be related to the fact that addition of hydrazine does not change the environment sufficiently to move the pH away from pH$_{IEP}$. Hence the contrasting results compared to the AVT(R) pH = 9.8 case. The impedance spectra for the hydrazine tests (sample AVTH-1 and AVTH-2) established a baseline for cases with deposition on the surface. The magnitude of impedance was around 10^6 Ω for both the hydrazine residuals tested. Correlating to visual observations, we can concur that deposition on the substrate results in high values of impedance for the system.

In the case of the filming amine chemistry tested with HRSG-02, there were regions where the deposition was mitigated, but also regions where tightly packed magnetite particles were deposition on the surface. There is a clearly some influence of the filming amine on the deposition process, however it is not possible to explain the mechanisms involved without obtaining a full picture of the solution speciation model. HRSG-02 being a proprietary product and a blend of multiple amines, the speciation model at 300 °C has not been fully developed. Using OLI Analyzer, a simple speciation model was developed using the blend of neutralizing amines in the proportions specified in Table 1-3. This model was used to calculate an approximate pH$_{300 °C}$ for the HRSG-02 boiler water. This pH is an approximation because the filming compound is not included in the model. The data for the organic filming compounds was not available.

Table 6-3. pH and Ionic strength values at 25 °C (experimental) and 300 °C (approximate/partial model) for HRSG-02

HRSG-02 Concentration	Measured $pH_{25°C}$	Approx. $pH_{25°C}$	Approx. $pH_{300°C}$	Approx. Ionic strength [mol/kg]
2.5 ppm	9.3	9	5.81	3.01×10^{-6}
5 ppm	9.9	9.3	5.91	3.75×10^{-5}

The approximate values were calculated using OLI Analyzer (MSE Thermodynamic data bank) without the inclusion of film forming compounds. Hence the difference between measured and approximately calculated values.

Table 6-3 shows pH and ionic strength values at 25 °C (experimental) and 300 °C (approximate/partial model) for HRSG-02. The approximate $pH_{300°C}$ values for the HRSG-02 tests are not very far from the pH_{PZC} of magnetite at 300 °C. However, the actual pH will be slightly different because of the contribution from the other amines in the blend. Considering that deposition was observed on the sample, it can be speculated that the actual $pH_{300°C}$ is not much higher than approximated value. However, this does not account for potential interactions between the amines and magnetite particles. Surface analyses showed types of deposits which were unique to the filming amine tests. This could also be a result of the amine magnetite interactions. EDS was unable to confirm any bonding between the amine and the magnetite particles and more specific tests would be required. The varying nature of the deposits on the samples FFA-1 and FFA-2 indicate possible amine-magnetite interactions both in bulk as well as on the substrate. There is evidence of certain filming amine causing the zeta potential of magnetite to change due to interactions between the amine and oxide.

Although the substrates were only partially covered with magnetite, the magnitude of the impedance for sample FFA-1 and FFA-1 were around 100 MΩ. This is in the same range as cases with full surface coverage. This is unexpected as the exposed metal substrate (partially covered) should provide a path of lower resistance. However, a possible explanation for this observation is the formation of a protective film on the substrate due to the presence of film forming compounds in the water chemistry. Impedance spectra were also used to identify the changes in the substrate before and after exposure at 300 °C, providing some insight into the way the filming amines function.

The effect of increasing the particle size on magnetite deposition on 304 SS substrates in boiler type environment was successfully studied. Visual observation of the samples showed that

increased particle size reduces deposition in the test environment. In simple Derjaguin, Landau, Verwey, Overbeek (DLVO) model, the interaction of the particles can be considered to be governed by the Van der Waals attractive forces and the electrostatic repulsion forces. It has been shown that under the AVT regime, when $pH_{25°C}$=9.3 using NH_4OH(aq), there is negligible electrostatic interaction between the particles [3,4]. Since, Test B has the same aqueous environment, there is would be no electrostatic interactions. Van der Waals interactions are directly proportional to the size of the interacting particles. Hence, an increase in the particle size distribution would increase the Van der Waals interactions [5].

However, another factor that must be considered in these conditions is the particle aggregation kinetics. The most common aggregation mechanisms are (i) Brownian motion or perikinetic aggregation, (ii) fluid motion or orthikinetic aggregation and (iii) differential sedimentation. Brownian aggregation is not dominant when the particle sizes are small or in dilute suspensions. Orthokinetic aggregation, which is caused by particle transport due to fluid motion is usually a more dominant force in aggregation. Orthokinetic aggregation is predominant when the particle size ranges from 1 μm to 10 μm. The particles are also affected by gravitational forces, buoyancy and other forces. The balance between the forces causes all particles to eventually sediment and settle down. This type of aggregation mechanism is called differential sedimentation. This type of collision mechanism is important when the particles are large as it can promote aggregation. Larger particles will sediment faster than smaller ones and will capture the smaller suspended particles as they fall [5]. The typical aggregation vs particle diameter for the different types of aggregation is shown in Figure 6-1
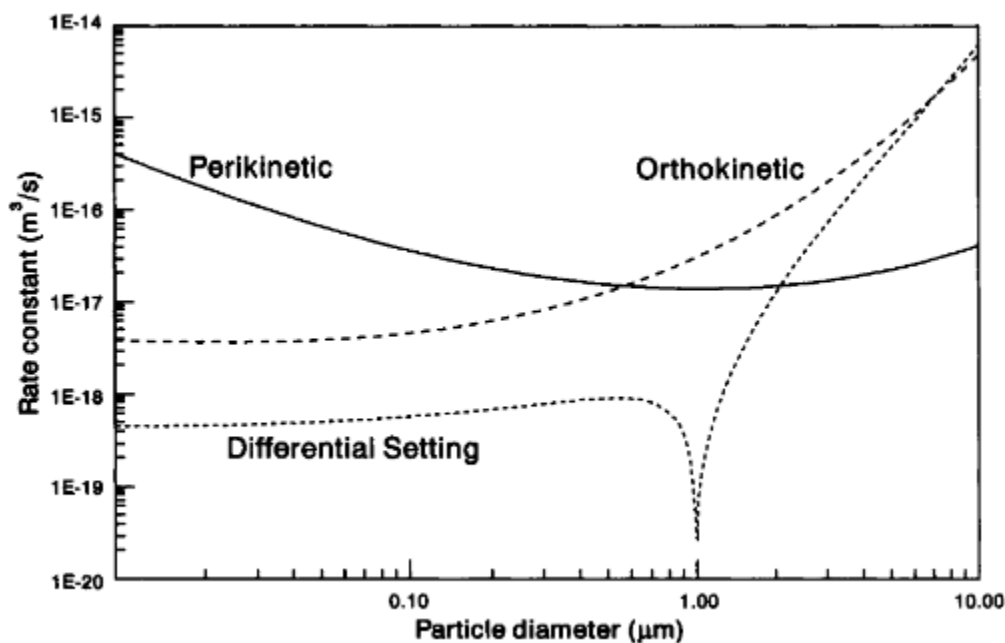
Figure 6-1 Comparison of collision rate constants for different transport mechanisms. Ambient conditions [5] [11].

Aggregation kinetics plays greater role in Test B, where the particle size of the suspended magnetite is higher than what was used in Test A. Increasing the particle size beyond 1 micron drastically increases the aggregation rates especially due to contribution from the orthokinetic and differential settling mechanisms. Hence, as the particles start to aggregate the sediment at a faster rate and are no longer in suspension. This implies that in the test system considered here, the number of particles available for deposition on the substrate is constantly decreasing. Although the aqueous environment is conducive for deposition, the availability of suspended particles could play a key role in deposition and can provide information on the time dependence of the deposition process.

Consistent with the trends observed in the previous cases, the partially covered substrate resulted in a lower value of impedance compared to samples completely covered with magnetite (except the filming amine case). The exposed metal results in a path of lower resistance compared to regions covered with oxide and hence the value of impedance is lower. Unlike the filming amine tests, there is no protective film in this case to increase the impedance. Comparing the results with the hydrazine case (sample AVTH-1 and AVTH-2), where the electrode assembly

was the same and the boiler water chemistry was very similar, one can state that lesser extent of deposition results in lower impedance values.

In all the treatment chemistries tested here, the size of the particles deposited on the substrates was much larger than the size of the magnetite particles added to the system (50-100 nm). Apart from just Ostwald's ripening, this indicates that there is agglomeration of magnetite particles in the bulk solution. This argument is supported by the high value agglomeration probability for magnetite-magnetite particle interactions in the AVT Low chemistry regime. Apart from just deposition of magnetite on the substrate, there is also agglomeration of magnetite particles in the bulk solution. The agglomerates can then be potentially deposited on the substrate. Evidence of this is also seen in sample AVTPS where the particle size of the magnetite added to the system was higher.

Overall, the deposition or lack thereof in all traditional water chemistries can be explained by the influence of the physicochemical environment on the behavior of the suspended magnetite particles. This has been verified using DLVO interaction energy calculations for the AVT regime. The interaction energy calculations can be extended to other treatment chemsitries, based on the availability of experimental zeta potential data to identify the limits and thresholds to mitigate deposition by tuning the water chemistry alone. EIS has also been successfully used to qualitatively monitor the solution substrate interface in situ. Based on the EIS spectra, impedance values in the order of $M\Omega$ or higher indicates high rates of deposition on the substrate. It must be kept in mind that these results are for a case where magnetite is readily available in the bulk solution (accelerated deposition) and for an arbitrarily chosen time period of 65 hours. However, this clearly demonstrates the applicability of EIS as a technique that can be used to monitor metal surfaces in boilers and power plants to track the buildup of deposits.

References

[1] R. Hunter, Foundations of Colloid Science, Oxford University Press, 2001. [book]

[2] S. Vidojkovic, V. Rodriguez-Santiago, M. V. Fedkin, D.J. Wesolowski, S.N. Lvov, Electrophoretic mobility of magnetite particles in high temperature water, Chem. Eng. Sci. 66 (2011) 4029–4035. doi:10.1016/j.ces.2011.05.021. [scientific journal]

[3] B. Raman, D.M. Hall, S.J. Shulder, M.F. Caravaggio, S.N. Lvov, An Experimental Study of Deposition of Suspended Magnetite in High Temperature-High Pressure Boiler Type Environments, Colloids Surfaces A Physicochem. Eng. Asp. (2016). [scientific journal]

[4] B. Raman, D.M. Hall, S.J. Shulder, M. Caravaggio, S.N. Lvov, Deposition of Suspended Magnetite in High Temperature High Pressure Boiler Environments, ECS Trans. 66 (2015) 43–56. doi:10.1149/06621.0043ecst. [scientific journal]

[5] M. Elimelech, J. Gregory, X. Jia, Particle deposition and aggregation: measurement, modelling and simulation, Butterworth-Heinemann, 2013. [book]

Chapter 7

Conclusion

The deposition of suspended magnetite on orifice plates and tube walls is an important issue for forced circulation fossil fuel plants. A suspended magnetite deposition cell was successfully designed to study the deposition of magnetite under different boiler water chemistry. The cell provided the scope to test multiple boiler water treatment chemistry at the conditions of 300 ˚C (572 °F) and 10 MPa (1450 psi). By adding excess magnetite to the test environment, accelerated deposition was successfully replicated. The experimental system was also designed to carry out in-situ electrochemical measurements with the help of a special electrode assemblies designed to function in extreme environments. Multiple boiler water chemistry were successfully tested and their influence on magnetite deposition was observed. The results indicated that the presence of suspended magnetite particles at a $pH_{25°C} = 9.3$, controlled by ammonium hydroxide, caused the particles to aggressively deposit on the stainless steel surface. In the control experiment, without any added magnetite, lack of a visible deposit indicated that the duration of the test was not sufficient to form an easily visible layer from corrosion that was comparable to the added magnetite test results. This again reiterates the fact that presence of magnetite at the above specified conditions resulted in the formation of an easily visible, friable, deposit on the sample surface. On the other end of the AVT spectrum, when tested at $pH_{25°C} = 9.8$, no visually observable deposits were found on the surface of the steel. These results are in agreement with what was expected according to the theory on behavior of suspended particles in aqueous solutions and Derjaguin-Landau-Verwey-Overbeek theory. The results showed that the zeta potential, which is influenced by the pH of the solution, could be the major factor dictating the susceptibility of deposition at these conditions. In case of the caustic treatment and phosphate treatment, it was seen that the compression of the double layer due to the additional electrolytes in the system could be influencing the deposition process even when the pH of the system is higher than the pH under AVT conditions. These results also proved the success of the experimental setup developed in this project for simulating the boiler environments of interest and for studying the deposition phenomena commonly faced in boilers.

The EIS measurements, when compared with control experiments, were used to qualitatively establish the feasibility of the EIS studies and provide evidence for developing a monitoring tool to observe the deposition process in-situ. Based on the EIS spectra, impedance values in the order of MΩ or higher indicates high rates of deposition on the substrate. Samples with lack of deposits or partial deposition showed much lower values of impedance. EIS was also successfully used to identify the effect of the film forming amines on the substrate. With more controlled EIS studies, the contribution of the deposition process can be isolated in the impedance spectra. The novel experimental setup also provided an opportunity to study different boiler/feedwater chemistry and their effects on corrosion and deposition. A clear trend in the influence of boiler water chemistry on the deposition process was established.

The three-different boiler water chemistry evaluations would suggest the following operating conditions:

- AVT – The pH closer to the top end of the pH range (9.6) if all-ferrous metallurgy feedwater system. Units with mixed-metallurgy systems should consider a solid alkali treatment.

- PT/CT – Alkali should be at lower end of range necessary to maintain ammonia corrected pH.

The effect of hydrazine addition, filming amine chemistry and increased particle size on magnetite deposition was successfully tested in boiler type environments. The results have been corroborated using three different techniques, (i) visual observations, (ii) surface analysis and (iii) *in situ* EIS. Two different residual concentrations of hydrazine, 30 ppb and 90 ppb, were tested at boiler like conditions of 300 °C (572 °F) and 10 MPa (1450 psi). The test solution was conditioned to the base case $pH_{25°C}$ = 9.3 using $NH_4OH(aq)$. From the results of testing, it could be concluded that hydrazine, at the concentrations tested here, does not significantly alter the deposition of magnetite on 304 stainless steel. The substrates exposed at both the test conditions showed black colored deposits on the surface. Macroscopically, both the samples looked uniformly covered. The visual observations were verified using the SEM images. SEM showed there were no significant changes in the nature or type of the deposits. These observations were consistent across the samples tested. The EIS data again showed no significant differences between the 90 ppb and 30 ppb residual concentrations. When combined with visual observations, SEM analysis and solution speciation provides sufficient evidence that the tests conducted at 30 ppb and 90 ppb residual hydrazine concentration are not significantly different. From these results and the solution speciation model, it can be concluded that 30 ppb and 90 ppb

hydrazine residuals have no influence on magnetite deposition on stainless steel. It is likely that at the operating conditions, residual hydrazine would have decomposed to ammonia. However, based on the concentrations of hydrazine present, ammonia generated would not have altered the pH of the solution enough (see Table 1) to drastically affect the deposition mechanism.

The tests with the filming amine did not mitigate deposition completely, but the presence of the HRSG-02 affected the nature of deposits observed on the substrate. Macroscopically the substrate appeared to be covered with deposits and some darker regions. Surface analyses showed regions of no, moderate and high surface coverage. SEM images also showed the number of particles on the surface increased with increasing concentration of HRSG-02. However, the approximate calculations of the at-temperature pH suggest that the solution pH could be away from the pH_{IEP} of magnetite at 300 °C. This could be due to the neutralizing amines alone or a combined effect of the neutralizing amines and filming amine. It is not possible to verify this unless further information is available regarding the solution chemistry at 300 °C. EIS was successfully used in identifying possible changes on the surface. Albeit, not accounting for a possible change in solution chemistry in the filming amine tests, EIS has proved to be a viable option for *in situ* interface monitoring. EIS was also used to show that HRSG-02 could offer valuable corrosion protection when units are offline post treatment with the amine.

Increasing the particle size distribution clearly showed a decrease in the deposition even though the boiler water chemistry was conducive for deposition. This was justified based on the particle aggregation kinetics. EIS was also used to verify that the substrate indeed behaved like a partially covered electrode. Although, controlling the particle size is not an option for utility boilers, these tests provide further insight into understanding deposition at high temperatures in boiler type environments. Even when the aqueous environment is conducive for deposition, as is the case in both Test A and Test B, as the particle size increases, the deposition will gradually decrease due to increasing rates of aggregation and particles settling down out of suspension. This can be further investigated using computational models for particle aggregation kinetics and settling time in boiler type environments.

Colloidal interactions govern the stability and behavior and suspended particles in aqueous media. Quantifying such interactions not only supports the experimental results, but also allows one to predict the behavior of suspended particles. In this study, DLVO theory has been used to calculate the interaction energies for magnetite-magnetite particle interactions and magnetite-steel interactions. The agglomeration probability (aggregation percentage) has also been calculated for magnetite-magnetite particle interactions and magnetite-steel interactions in

the AVT regime. Based on the interaction energies and agglomeration probabilities, it is seen that, boilers operating under the AVT Low regime provide a more conducive environment for magnetite deposition at 300 °C. This can be explained by the fact that at 300 °C, the pH of the boiler water is close to the IEP of magnetite. This eliminates any repulsive interactions between the particles. In the case of magnetite steel interactions, it is seen that when the zeta potential of magnetite is ~ 0 mV, the net interaction energy favors attraction for a range of zeta potential values of steel. The DLVO calculations predict magnetite agglomeration in the bulk solution as well as deposition of magnetite on stainless-steel substrates when operating in the AVT Low regime. The inferences from the DLVO calculations agree with previously published experimental results. On the other hand, the total interaction energy does not favor aggregation or deposition of magnetite when the boiler water treatment is changed to AVT High. Neither magnetite-magnetite agglomeration nor magnetite deposition on stainless steel is favored in this case. This argument is supported by the results from the experimental studies, where no deposition was observed on the surface of the substrates. Such calculations can be extended to other boiler water treatments, oxides and substrates, provided zeta potential values are available for the specific physicochemical environment. Supported by experimental results, DLVO calculations can be used to identify thresholds and limits in boiler water treatments to mitigate deposition and fouling. The work presented here provides a template which can be easily extended to other oxides and treatment chemistries to predict the behavior of suspended particles in boiler water.

In summary, this study has clearly established a link between the solution chemistry at 300 °C (572 °F) to the deposition of magnetite on 304 SS. AVT, CT, PT and AVT(R) have been tested. The tests here explored a new chemistry in the poly amine treatment with filming amines. The results also validate the conclusions of the previous study and establish the influence of DLVO forces in deposition. The DLVO interactions for the AVT regime have been quantified and the capability of DLVO interaction energy calculations to predict the behavior of suspended particles in boiler water has been established. The importance of particle aggregation in governing deposition has also been shown. Although the theory of aggregation and DLVO interaction have been around for decades, the applicability has been proven for the first time in boiler type environments and such studies provide means to understanding the deposition process and tuning the physicochemical environment in a manner to mitigate the deposition. This will save time and money by removing the frequent need to physically remove the deposits and clean the boiler.

Appendix A

Electrochemical Impedance Spectroscopy as a Tool to Link Cycle Chemistry Properties to Fouling in Power Generating Systems

The content of this chapter was originally published in the proceedings of the 11th International Conference on Cycle Chemistry, St. Louis, MO, July 14-17, 2015 and is referenced as Raman, Hall, Lvov, Shulder and Caravaggio, '*Electrochemical Impedance Spectroscopy as a Tool to Link Cycle Chemistry Properties to Fouling in Power Generating Systems*', in 11th International Conference on Cycle Chemistry in Fossil & Combined Cycle Plants with Heat Recovery Steam Generator (Saint Louis: EPRI, 2015).

Abstract

Electrochemical Impedance Spectroscopy (EIS) is a non-destructive alternating current (ac) analytical technique that can provide in-situ electric impedance values. These values relate directly to processes that affect the passage of electric current through media with some degree of electric conductivity. As such, EIS can be used as a tool to monitor both cycle chemistry and metal surface properties, provided that the properties of interest alter the measured electric impedance in some observable manner. Issues that plague power plants such as fouling and corrosion are prime examples of processes that have observable effects on the electric impedance that exists between metal surfaces in contact with the feedwater flowing within a power cycle. With well-designed experiments and the proper equipment, in-situ EIS measurements can be used to quantify the effects of changes to cycle chemistries, flow rate and time on processes such as corrosion and fouling. In this work, laboratory scale experiments were carried out to study deposition of metal oxide on metal substrates, simulating the fouling experienced in boiler units. An autoclave pressure vessel was used to create boiler type environments of 300 ℃ and 100 bar. Metal oxide particles were added along with the test solution, to simulate boiler water chemistry prone to fouling. A three-electrode assembly that consisted of the metal substrate as the working electrode, a counter electrode and a reference

electrode was used with a potentiostat for the *in-situ* EIS measurements. EIS was used successfully to detect changes on the surface of the stainless-steel substrate due to the metal oxide deposition.

Introduction

Corrosion & Fouling

The primary water systems in a steam generation facility are (i) feedwater/boiler water/after boiler circuit, (ii) makeup system, (iii) condenser cooling, (iv) closed cooling water [1]. Primarily constructed out of metals and alloys, all of the above systems are prone to corrosion and fouling. Each of the systems operate under unique conditions and provide different environments for the metal solution interaction. Corrosion of metals is due to an irreversible oxidation reduction reaction between the metal and an oxidizing agent in the environment. Corrosion degrades the material's functional properties, making it unsuitable for the intended use [2]. Fouling is defined as the collection and/or formation of unwanted materials on the surface. Fouling has adverse effects, especially on heat transfer surfaces, where it reduces the heat transfer efficiency. In the case of orifices, fouling can affect the pressure differential across the orifices, altering the flow and causing inefficiencies. Fouling is typically caused by accumulation of particulates, precipitation, chemical reaction or concentration of corrosion products [3]. Corrosion is one of the primary reasons for boiler tube and equipment failure in steam generation systems [4,5]. Fouling causes erosion-corrosion of steel piping, boiler tube failures, scaling and deposition on tubes and pipes [6].

Dissolved oxygen is a strong oxidizing agent and one of the major causes of corrosion in power plants [1]. In the case of steel in boilers, the iron corrodes to its oxides according to the following reaction, [1,5]

$$Fe(s) \rightarrow Fe^{2+}(aq) + 2e^- \qquad (1)$$

Although the dissolved oxygen in the boiler water can be eliminated, iron can still be oxidized to form magnetite (Fe_3O_4) films [5,7] according to the following reaction,

$$3Fe(s) + 4H_2O(l) \rightarrow Fe_3O_4(s) + 4H_2(g) \qquad (2)$$

The magnetite (Fe_3O_4) forms a dark protective layer on the boiler tube surface and prevents further corrosion. However, multiple layers of magnetite results in porous deposits,

which have lower heat transfer coefficients and cause inefficiencies. Fouling of the tubes causes localized heating and create concentration sites for corrosive chemicals or cause other salts to crystallize on the surface [1].

Magnetite can also be further oxidized to ferric oxide, also called hematite according to the following reaction,

$$2Fe_3O_4(s) + \frac{1}{2} O_2(g) \rightarrow 3Fe_2O_3(s) \tag{3}$$

Ferric oxide (Fe_2O_3) is brownish-red in color and does not form a protective layer. This causes further corrosion of the base metal. Ferric oxide can also enter the water stream and can be transported downstream [1].

Cost of Corrosion

As reported by NACE in 2002, utilities accounted for the maximum share of industrial corrosion costs. Out of the $49 billion (in terms of 1998 dollars) in corrosion costs borne by the utility sector, the electric power generation industry had $6.9 billion attributed to corrosion costs. It was estimated that corrosion related issues cost the nuclear power sector $4.2 billion and the fossil fuel based power generation industries $1.9 billion [8]. These numbers represent only the direct costs of corrosion which are related to replacement of materials and equipment ruined by corrosion. The indirect costs, which include cost of repair, loss of production and downtime, often exceed the direct costs of corrosion. Failures due to corrosion can also result in an unsafe environment for operation. The different types of expenses involved make the estimation of total cost of corrosion difficult [2].

Controlling and Monitoring Corrosion

Corrosion and fouling can be detrimental to the operation of power plants and measures must be taken in order to control corrosion. Reducing boiler tube failures and establishing treatment programs to prevent fouling has been the focus of the power generation sector for decades [4,6,9-13]. The most common method employed to minimize corrosion in water systems is controlling the water chemistry. Corrosion and fouling strongly depend on temperature, concentration of chemical species, pH and properties of metal surface [6]. Hence, careful control

of boiler water chemistry is required to maintain an environment which minimizes corrosion. Water in steam generation units is maintained at a high pH and low dissolved oxygen concentration [1]. The de-aerated alkaline water creates a reducing environment at the metal solution interface, slowing down corrosion. Boiler and feed water treatment programs have been employed for many years now and established standards are available.

Treatment programs employed will be ineffective if they are not monitored constantly [1]. Corrosion monitoring provides information on the extent of damage and the rate at which the damage due to corrosion is occurring. Monitoring also informs one about the effectiveness of any corrosion control/inhibition method employed [14]. Nondestructive monitoring techniques are very effective in the power plant environment and a lot of effort has been put on designing proper sampling techniques to obtain representative samples [1]. Water systems in the steam generation units are maintained at high temperatures and the properties of aqueous systems vary significantly with temperature [15]. *In situ* monitoring techniques are very attractive for this purpose as they do not require the sample to be cooled down, causing the physiochemical properties to change.

Electrochemical Sensors

Electrochemical sensors have been widely used for detection of oxygen, carbon monoxide, hydrazine, measuring pH and conductivity, etc. primarily because of ease of use and accuracy [16]. Corrosion, being an electrochemical process, can be studied using electroanalytical techniques [17]. Electrochemical sensors are well established in multiple industries and provide real time information of the processes *in situ* [18]. Direct analytical methods such as weight lost measurements or solution analysis require high exposure time or expensive analytical equipment. Electrochemical sensors obtain information in the form of an electrical signal generated by the interaction of the surface in question and the environment. Electrochemical methods are based on Faraday's law to relate mass and current flux. Electrochemical probes have very small measurement times, high accuracy and provide an option for continuous monitoring [19]. A typical electrochemical sensor consists of a working electrode, which is the material of interest, a counter electrode, which is a large area current collector and a reference electrode, with respect to which all the potentials are measured. A review of electrochemical sensors that can be used in high temperature/high pressure aqueous solutions is given in Ref. [20].

Direct Current Techniques

There are multiple direct current (dc) based techniques involving polarization of the working electrode over a range of potential and analyzing the current response. Frequently used is the linear polarization resistance (LPR), which is a dc sweep method where multiple potentials across a small range are applied to the working electrode around the open circuit potential and the current response is recorded. The current response of a system is directly related to the rate of the electrochemical reactions occurring at the surface. While monitoring corrosion, the current response of a surface to applied potential can be easily converted to corrosion rate in millimeters per year using the Stern-Geary equation [14,21], which is given as,

$$CR = j_{corr}M_M/\rho_M zF \tag{4}$$

CR, is the corrosion rate in units of length per time, $j_{corr,}$ is the corrosion current density in A/cm^2, M_M is the molar mass of the corroding metal in g/mol, ρ_M is the density of the corroding metal in g cm^{-3}, *F* is the Faraday constant, 96485 C/mol and *z* is the charge number of the oxidized metal species.

This technique is a quick and easy method to obtain the instantaneous corrosion rates. However, polarization resistance measurements have to be compensated for internal solution resistance measurements, especially in low conductivity solutions [14,22]. The aqueous systems in steam generating plants are maintained at very low conductivity. Failure to correct for solution resistance results in corrosion rates being underestimated. Correcting for internal resistance requires additional tests to estimate the solution resistance. Additionally, LPR can sometimes not be reliable when the surface is covered with scales or deposits [23]. The dc techniques, although valuable, are limited in the amount of information that can be obtained.

Alternating Current Impedance Techniques

The technique of characterizing electrochemical processes using impedance measurements is called electrochemical impedance spectroscopy. In this technique, the current response of the system to the application of a periodic small amplitude potential signal is studied. The response is recorded for a range of frequencies and hence the term spectroscopy is used [24]. As ac impedance measurements are often used to determine the conductivity of solutions this technique offers clear advantages by being incorporated into use in addition to dc polarization

techniques [22]. The ac measurements permit separation of frequency dependent elements of the processes such as solution conductivity from electrochemical reactions [14]. In theory, if the impedance measurements are carried over an infinite range of frequencies, it would contain all the information that can possibly be extracted by electrical perturbation on the system [25,26]. As such, it is not surprising that impedance data has been shown to be useful in studying complex electrochemical processes like, anodic behavior of metals, corrosion, batteries and surface characterization of electrodes [26].

Electrochemical Impedance Spectroscopy (EIS): An Introduction

In ac impedance methods, a sinusoidal potential modulation of small amplitude is applied at different frequencies and the response of the electrode is measured. If ΔE is defined as the difference between the steady state potential and the applied potential, the sinusoidal input signal as a function of time t can be given by,

$$\Delta E = |\Delta E| \sin(\omega t) \tag{5}$$

ω, is the radial frequency.

In order to maintain linearity of the system, the modulation amplitude is typically kept small, usually on the order of about 10 mV. This sinusoidal perturbation potential causes a current response from the system. The resulting sinusoidal current is superimposed onto the steady state current. If the perturbation potential is applied around the open circuit potential, then the steady state current is 0. The current response is given by,

$$\Delta I = |\Delta I| \sin(\omega t - \varphi) \tag{6}$$

φ, is the phase difference between the input and output signals, also called the phase angle.

The sinusoidal signals can be represented in polar coordinates with the amplitude as the radius and phase angles as the radial frequency. Representing the sinusoidal perturbation in a complex radial plane,

$$\Delta E = \Delta E_{Re} + i\Delta E_{Im} \tag{7}$$

$$\Delta E_{Re} = |\Delta E| \cos(\omega t) \tag{8}$$

$$\Delta E_{Im} = |\Delta E| \sin(\omega t) \tag{9}$$

where i, is the square root of -1.

Using Euler's identities, we obtain,

$$\Delta E = |\Delta E| \exp(i\omega t) \tag{10}$$

$$\Delta I = |\Delta I| \exp(i(\omega t-\varphi)) \tag{11}$$

The impedance is defined as the ratio of the potential perturbation to the current response of the system and is given by,

$$Z = \Delta E/\Delta I = [|\Delta E| \exp(i\omega t)] / [|\Delta I| \exp(i(\omega t-\varphi))] \tag{12}$$

If,

$$|Z| = |\Delta E|/|\Delta I|$$

Then,

$$Z = |Z|\exp(-\varphi) \tag{13}$$

Similar to the potential and current, the impedance can be represented in a complex plane where the impedance vector is characterized by a modulus $|Z|$ and the phase angle φ. This enables the representation of the total impedance as a sum of the real and imaginary parts

$$Z = Z_{Re} + iZ_{Im} \tag{14}$$

Measuring Impedance

A typical EIS setup has a three electrode cell with a working electrode, a counter electrode and a reference electrode. The electrodes are connected to a potentiostat, which can maintain a constant potential difference between the working and the reference electrode. The potentiostat can also measure the current, which is the response of the system. The current is calculated by measuring the potential across a known resistance or by using a current follower. While performing an EIS, the potentiostat applies the ac potential perturbation and measures the current response. The impedance is calculated by a frequency response analyzer. A reference ac wave of a certain frequency is superimposed on a set dc potential and applied to the working electrode. The analyzer in the potentiostat receives the signal from the system, which is then multiplied by the reference sine or cosine wave before integrating it to obtain the impedance values. Such integration extracts the real and imaginary parts of the response signal [24,27].

Equivalent Circuit of an Electrochemical System

It is good practice to interpret impedance measurements using reaction models that represent the phenomena occurring in the physical system. A model of the system in question allows one to calculate the impedance as a function of frequency and connect measured impedance values to key model parameters such as solution conductivity, species diffusion coefficients and coating thicknesses [27]. When using these models, comparisons between the theoretical and experimental impedances is a common method for accepting or rejecting a circuit model. Multiple processes contribute to the impedance response of a system. In such cases, it is easy to treat the processes independently and combine them using equivalent electrical circuits [28]. Equivalent circuits are electrical analogs of the electrochemical system that exhibit the same impedance-frequency behavior as the physical system. Equivalent circuits typically consist of a combination of passive elements like resistors, capacitors or inductors arranged either in series or parallel. Passive circuit elements are those that do not generate any power, but store or dissipate the energy in the form of a voltage drop or current [27]. Each of the elements has a typical impedance response, which can be related to some of the physical processes occurring in the system. Processes like conductivity, faradaic charge transfer and double layer charging can be well represented by passive elements like the resistors and capacitors [28]. Apart from the traditional electrical equivalents mentioned above, there are also elements like the Warburg element, which accounts for diffusion processes. The Warburg element has a mathematical basis derived from Fick's laws and has an impedance response similar to some of the diffusion processes observed in a physical system.

The key in using equivalent circuits is to ensure that the electrical analog is a close representation of the physical model of the system. Multiple equivalent circuits can exhibit the same impedance frequency behavior and the experimental impedance data can be fit to multiple circuits using a number of parameters [25,28]. Reaction models on the other hand are representative of the physics of the system and are unique only each system. The equivalent circuit representation must be designed in a manner that the elements represent the electrochemical system physically [25]. Not all equivalent circuits represent the physical electrochemical system even though they may have the same impedance response. Equivalent circuits are useful tools that allow understanding of the impedance behavior, but the appropriate equivalent circuit must be decided based on knowledge of the electrochemical system and not the data fit [2,25].

Impedance of Passive Elements

The equivalent circuits which represent electrochemical systems typically constitute of passive elements and hence it is useful to study the current response of individual elements [2,27]. The three passive elements most commonly present are resistor, capacitor and inductor. The resistor denotes any ohmic resistance, wherein the potential and the current are in the same phase. The current potential relationship is given by Ohm's law. In a capacitor and inductor, the current and potential are separated by a phase shift. The relevant information about the three passive elements are given in Table 1 [17] where C represents the capacitance and L is the inductance of the system.

Table A-1. Passive elements and their impedance response

Element	Current Potential Relationship	Impedance	Phase Shift (in degrees)
Resistor	$\Delta E = \Delta I\, R$	$Z = \Delta E/\Delta I = R$	0
Capacitor	$\Delta I = C\, d(\Delta E/dt)$	$Z_C = |Z|\exp(j\varphi) = -i/\omega C$	-90
Inductance	$\Delta E = L\, (d\Delta I/dt)$	$Z_L = |Z|\exp(j\varphi) = i\omega L$	90

For alternating current in an electrical circuit, the impedance is analogous to ohmic resistance for direct current. Hence, for individual elements with impedance, Z_K connected in series,

$$Z = \Sigma\, Z_K \tag{15}$$

And for individual elements connected in parallel,

$$1/Z = \Sigma\, 1/Z_K \tag{16}$$

Representation of Impedance Data

Electrochemical systems are often represented using equivalent electrical circuits which give a similar impedance response. Based on equations X-Y, the impedance can be separated in to real and imaginary components. The most classic example of an equivalent circuit derived from a physical model is the simplified Randles cell, which represents the impedance response of an electrochemical system that can be characterized using passive elements like a resistor and a capacitor. Physically, this model represents a charging current and a faradaic current passing through an electrode/electrolyte interface with the total current conducted by the electrolyte [28].

The charging current is associated with the double layer capacitance of the metal electrode and the faradaic current is associated with any electron transfer processes occurring at the surface. The electrolyte has an internal resistance of its own. The ohmic resistance of the solution, R_s, is in series with the impedance due to the processes occurring at the metal-solution interface. The simplified Randles cell can be used to represent a system in which a metal (electrode) is immersed in an electrolyte and is undergoing corrosion (oxidation) in the absence of any mass transfer [27]. The equivalent circuit shown in Figure 1, represents the electrochemical system described above. The capacitance element, C_{dl}, represents the impedance of the electric double layer on the electrode solution interface. R_{ct}, represents the charge transfer resistance, which is arising due to electrochemical reactions occurring at the interface [28].
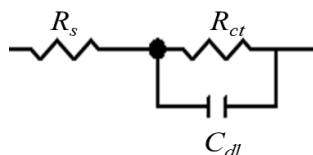
Figure A-1. Equivalent electrical circuit for a simplified metal solution interface.

If Z_C, is the impedance of the capacitance element, the total impedance of the circuit can be expressed as

$$Z = R_s + [Z_C R_{ct}/Z_C + R_{ct}] \tag{17}$$

$$Z_C = -i/\omega(C_{dl}) \tag{18}$$

The impedance can be separated in to real and imaginary components and can be represented in a complex plane diagram, i.e. using real impedance and imaginary impedance axes, for different frequencies. This representation is called the Nyquist plot [2,26]. Figure 2 shows the Nyquist plot for the impedance response of equivalent circuit shown in Figure 1. The impedance response was generated with $R_s = 1500$ Ω, $R_{ct} = 5000$ Ω and $C_{dl} = 1$ μF.
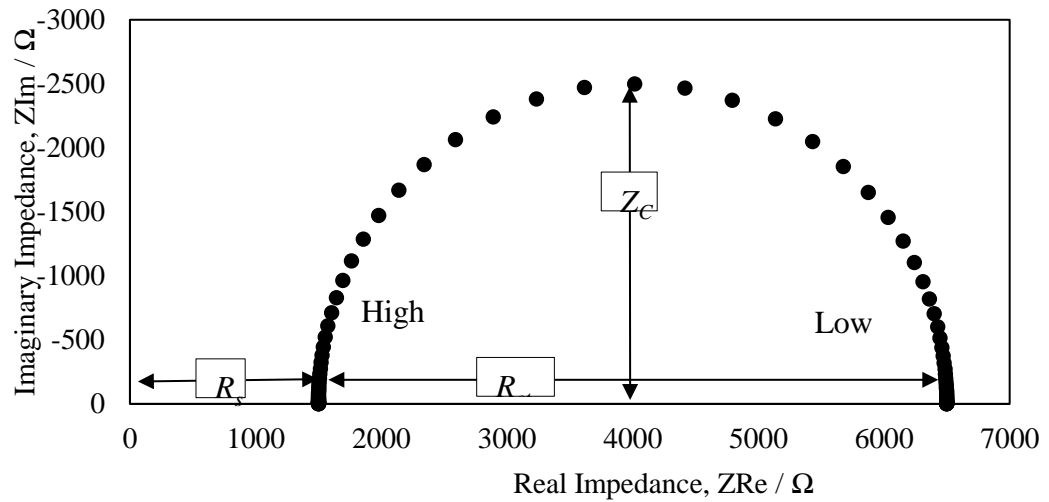
Figure A-2. Nyquist plot for the equivalent circuit described above.

The Nyquist plot does not inherently convey the frequency of each point. However, the values of the different circuit elements can be obtained from the Nyquist plot. The capacitance can be obtained from the value of the impedance, Z_C, and frequency at the maximum.

Another representation of the impedance data is the Bode diagram, which shows the modulus of impedance and phase angle as a function of the frequency [2,26]. For ease of interpretation the frequency is plotted in a logarithmic axis. Figure 3 shows the Bode plot for the circuit given in Figure 1.
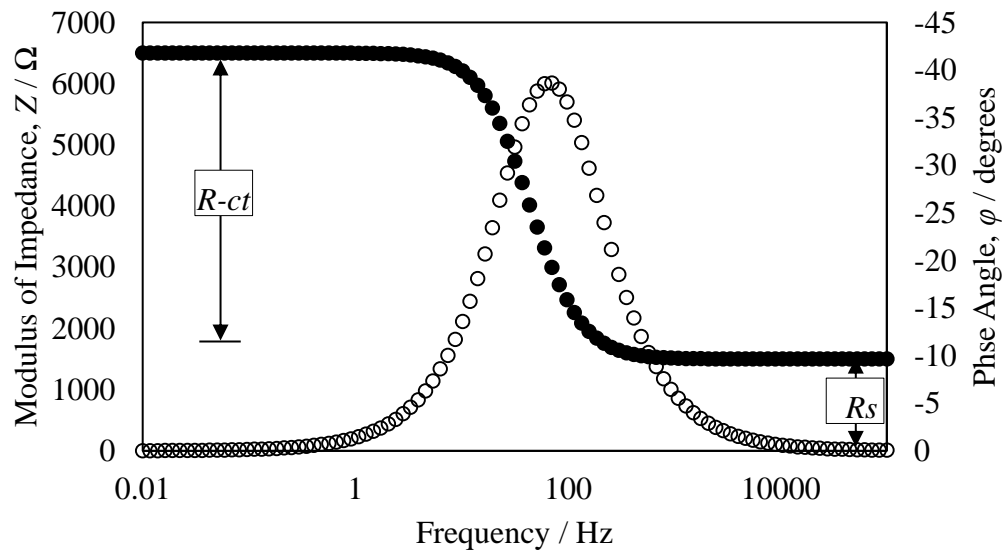
Figure A-3. Bode Diagram for the equivalent circuit described above: [●] Modulus of Impedance, [○] Phase Angle.

The simplified Randles cell is one of the simplest models and is often not the best fit for many real systems. As more processes influence the passage of current across an interface, the simplest model needed to represent a system becomes more complicated with each process that contributes to the impedance. In many cases the *R-ct* element is replaced by a general impedance element, which encompasses the different processes. The nature of the impedance response depends on the reaction mechanism and kinetic model of the processes. For Faradaic processes, the current can be expressed as a function of physical properties such as interfacial potential, concentration of the bulk species and/or surface coverage. These general expressions aid in the development of models from proposed reaction mechanisms [27].

Mixed Charge Transfer and Diffusion Control

In many processes, the rate of electrochemical reactions depends on transport of reacting species to the electrode surface [28]. In such cases, concentration gradients and diffusion effects can limit how and when the processes occur and hence, influence the impedance response. In a typical case, mass transport phenomena are slow compared to the kinetic charge transfer phenomena and are observed when the electrode is polarized for a significant amount of time i.e. low frequencies. Warburg developed the theory of impedance of diffusional transport of electroactive species to the electrode surface using Fick's law [25]. The impedance due to diffusion is called Warburg impedance, Z_W.

$$Z_W = \sigma(\omega)^{-1/2}(1\text{-}i) \tag{19}$$

$$\sigma = RT/n^2F^2A\sqrt{2}\ [\{1/(C_{Ox}{}^*\sqrt{D_{Ox}})\} + [\{1/(C_{Red}{}^*\sqrt{D_{Red}})\}] \tag{20}$$

n, is the number of electrons involved, R, is the gas constant, A, is the area of the electrode, $C_O{}^*$, is the bulk concentration of the oxidant, D_{Ox}, is the diffusion coefficient of the oxidant. The subscript Red denotes the parameters for the reductant.

From the expression of the Warburg impedance, it is straightforward that the phase shift is 45 degrees. Hence, on a complex plane diagram, the Warburg can be identified by a straight diagonal line with a slope of 45 degrees.

The above formulation of the Warburg impedance is valid only where the diffusion layer can grow to an infinite thickness also known as the semi-infinite diffusion case [28]. This is however not what is observed in some systems. In some cases, processes such as convection will

limit the thickness of the diffusion layer to a finite value, δ, also called the Nernst diffusion layer, and becomes the boundary for the diffusing species. Beyond this thickness, the solution is considered bulk. The diffusion impedance in this case takes the form

$$Z_W = \sigma(\omega)^{-1/2}(1\text{-}j)\tanh(\delta(j\omega/D)^{-1/2}) \qquad\qquad (21)$$

D, is an average value of the diffusion coefficients of the diffusing species.

There is no corresponding simple passive electrical element for diffusion such as a pure resistor, capacitor, etc. Hence in equivalent electrical circuits, a Warburg element is used, the impedance response of which is based on the impedance relationships described above. In addition to this, impedance analysis has been extended to account for homogenous bulk reactions, adsorption, reactions involving intermediates and surface inhomogeneity as well [28].

Impedance measurements have rendered a new approach to studying the electrode-solution interface. EIS probes can be used to monitor the multiple processes like chemical reactions and adsorption of species, which occur at the electrode-electrolyte interface [26].

Monitoring Power Plant Water Systems using EIS

Conductivity

Conductivity measurements are made regularly in power plant systems to monitor the purity. High purity water has very low conductivity. When chemicals are added to control the pH, the conductivity changes accordingly. Dissolved corrosion products or impurities can affect the conductivity of the solutions by changing the ionic composition of the solution. There are set standards for permissible conductivity of feedwater at different points for different types of boiler units. Hence solution conductivity is an important parameter which is regularly monitored [29]. Based on the impedance formulations, at high frequencies ($\omega \to \infty$), all contributions to impedance except the series electrolyte resistance can be neglected [21]. Therefore, high frequency impedance values from the Nyquist and the Bode plots can be approximated as the solution resistance [28]. The Nyquist plots shown in Figure 2 indicate how easily the value of the internal resistance, Rs, can be obtained in the case of the simplified Randles cell. Given a fixed electrode geometry i.e. known cell constant, the conductivity of the solution can be determined. Hence EIS is a quick and reliable method to obtain the conductivity of the solution.

Corrosion

EIS has been extensively used in studying metal corrosion. The dissolution of metal when exposed to corrosive solutions has been studied not only in terms of corrosion rates, but also from a mechanistic perspective accounting for changes on the surface [17,30]. Impedance spectroscopy has been applied to understand corrosion on inhomogeneous surfaces, defects in films and coatings and the properties of passive oxide coatings [31]. Passivity is the phenomenon where the metal is covered by a protective layer, usually oxide, and has extremely low corrosion rates [17]. The waterside of the tubes walls in steam generation units develop a dense layer of magnetite [1]. Passivity has been studies extensively using EIS. EIS has been used to delineate the processes occurring at the metal film interface, in the film and at the film solution interface. Multiple models have been developed for studying crystalline deposits and porous films of iron oxides, which constitute the bulk of the boiler tube deposits [17]. EIS has also been successfully applied in studying films and coatings which act as corrosion inhibitors [32]. Coating are not fully impervious to ions and so the corrosion reactions occur at the metal coating interface at a very low rate. However, the transport of the reactive species through the films makes the overall process a very complicated one [17]. EIS is being extensively used to evaluate protective films and coatings on metal surfaces [17,30,33]. The effectiveness of the inhibitors can be well characterized using EIS, not only by measuring polarization resistance, but also the film thickness (from coating capacitance) and the effectiveness of surface coverage, which is obtained from the electrical double layer capacitance at the metal interface [31].

Fouling and Deposition

Particulate fouling and deposition causes a change at the metal solution interface. EIS can be used to detect these changes on the surface of the metal. Impedance measurements have not only been used to detect the formation of scales, but also have been used to identify the properties of the scales formed under different conditions [23]. Zebardast et al. (2013) have used EIS to detect the presence of magnetite particles on the surface of a platinum electrode in a controlled environment. The deposition was monitored by observing the change in the electric double layer capacitance on the platinum [34]. EIS has also been used to study particle-substrate interactions, which forms the basis of deposition and fouling [35]. Research is currently being carried out at

the EMS Energy Institute's Electrochemical Technologies Program of the Pennsylvania State University on using EIS to detect and monitor oxide deposition process in high temperature high pressure boilers. Growth of such oxide films have been modeled using a transmission line equivalent circuit, which takes in account the porosity of the oxide films [36].

The versatility of EIS makes it a very useful tool for monitoring the environment in the water systems in a steam generation unit. EIS offers a distinct advantage by providing a holistic picture of the electrode electrolyte environment. By designing in-situ electrochemical probes and using EIS, detailed, real time information about the metal solution environment can be obtained. Studies have proved that EIS can be used to both detect changes on the surface as well as understand the processes occurring at the interface. Effective understanding of impedance measurements requires significant knowledge of electrochemistry and of the physiochemical processes that could occur at the interface in addition to sophisticated modeling software and knowledge to interpret the EIS data.

References

[1] B. Buecker, Power Plant Water Chemistry: A Practical Guide, PennWell Publishing Company, 1997.

[2] D. Landolt, Corrosion and surface chemistry of metals, CRC Press, 2010.

[3] M.M. Awad, Fouling of Heat Transfer Surfaces, in: Heat Transf. - Theor. Anal. Exp. Investig. Ind. Syst., INTECH Open Access Publisher, 2011: pp. 505–542.

[4] B. Dooley, A vision for reducing boiler tube failures, Power Eng. 96 (1992).

[5] D.I. Bain, J. Bates, Corrosion Monitoring in Fossil-Fired Utility Steam Generators, Ultrapure Water. 22 (2005) 21.

[6] P.O. Jonas, Effective Cycle Chemistry Control, (2000).

[7] J. Robertson, The mechanism of high temperature aqueous corrosion of steel, Corros. Sci. 29 (1989) 1275–1291. doi:10.1016/0010-938X(89)90120-0.

[8] G. Koch, M. Brongers, N. Thompson, P. Virmani, J. Payer, Corrosion Costs and Preventive Strategies in the United States, 2002.

[9] B. Buecker, The Evolution of Power Plant Water/Steam Chemistry, Power Eng. 10 (2012).

[10] B. Buecker, Utility water chemistry update, Power Eng. 105 (2001) 12. [11] B. Buecker, Monitoring the chemistry program change of the condensate/feedwater in a utility drum boiler, Mater. Perform. 44 (n.d.) 42–45.

[12] B. Dooley, A vision for reducing boiler tube failures. Part 2, Power Eng. 95 (1992).

[13] R.B. Dooley, R. Tilley, Guidelines for controlling flow-accelerated corrosion in fossil and combined cycle plants, EPRI Rep. 1008082 (2005).

[14] G.C. Moran, P. Labine, Corrosion monitoring in industrial plants using nondestructive testing and electrochemical methods: a symposium, Astm International, 1986.

[15] R. Fernandez-Prini, A.H. Harvey, D.A. Palmer, Aqueous systems at elevated temperatures and pressures: Physical chemistry in water, steam and hydrothermal solutions, Academic Press, 2004.

[16] J.R. Stetter, W.R. Penrose, S. Yao, Sensors, chemical sensors, electrochemical sensors, and ECS, J. Electrochem. Soc. 150 (2003) S11–S16.

[17] E. Barsoukov, J.R. Macdonald, Impedance spectroscopy: theory, experiment, and applications, John Wiley & Sons, 2005.

[18] U. Guth, W. Vonau, J. Zosel, Recent developments in electrochemical sensor application and technology, Meas. Sci. Technol. 20 (2009) 42002.

[19] W.J. Lorenz, F. Mansfeld, Determination of corrosion rates by electrochemical DC and AC methods, Corros. Sci. 21 (1981) 647–672. doi:10.1016/0010-938X(81)90015-9.

[20] S.N. Lvov, Electrochemical Techniques for Studying High-temperature Subcritical and Supercritical Aqueous Solutions, Encycl. Electrochem. (2007).

[21] S.N. Lvov, Introduction to Electrochemical Science and Engineering, CRC Press, 2014.

[22] G.W. Walter, Problems arising in the determination of accurate corrosion rates from polarization resistance measurements, Corros. Sci. 17 (1977) 983–993. doi:10.1016/S0010-938X(77)80013-9.

[23] B. Kinsella, Y.J. Tan, S. Bailey, Electrochemical impedance spectroscopy and surface characterization techniques to study carbon dioxide corrosion product scales, Corrosion. 54 (1998) 835–842.

[24] A. Lasia, Electrochemical impedance spectroscopy and its applications, in: Mod. Asp. Electrochem., Springer, 2002: pp. 143–248.

[25] D.D. Macdonald, Reflections on the history of electrochemical impedance spectroscopy, Electrochim. Acta. 51 (2006) 1376–1388. doi:10.1016/j.electacta.2005.02.107.

[26] S.-M. Park, J.-S. Yoo, Electrochemical impedance spectroscopy for better electrochemical measurements, Anal. Chem. 75 (2003) 455–A.

[27] M.E. Orazem, B. Tribollet, Electrochemical Impedance Spectroscopy, John Wiley & Sons, Inc., 2008. doi:10.1002/9780470381588.

[28] M. Sluyters-Rehbach, Impedances of electrochemical systems: Terminology, nomenclature and representation-Part I: Cells with metal electrodes and liquid solutions (IUPAC Recommendations 1994), Pure Appl. Chem. 66 (1994) 1831–1891.

[29] D. Friend, R. Dooley, Technical Guidance Document: Volatile Treatments for the steam-water circuits of fossil and combined cycle/HRSG power plants, Niagara Falls, Canada, 2010. http://www.iapws.org/techguide/Volatile.pdf.

[30] F. Mansfeld, Use of electrochemical impedance spectroscopy for the study of corrosion protection by polymer coatings, J. Appl. Electrochem. 25 (1995). doi:10.1007/BF00262955.

[31] K. Jüttner, W.J. Lorenz, Electrochemical impedance spectroscopy (EIS) of corrosion processes on inhomogeneous surfaces, in: Mater. Sci. Forum, Trans Tech Publ, 1991: pp. 191–204.

[32] Y.J.Y.-J. Tan, S. Bailey, B. Kinsella, An investigation of the formation and destruction of corrosion inhibitor films using electrochemical impedance spectroscopy (EIS), Corros. Sci. 38 (1996) 1545–1561. doi:10.1016/0010-938X(96)00047-9.

[33] W. Kuang, J. a. Mathews, M.L. Taylor, D.D. Macdonald, The effect of Anodamine on the corrosion behavior of 1018 mild steel in deionized water: II. Electrochemical Impedance Analysis, Electrochim. Acta. 136 (2014) 493–503. doi:10.1016/j.electacta.2014.05.146.

[34] H.R. Zebardast, S. Rogak, E. Asselin, Electrochemical detection of corrosion product fouling in high temperature and high pressure solution, Electrochim. Acta. 100 (2013) 101–109. doi:10.1016/j.electacta.2013.03.108.

[35] H.R. Zebardast, S. Rogak, E. Asselin, Interfacial electrochemistry study of particle–wall interaction using electrochemical impedance spectroscopy, J. Electroanal. Chem. 670 (2012) 67–77. doi:10.1016/j.jelechem.2012.02.002.

[36] J.R. Park, D.D. Macdonald, Impedance studies of the growth of porous magnetite films on carbon steel in high temperature aqueous systems, Corros. Sci. 23 (1983) 295–315. doi:10.1016/0010-938X(83)90063-X.

[37] B. Raman, D. Hall, S. Shulder, M. Caravaggio, S.N. Lvov, Deposition of Suspended Magnetite in High Temperature High Pressure Boiler Environments, University Park, 2015.

Contributions of Colleagues

The experimental system was designed and built by the primary author with some inputs from D. Hall. The experiments and analyses were carried by the primary author. D. Hall provided advise on thermodynamic calculations and OLI modeling. S.J. Shulder and M. Caravaggio aided in ensuring that the experimental conditions closely matched industrial practices. Dr. S. Lvov provided guidance throughout the process of completing this study.

VITA

Balaji Raman

balajiraman.chem@gmail.com

Education

- Ph. D Energy & Mineral Engineering, with Minor in Electrochemical Engineering
  Pennsylvania State University, 2017

- M.S. in Energy and Mineral Engineering, with option in Energy Management &
  Policy
  Pennsylvania State University, 2016

- B. Tech in Chemical Engineering
  National Institute of Technology, Trichy, India, 2011

Work Experience

- Graduate Research Assistant, EMS Energy Institute, 2014-2017
- Electrochemistry Intern, TE Connectivity, 2016

Publications

- B. Raman, D.M. Hall, S.J. Shulder, M.F. Caravaggio, S.N. Lvov, An Experimental
  Study of Deposition of Suspended Magnetite in High Temperature-High Pressure
  Boiler Type Environments, Colloids Surfaces A Physicochem. Eng. Asp. (2016).
  [Paper]

- B. Raman, D. Hall, S.N. Lvov, Deposition Mechanism and Control of Lower Orifice
  Header Fouling in Forced Circulation Units, Palo Alto, CA, 2015. doi:3002007082.
  [EPRI Report]

- B. Raman, D. Hall, S.N. Lvov, S. Shulder, M. Caravaggio, Electrochemical
  Impedance Spectroscopy as a Tool to Link Cycle Chemistry Properties to Fouling in
  Power Generating Systems, in: 11th Int. Conf. Cycle Chem. Foss. Comb. Cycle
  Plants with Heat Recover. Steam Gener., EPRI, Saint Louis, 2015. [Paper]

- B. Raman, D.M. Hall, S.J. Shulder, M. Caravaggio, S.N. Lvov, Deposition of
  Suspended Magnetite in High Temperature High Pressure Boiler Environments, ECS
  Trans. 66 (2015) 43–56. doi:10.1149/06621.0043ecst. [Paper]